

NEW HORIZONS IN SPHERE PACKING THEORY, PART I: FUNDAMENTAL CONCEPTS & CONSTRUCTIONS, FROM DENSE TO RARE

THOMAS BEWLEY, PAUL BELITZ, & JOSEPH CESSNA

Abstract. The field of n -dimensional sphere packings is elegant and mature in its mathematical development and characterization. However, it is still relatively limited in its practical applications, especially for $n > 3$. The present line of research intends to open up two broad new areas for profitable application of this powerful body of mathematical literature in science and engineering. Towards this end, the present paper (Part I) reviews the essential results available in this field (reconciling the theoretical literature for dense and rare sphere packings, which today are largely disjoint), catalogs the key properties of the principle dense and rare sphere packings and corresponding nets available (including hundreds of values not previously known), and extends the study of regular rare sphere packings and nets to $n > 3$ dimensions (an area which up to now has been largely unexplored). These results are leveraged heavily in the practical applications addressed in Parts II and III. In particular, Part II builds from this presentation to develop a new algorithm for Lattice-Based Derivative-free Optimization via Global Surrogates (LABDOGS), leveraging dense sphere packings as an alternative to Cartesian grids to coordinate derivative-free searches; Part II also develops and uses a new algorithm for efficient solution of discrete Thomson problems restricted to nearest-neighbor points of a lattice. Part III builds from this presentation to develop new interconnect graphs for switchless multiprocessor computer systems, leveraging nets derived from rare sphere packings as alternatives to Cartesian grids to establish structured, fast, and inexpensive interconnects, paying particular attention to the improved coordination sequences facilitated by such nets. In both applications, Cartesian grids are used as the default choice today in almost all related realizations; the present sequence of papers establishes that significant performance improvements may be realized by leveraging n -dimensional sphere packings appropriately in such practical applications.

Key words. n -dimensional sphere packings, lattices, nets, coding theory, derivative-free optimization, switchless computational interconnects

AMS subject classifications. 11H31, 11H71, 52C17, 52C22, 68M10, 05B45

1. Introduction. An n -dimensional infinite *sphere packing* is an array of nodal points in \mathbb{R}^n obtained via the packing of identical n -dimensional spheres. By *packing*, we mean an equilibrium configuration of spheres, each with at least 2 nearest neighbors, against which a repellant force is applied. Many packings investigated in the literature are *stable* packings, meaning that there is a restoring force associated with any small movement of any node of the packing; this requires each sphere in the (n -dimensional) packing to have at least $n + 1$ neighbors. However, unstable packings with lower nearest-neighbor counts are also of interest. Note also that, by replacing each sphere in an n -dimensional packing with a nodal point (representing, e.g., a computer), and connecting those nodal points which are nearest neighbors, a *net* (a.k.a. *interconnect* or *contact graph*) is formed¹.

An n -dimensional real *lattice* (a.k.a. *lattice packing*) is a sphere packing which is shift invariant (that is, which looks identical upon shifting any nodal point to the origin); this shift invariance generally makes lattice packings simpler to describe and enumerate than their nonlattice alternatives. Note that there are many regular² sphere packings which are *not* shift invariant [the nonlattice packings corresponding to the honeycomb net in 2D and the diamond and quartz nets in 3D are some well-known examples]. We will focus our attention in this paper on those packings and nets which are at least *uninodal* (that is, which look identical upon shifting any nodal point to the origin and rotating and reflecting appropriately). For *dense* sphere packings, from a practical perspective, lattice packings are essentially³ as good a choice as their more cumbersome nonlattice alternatives for $n \leq 24$ in terms of

¹As introduced in the second-to-last paragraph of §2.3, it is natural with certain sphere packings (for example, D_n^* , A_n^* , and the packings associated with the T_n^{90} and T_n^{60} nets) to define nets which are *not* contact graphs of the corresponding sphere packings by connecting non-nearest-neighbor points.

²The regularity of a nonlattice packing is quantified precisely in §3.1.

³For $n = 10, 11, 13, 18, 20,$ and 22 , there exist nonlattice packings (denoted $P_{10c}, P_{11a}, P_{13a}, \mathcal{B}_{18}^*, \mathcal{B}_{20}^*, \mathcal{A}_{22}^*$) that are 8.3%, 9.6%, 9.6%, 4.0%, 5.2%, and 15.2% denser than the corresponding best known lattice packings (Conway & Sloane 1998, p. xix); to put this into perspective, the density of Λ_{22} is over 10^6 times the density of \mathbb{Z}^{22} .

the four metrics defined below (that is, for maximizing packing density and kissing number and minimizing covering thickness and quantization error). However, the best *rare* sphere packings (with small kissing number) are all nonlattice packings.

As illustrated in Figure 1.1 and Table 1, we may introduce the subject of n -dimensional sphere packings by focusing our attention first on the $n = 2$ case: specifically, on the *triangular*⁴ lattice (A_2), the *square* lattice (\mathbb{Z}^2), and the *honeycomb* nonlattice packing (A_2^+). The characteristics of such sphere packings may be quantified by the following measures:

- The *packing radius* (a.k.a. the *error-correction radius*) of a packing, ρ , is the maximal radius of the spheres in a set of identical nonoverlapping spheres centered at each nodal point.
- The *packing density* of a packing, Δ , is the fraction of the volume of the domain included within a set of identical non-overlapping spheres of radius ρ centered at each nodal point on the packing. Packings that maximize this metric are referred to as *close-packed*.
- The *covering radius* of a packing, R , is the maximum distance between any point in the domain and its nearest nodal point on the packing. The *deep holes* of a packing are those points which are at a distance R from all of their nearest neighbors. Typical vectors from a nodal point to the nearest deep holes in a lattice packing are often denoted $[1]$, $[2]$, etc.
- The *covering thickness* of a packing, Θ , is the number of spheres of radius R centered at each nodal point containing an arbitrary point in the domain, averaged over the domain.
- The *Voronoi cell* of a nodal point in a packing, $\Omega(P_i)$, consists of all points in the domain that are at least as close to the nodal point P_i as they are to any other nodal point P_j .
- The *mean squared quantization error per dimension* of a lattice or uninodal nonlattice packing, G , is the average mean square distance of any point in the domain to its nearest nodal point, normalized by n times the appropriate power of the volume, V , of the Voronoi cell. Shifting the origin to be at the centroid of a Voronoi cell $\Omega(P_i)$, it is given by

$$G = \frac{S}{nV^{\frac{n+2}{n}}} \quad \text{where} \quad S = \int_{\Omega(P_i)} |\mathbf{x}|^2 d\mathbf{x}, \quad V = \int_{\Omega(P_i)} d\mathbf{x}. \quad (1.1)$$

- The *kissing number* (a.k.a. the *error coefficient*) of a lattice or uninodal nonlattice packing, τ , is the number of nearest neighbors to any given nodal point in the packing. In other words, it is the number of spheres of radius ρ centered at the nodal points of the packing that touch, or “kiss”, the sphere of radius ρ centered at the origin.
- The *coordination number* of a net (derived from a sphere packing, as discussed previously) is the first number of the net’s *coordination sequence*, the k ’th element of which is given by $td_k - td_{k-1}$, where td_k , which quantifies the net’s *local topological density*, is the total number of nodes reached via k hops or less from the origin in the net⁵.

Certain applications, such as that explored in Part II of this work (Belitz & Bewley 2011), require dense lattices. There are two key drawbacks with Cartesian approaches for such applications. First, the *discretization of space is significantly less uniform* when using the Cartesian grid as opposed to the available alternatives, as measured by the packing density Δ , the covering thickness Θ , and the mean-squared quantization error per dimension, G (see Table 1). Second, the *configuration of nearest-neighbor gridpoints is significantly more*

⁴Note that many in this field refer to the A_2 lattice as “hexagonal”. We prefer the unambiguous name “triangular” to avoid confusion with the honeycomb nonlattice packing (see Figure 1.1).

⁵In most cases, the natural net to form from a sphere packing is the contact graph; in such cases, the kissing number, τ , and the coordination number are equal. As mentioned previously, it is natural with certain sphere packings to define nets which are *not* contact graphs by connecting non-nearest-neighbor points; in such cases, the kissing number (a property of the sphere packing) and the coordination number (as defined here, a property of a corresponding net) are, in general, *not* equal. We find this clear semantic distinction to be useful to prevent confusion between these two distinct concepts; note that some authors (e.g., Conway & Sloane 1998) do not make this distinction.

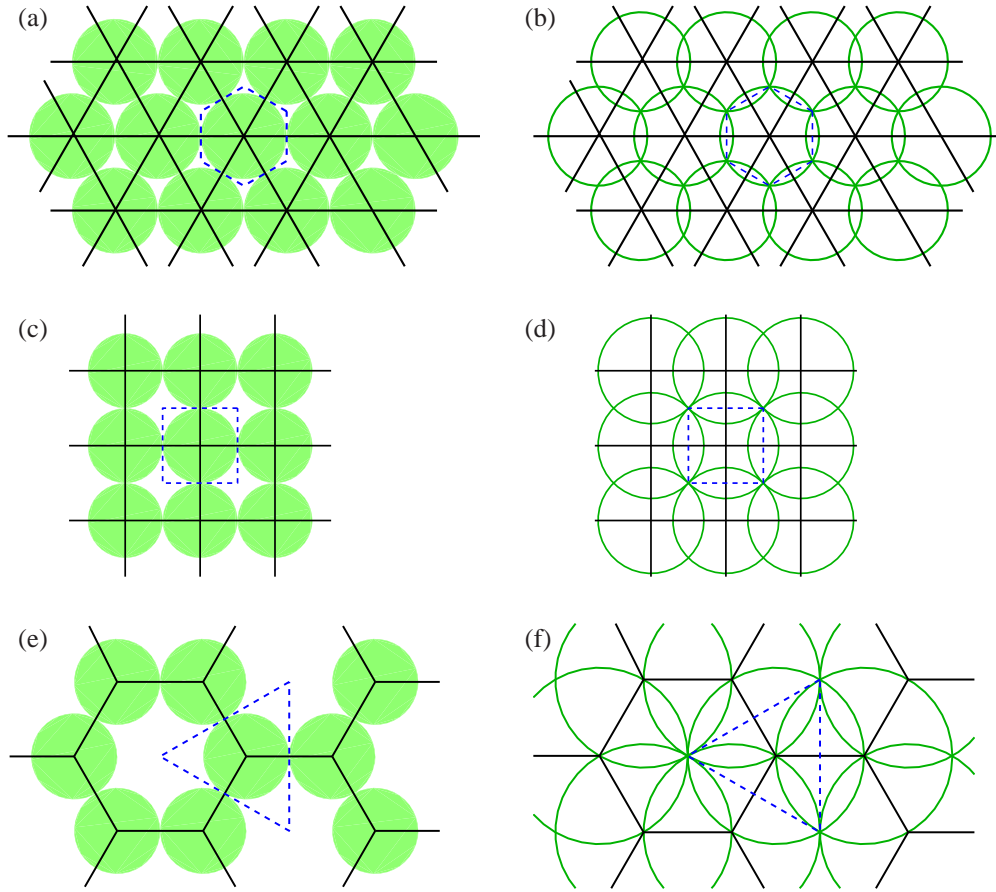


FIG. 1.1. The triangular lattice (a,b), the square lattice (c,d), and the honeycomb nonlattice packing (e,f). Indicated in the left three subfigures is the packing with spheres of radius ρ , the corresponding net or contact graph (solid lines), a typical Voronoi cell (dashed line), and the kissing number (that is, the spheres that contact a given sphere). Indicated in the right three subfigures is the covering with spheres of radius R . Looking at their respective packing densities Δ in Table 1, as compared with the square lattice, the triangular lattice is said to be **dense**, and the honeycomb nonlattice packing is said to be **rare**.

n	packing	name	Δ	Θ	G	τ	td_{10}	
2	A_2	triangular	0.9069	1.2092	0.08019	6	331	
	\mathbb{Z}^2	square	0.7854	1.5708	0.08333	4	221	
	A_2^+	honeycomb	0.6046	2.4184	0.09623	3	166	
8	E_8	Gosset	0.2537	4.059	0.07168	240	1,006,201,681	
	\mathbb{Z}^8	Cartesian	0.01585	64.94	0.08333	16	1,256,465	
	(unstable)	V_8^{90}		5.590e-4	49.89	0.09206	4	37,009
		\mathcal{V}_8^{90}		2.327e-4	87.31	0.09266	3	2290
24	Λ_{24}	Leech	0.001930	7.904	0.06577	196560	$> 10^{15}$	
	\mathbb{Z}^{24}	Cartesian	1.150e-10	4,200,263	0.08333	48	24,680,949,041	

Table 1. Characteristics of selected lattice and uninodal nonlattice packings and nets. Note that $n = 24$ is a natural stopping point in this study. It is special because it is the only integer $n > 1$ that satisfies $1^2 + 2^2 + \dots + n^2 = m^2$ where m is itself an integer; as a consequence, a particularly uniform lattice with a large number of symmetries is available in this dimension.

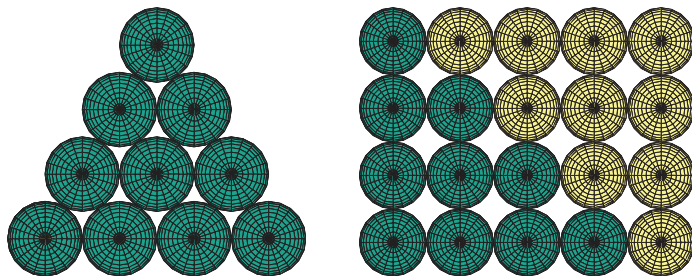


FIG. 1.2. (left) Ten marbles placed in a triangle [referred to by the Pythagoreans as a τετρακτύς, and upon which they placed a particular mystic significance], and (right) the Pythagoreans' placement of two triangular groups of marbles into an "oblong" $m \times (m + 1)$ rectangle, from which the formula for $T_{2,m}$ follows immediately.

limited when using the Cartesian grid, as measured by the kissing number τ , which is an indicator of the degree of flexibility available when selecting from nearest-neighbor points. As seen by comparing the $n = 2$, $n = 8$, and $n = 24$ cases in Table 1, these drawbacks become increasingly substantial as the dimension n is increased; by the dimension $n = 24$, the best available lattice has

- a factor of $0.001930/1.1501e - 10 \approx 17,000,000$ better (higher) packing density,
- a factor of $4,200,263/7.9035 \approx 530,000$ better (lower) covering thickness,
- a factor of $0.08333/0.0658 \approx 1.27$ better (lower) mean-squared quantization error, and
- a factor of $196560/48 \approx 4100$ better (higher) kissing number

than the corresponding Cartesian grid. Thus, the selection of the Cartesian grid, by default, for applications requiring dense (that is, uniform) lattices with $n > 3$ is simply untenable.

Other applications, such as that explored in Part III of this work (Cessna & Bewley 2011), require regular nets which, with low coordination number, connect to a large number of nodes with each successive hop from the origin, as quantified by the net's coordination sequence. As mentioned previously, a useful measure of a net's topological density is given, e.g., by td_{10} , which is the number of distinct nodes within 10 hops of the origin. Note that the coordination number of the n -dimensional Cartesian grid is $2n$; the coordination number of the alternative n -dimensional constructions introduced in §3 are as small as 3 or 4, while the topological density increases rapidly as n is increased (compare, e.g., the values of td_{10} for A_2^+ and \mathbb{Z}^2 , with $\tau = 3$ and $\tau = 4$ respectively, to those for Υ_8^{90} and \mathbb{V}_8^{90} in Table 1); it is thus seen that, for applications requiring graphs with low coordination number and high topological density, the selection of the Cartesian grid, by default, is also untenable.

We are thus motivated to make the fundamental results of both dense and rare n -dimensional sphere packing theory more broadly accessible to the science and engineering community, and to illustrate how this powerful body of theory may be put to use in two important new applications of practical relevance. Towards this end, the remainder of Part I succinctly reviews and extends several significant results in this mature and sophisticated field, inter-relating the literature on dense and rare packings, which is today largely disjoint. These results are leveraged heavily in the applications described in Parts II and III. We note that, beyond providing an up-to-date and synthetic review of this otherwise difficult subject in a (hopefully) accessible language, a significant number of new computations, constructions, algorithms, metrics, and codes are also reported in this document (Part I) [the reader is referred specifically to Tables 2-3, §3.4.1 through §3.4.7, §3.5, and §5.5].

The mathematical characterization of sphere packings has a long and rich history. Some recent articles and popular books recount this history in detail, including Zong (1999), Szpiro (2003), Hales (2006), and Aste & Weaire (2008). The purpose of the present article is not to repeat these historical retrospectives, which these sources do quite adequately, but to characterize, catalog, and extend the infinite packings available today to facilitate their practical

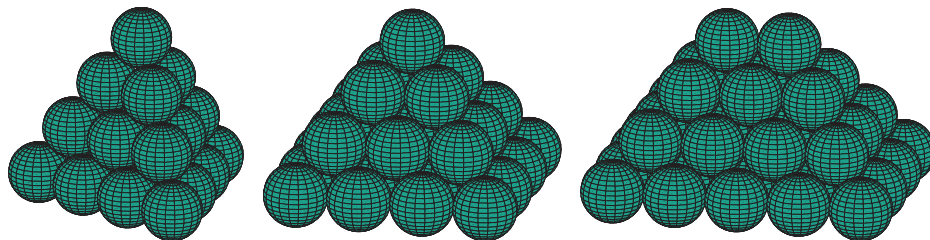


FIG. 1.3. Pyramidal stacks of spheres with triangular, square, and “oblong” (rectangular) bases. All three stacks are subsets of the face-centered cubic lattice, discussed further in §2.3.

application in new fields. Nonetheless, we would remiss if we didn’t at least provide a brief historical context to this field, which we attempt in the following two subsections.

1.1. Finite packings: mystic marbles, stacked spheres, permuted planets, cartoned cans, catastrophic sausages, and concealed origins. We begin by defining, for $m \geq 1$, a notation to build from:

$$T_{0,m} \triangleq 1, \quad T_{1,m} \triangleq \sum_{k=1}^m T_{0,k} = m \quad (\text{the positive integers}).$$

In the sixth century BC, Pythagoras and his secret society of numerologists, the Pythagoreans, discovered geometrically (see Figure 1.2, and pp. 43-50 of Heath 1931) the formula for the number of marbles placed in a (2D) triangle (that is, the “triangular numbers”):

$$T_{2,m} \triangleq \sum_{k=1}^m T_{1,k} = m(m+1)/2.$$

The earliest known mathematical work to discuss the (3D) stacking of objects is a Sanskrit document *The Aryabhatiya of Aryabhata* (499 AD; see Clark 1930, p. 37), which states:

“In the case of an *upaciti* [lit., ‘pile’] which has ... the product of three terms, having the number of terms for the first term and one as the common difference, divided by six, is the *citighana* [lit., ‘cubic contents of the pile’]. Or, the cube of the number of terms plus one, minus the cube root of this cube, divided by six.”

Thus, Aryabhata establishes, in words, two equivalent expressions for the number of objects (“cubic contents”) in a (3D) triangular-based pyramid (“pile”) with m objects on each edge:

$$T_{3,m} = \frac{m(m+1)(m+2)}{3!} = \frac{(m+1)^3 - (m+1)}{6};$$

note also that $T_{3,m} \triangleq \sum_{k=1}^m T_{2,k}$.

Thomas Harriot was apparently the first to frame the problem of sphere packing mathematically in modern times (see, e.g., the biography of Harriot by Rukeyser 1972). At the request of Sir Walter Raleigh, for whom Harriot served, among other capacities, as an instructor of astronomical navigational and on various problems related to gunnery, Harriot (on December 12, 1591) computed, but did not publish, the number of cannonballs in a pile with a triangular, square [$m \times m$], and rectangular [$m \times (m+1)$, a.k.a. “oblong”] base, as illustrated in Figure 1.3, obtaining $T_{3,m}$, S_m , and R_m respectively, where

$$S_m = \sum_{k=1}^m k^2 = \frac{m(m+1)(2m+1)}{6}, \quad R_m = \sum_{k=1}^m k(k+1) = S_m + T_{2,m} = \frac{m(m+1)(2m+4)}{6}.$$

In 1614, Harriot wrote *De Numeris Triangularibus Et inde De Progressionibus Arithmetiis: Magisteria magna (On triangular numbers and thence on arithmetic progressions: the great*

doctrine)⁶. Looking closely at the triangular table of binomial coefficients⁷ on pp. 1-3 (folios 108-110) of this remarkable document, it is seen that Harriot understood the *geometric* relationship between the positive integers $T_{1,m}$, the “triangular numbers” $T_{2,m}$ [that is, the number of spheres in a (2D) triangle with m spheres on each edge], the “pyramidal numbers” $T_{3,m}$ [that is, the number of spheres in a (3D) triangular-based pyramid with m spheres on each edge], and the next logical steps in this arithmetic progression, given by:

$$T_{4,m} \triangleq \sum_{k=1}^m T_{3,k} = \frac{m(m+1)(m+2)(m+3)}{4!}, \quad T_{5,m} \triangleq \sum_{k=1}^m T_{4,k} = \frac{m(m+1)(m+2)(m+3)(m+4)}{5!},$$

etc. In particular, Harriot noticed that the $(n+1)$ 'th element of the $(n+m)$ 'th row of this triangular table is $T_{n,m}$. Accordingly, we may think of $T_{n,m}$ as the number of spheres in an “ n -dimensional pyramid” with m spheres on each edge, with $T_{n,2}$ representing $n+1$ spheres configured at the corners of a regular n -dimensional simplex. It is thus natural to credit Harriot (1614) with the first important steps towards the discovery of laminated lattices, discussed further in §2.4 and §2.6.

Harriot also introduced the packing problem to Johannes Kepler, ultimately leading Kepler (1611), in another remarkable document *Strena seu de nive sexangula (The six-cornered snowflake)*, which also hypothesized about a related atomistic physical basis for hexagonal symmetry in crystal structures of water, to conjecture that

“The (cubic or hexagonal close) packing is the tightest possible, such that in no other arrangement can more spheres be packed into the same container.”

Kepler's conjecture is, of course, patently false if considered in a finite container of a specified shape. For instance, a $2d \times 2d \times 2d$ cubic container can fit 8 spheres of diameter d if arranged in Cartesian configuration, but can only fit 5 spheres if arranged in a “close-packed” configuration⁸. It is presumed that Kepler in fact recognized this, and thus Kepler's conjecture is commonly understood as a conjecture regarding the densest packing possible in the limit that the size of the container is taken to infinity (for further discussion, see §1.2).

Note in Figure 1.3 that any sphere (referred to as a “sun”) on the interior of the piles has 12 nearest neighbors (referred to as its “planets”). Considering this sun and its 12 planets in isolation, there is in fact adequate room to permute the planets to different positions while keeping them in contact with the sun, something like a 12-cornered Rubik's cube with spherical pieces (see Figure 1.4). Due to the extra space available in this configuration, it is unclear upon first inspection whether or not there is sufficient room to fit a 13'th planet in to touch the sun while keeping all of the other 12 planets in contact with it. In 1694, Isaac Newton conjectured this could not be done, in a famous disagreement with David Gregory, who thought it could. Newton turned out to be right, with a complete proof first given in Schütte & van der Waerden (1953), and a substantially simplified proof given in Leech (1956).

Moving from 16th-century stacks of cannonballs to 21st-century commerce, the question of dense finite packings of circles and spheres finds practical relevance in a variety of packaging problems. For example, to form a rectangular cardboard carton for 12 fl oz soda cans, 164 cm² of cardboard per can is needed if 18 cans are placed in a cartesian configuration with 3 rows of 6 cans per row, whereas 3.3% less cardboard per can is needed if 18 cans are placed in a triangular configuration (within a rectangular box) with 5 rows of {4,3,4,3,4} cans per row. If an eye-catching (stackable, strong, “green”...) hexagonal cardboard carton for the soda cans is used, with 19 cans (described in marketing terms as “18 plus 1 free”) again placed in a triangular configuration, 17.7% less cardboard per can is required.

Two new questions arise when one “shrink-wraps” a number (m) of n -dimensional spheres (resulting in a convex, fitted container), namely: what configuration of the spheres minimizes

⁶Harriot (1614) passed through several hands before finally being published in 2009, almost 4 centuries later.

⁷This now famous triangular table of binomial coefficients is incorrectly attributed by many in the west to Blaise Pascal (b. 1623), though it dates back to several earlier sources, the earliest being Pingala's Sanskrit work *Chandas Shastra*, written in the fifth century BC.

⁸For larger containers, the arrangements which pack in the greatest number of spheres (or other objects) must in general be found numerically (see Gensane 2004, Schürmann 2006, and Friedman 2009).

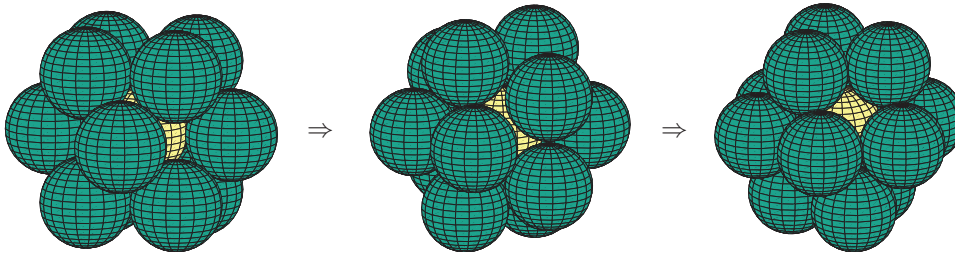


FIG. 1.4. Illustration of the 13 spheres (a.k.a. Newton-Gregory) problem and planetary permutations. Configuration (a) is 13 of the spheres taken from the second, third, and fourth layers of the stack in the orientation shown in Figure 1.3b, whereas configuration (c) is 13 of the spheres taken from the third, fourth, and fifth layers of the stack in the orientation shown in Figure 1.3a [extended by one additional layer]. In both configurations, the 12 “planets” (positioned around the central “sun”) are centered at the vertices of a cuboctahedron. The planets can be permuted by “pinching” together two of the four planets on the corners of each square face, in an alternating fashion, to form a symmetric icosahedral configuration with significant space between each pair of planets [configuration (b)], then “pushing” apart pairs of planets in an analogous fashion to form a different cuboctahedron. Alternatively, starting from configuration (b), identifying any pair of opposite planets as “poles”, and slightly shifting the five planets in each of the “tropics” as close as possible to their nearest respective poles, the resulting northern and southern groupings of planets can be rotated in relation to each other along the equator. Repeated application of these two fundamental motions can be used to permute the planets arbitrarily.

the surface area of the resulting container, and what configuration minimizes the volume of the resulting container? Both questions remain open, and are reviewed in Zong (1999). Regarding the minimum surface area question, it was conjectured by Croft, Falconer, & Guy (1991) that the minimum surface area, for $n \geq 2$ and large m , is achieved with a roughly spherical arrangement. In contrast, regarding the minimum volume question, it was conjectured by L. Fejes Tóth (1975) that the minimum volume, for $n \geq 5$ and any m , is achieved by placing the spheres in a line, leading to a shrink-wrapped container in the shape of a “sausage”. For $n = 3$, it has been shown that a roughly spherical arrangement minimizes the volume for $m = 56$, $m = 59$ to 62 , and $m \geq 65$, and it is conjectured that a sausage configuration minimizes the volume for all other m (see Gandini & Willis 1992); for $n = 4$, there appears to be a similar “catastrophe” in the volume-minimizing solution, from a sausage configuration to a roughly spherical configuration, as m is increased beyond a critical value (Willis 1983 conjectures this critical value to be $m \approx 75000$, whereas Gandini & Zucco 1992 conjectures it to be $m = 375769$).

Finally, L. Fejes Tóth (1959) presents a curious set of questions that arise when considering the blocking of light with a finite number of opaque unit spheres packed around the origin. The first such question, known as Hornich’s Problem, seeks the smallest number of opaque unit spheres that completely conceal light rays emanating from a point source at the center of a transparent unit sphere at the origin. A related question, known as L. Fejes Tóth’s Problem, seeks the smallest number of opaque spheres that completely conceal light rays emanating from the surface of a unit sphere at the origin (e.g., in Figure 1.4, adding additional outer planets to completely conceal the view of the sun from all angles). In 2D, the (trivial) answer to both problems is 6, via the triangular packing indicated in Figure 1.1a. In higher dimensions, both questions remain open, and the answer differs depending on whether or not the sphere centers are restricted to the nodal points of a lattice. For the L. Fejes Tóth’s Problem, for $n \geq 3$, the answer is unbounded if restricted to lattice points, and bounded if not. For Hornich’s Problem, the answer is bounded in both cases, with the number of spheres, h , required in the 3D case, when not restricted to lattice points, being somewhere in the range $30 \leq h \leq 42$. Zong (1999) derives several of the known bounds available in both problems.

1.2. Infinite packings. In the last 300 years, many different constructions of infinite lattice and nonlattice packings have been proposed in each dimension. These packings each have different packing density, covering thickness, mean-squared quantization error, and kissing number, and their corresponding nets each have different topological density; knowledge

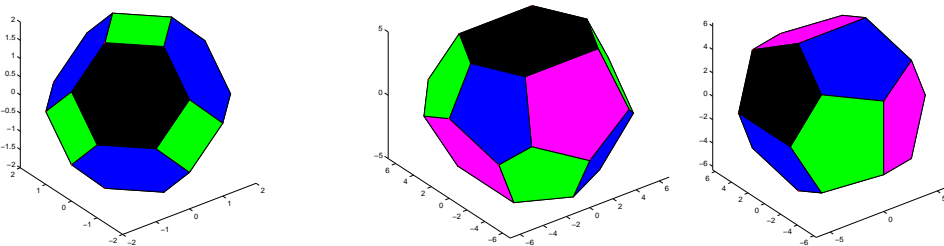


FIG. 1.5. (a) A regular truncated octahedron, used to tile \mathbb{R}^3 in Kelvin's conjecture; (b) an irregular tetrakaidecahedron and dodecahedron, used to tile \mathbb{R}^3 in the Weaire-Phelan structure.

of these properties is essential when selecting a packing or net for any given application. We have thus attempted to catalog these constructions and their properties thoroughly in the remainder of this review.

In the characterization of density, amongst all *lattice* packings of a given dimension, the A_2 , A_3 , D_4 , D_5 , E_6 , E_7 , E_8 , and Λ_{24} constructions given in §2 have been proven to be of maximum density, in Lagrange (1773) for $n = 2$, Gauss (1831) for $n = 3$, Korkine & Zolotareff (1873, 1877) for $n = 4$ and 5, Blichfeldt (1935) for $n = 6$ through 8, and Cohn & Kumar (2009) for $n = 24$. There are no such proofs of optimality for other values of n , though the lattices Λ_n and K_n introduced in §2.6 are likely candidates in the range $9 \leq n \leq 23$.

Remarkably, if one considers both lattice *and* nonlattice packings, proof of which packing is of maximum density in a given dimension is still open for $n > 3$. It was established in Thue (1892) that A_2 has the maximum density amongst all lattice and nonlattice packings for $n = 2$. Considerable attention has been focused over the centuries on the corresponding question for A_3 in dimension $n = 3$, that is, on Kepler's conjecture (posed in 1611) in the limit that the container size is taken to infinity. Indeed, David Hilbert, in his celebrated list of 23 significant open problems in mathematics in 1900, included a generalization of Kepler's conjecture as part of his 18th problem (see, e.g., Milnor 1976).

Note that it is not at all obvious that an infinite packing as regular as A_3 would necessarily be the packing that maximizes density. Indeed, as mentioned in footnote 3 on page 1, nonlattice packings are known in dimensions $n = 10, 11, 13, 18, 20$, and 22 that are each slightly denser than the densest known lattice packings in these dimensions.

In three dimensions, physiologist Stephen Hales (1727), in his groundbreaking work *Vegetable Staticks*, reported a curious experiment:

"I compressed several fresh parcels of Pease in the same Pot, . . . by the great incumbent of weight, pressed into the interstices of the Pease, which they adequately filled up, being therefore formed into pretty regular dodecahedrons."

This report implied that many of the dilated peas in this experiment had 12 nearest neighbors and/or pentagonal faces. However, the "pretty regular" qualification left a certain ambiguity, and this experiment left mathematicians puzzled, as it is patently impossible to tile \mathbb{R}^3 with regular dodecahedra. Kelvin (1887) formalized the question inherent in Hales' dilated pea experiment by asking how \mathbb{R}^3 could be divided into regions of equal volume while minimizing the partitional area. He conjectured the answer to be a regular tiling of \mathbb{R}^3 with truncated octahedra, which are in fact the Voronoï cells of the A_3^* lattice (see §3.4.3). [Note that the Voronoï cell of the A_3 lattice is the (face-transitive) *rhombic* dodecahedron, which is dual to the cuboctahedron illustrated in Figures 1.4a,c and tiles \mathbb{R}^3 with slightly greater partitional area than does the tiling with truncated octahedra.] Kelvin's conjecture stood for over 100 years, until Weaire & Phelan (1994) discovered a tiling of \mathbb{R}^3 based on irregular tetrakaidecahedra (with 2 hexagonal faces and 12 pentagonal faces) and irregular dodecahedra (with 12 pentagonal faces); this tiling has 0.3% less partitional area than the much more regular tiling with truncated octahedra considered by Kelvin (see Figure 1.5). In hindsight, it is quite pos-

sible that Hales might have in fact stumbled upon the Weaire-Phelan structure in his cooking pot (in 1727!) and, seeing all of those pentagonal faces and 12-sided (as well as 14-sided) dilated peas, asserted that what he was looking at was a culinary approximation to a tiling of \mathbb{R}^3 with regular dodecahedra, even though such a tiling is impossible.

Returning to Kepler's conjecture, in 1998, Thomas Hales (no relation to Stephen) announced a long-sought-after proof, in a remarkably difficult analysis making extensive use of computer calculations. This proof was spread over a sequence of papers published in the years that followed (see Hales 2005). An extensive discussion of this proof, which is still under mathematical scrutiny, is given in Szpiro (2003). Inspiration for this proof was based, in part, on a strategy to prove Kepler's conjecture proposed by L. Fejes Tóth (1953), the first step of which is a quantitative version of the Newton-Gregory problem discussed in §1.1.

2. Dense lattice packings for $n \leq 24$. There are many dense lattices more complex than the Cartesian lattice that offer superior uniformity and nearest-neighbor configuration, as quantified by the standard metrics introduced in §1 (namely, packing density, covering thickness, mean-square quantization error, and kissing number). This section provides an overview of many of these lattices; *the definitive comprehensive reference for this subject is Conway & Sloane (1998), to which the reader is referred for much more detailed discussion and further references on many of the topics discussed in §2*. Note that the subject of coding theory, reviewed in §4, is very closely related to the subject of dense lattice packings. As mentioned in the abstract, the practical application explored in Part II of this work also leverages these constructions heavily.

2.1. Lattice terminology. The notation $L_n \cong M_n$ means that the lattices L_n and M_n are *equivalent* (when appropriately rotated and scaled) at the specified dimension n . Also note that the four most basic families of lattices introduced in §2, denoted \mathbb{Z}^n , A_n , D_n , and E_n , are often referred to as *root lattices* due to their relation to the root systems of Lie algebra.

There are three primary methods⁹ to define any given n -dimensional real lattice:

- As an *explicit description* of the points included in the lattice.
- As an *integer linear combination* (that is, a linear combination with integer coefficients) of a set of n basis vectors \mathbf{b}^i defined in \mathbb{R}^{n+m} for $m \geq 0$; for convenience, we arrange these basis vectors as the columns¹⁰ of a *basis matrix*¹¹ B .
- As a *union of cosets*, or sets of nodal points, which themselves may or may not be lattices.

The standard form of these definitions, as used in §2, makes it straightforward to generalize application codes that can build easily upon any of the lattices so described.

Any real (or complex) lattice L_n has associated with it a *dual lattice* L_n^* defined such that

$$L_n^* = \{ \mathbf{x} \in \mathbb{R}^n \text{ (or } \mathbb{C}^n) : \mathbf{x} \cdot \bar{\mathbf{u}} \in \mathbb{Z} \text{ for all } \mathbf{u} \in L_n \}, \quad (2.1)$$

where \mathbb{Z} denotes the set of all integers, dot denotes the usual scalar product, and overbar denotes the usual complex conjugate. If B is a square basis matrix for L_n , then B^{-T} is a square basis matrix for L_n^* .

Unless specified otherwise, the word lattice in this paper implies a real lattice, defined in \mathbb{R}^n . However, note that it is straightforward to extend this work to complex lattices, defined

⁹A convenient alternative method for building a cloud of lattice points near the origin is based on the stencil of nearest-neighbor points to the origin in the lattice, repeatedly shifting this stencil to each of the lattice points near the origin determined thus far in order to create additional lattice points in the cloud. Unfortunately, this simple alternative method does not work for all lattices, such as D_n^* and A_n^* (see §2.3 and 2.4).

¹⁰In the literature on this subject, it is more common to use a *generator matrix* M to describe the construction of lattices. The basis matrix convention B used here is related simply to the corresponding generator matrix such that $B = M^T$; we find the basis matrix convention to be more natural in terms of its linear algebraic interpretation.

¹¹Note that integer linear combinations of the columns of most matrices do *not* produce lattices (as defined in the second paragraph of §1). The matrices listed in §2 as basis matrices are special in this regard. Note also that basis matrices are not at all unique, but the lattices constructed from alternative forms of them are equivalent; the forms of the basis matrices listed in §2 were selected based on their simplicity.

in \mathbb{C}^n . To accomplish this extension, it is necessary to extend the concept of the integers, which are used to construct a lattice via the “integer” linear combination of the basis vectors in a basis matrix B , as described above. There are two primary such extensions:

- The *Gaussian integers*, defined as $\mathcal{G} = \{a + b\iota : a, b \in \mathbb{Z}\}$ where $\iota = \sqrt{-1}$, which lie on a square array in the complex plane \mathbb{C} .
- The *Eisenstein integers*, defined as $\mathcal{E} = \{a + b\omega : a, b \in \mathbb{Z}\}$ where $\omega = (-1 + \iota\sqrt{3})/2$ [note that $\omega^3 = 1$], which lie on a triangular array in the complex plane \mathbb{C} .

We may thus define three types of lattices from a basis matrix B :

- a real lattice, defined as a linear combination of the columns of B with integers as weights;
- a (complex) \mathcal{G} lattice, defined as a linear combination of the columns of B with Gaussian integers as weights; and
- a (complex) \mathcal{E} lattice, defined as a linear combination of the columns of B with Eisenstein integers as weights.

The special n -dimensional real, \mathcal{G} , and \mathcal{E} lattices formed by taking $B = I_{n \times n}$ are denoted \mathbb{Z}^n , $\mathbb{Z}[\iota]^n$, and $\mathbb{Z}[\omega]^n$ respectively. Note also that, for any complex lattice with elements $\tilde{\mathbf{z}} \in \mathbb{C}^n$, there is a corresponding real lattice with elements $\tilde{\mathbf{x}} \in \mathbb{R}^{2n}$ such that

$$\tilde{\mathbf{x}} = (\Re\{\tilde{z}_1\} \quad \Im\{\tilde{z}_1\} \quad \dots \quad \Re\{\tilde{z}_n\} \quad \Im\{\tilde{z}_n\})^T. \quad (2.2)$$

The present sequence of papers focuses on the practical use of real lattice and nonlattice packings with $n > 3$. Thus, in the present Part I, we only make brief use of complex lattices to simplify certain constructions.

2.2. The Cartesian lattice \mathbb{Z}^n . The *Cartesian lattice*, \mathbb{Z}^n , is defined $\mathbb{Z}^n = \{(x_1, \dots, x_n) : x_i \in \mathbb{Z}\}$, and may be constructed via integer linear combination of the columns of the basis matrix $B = I_{n \times n}$. The Cartesian lattice is self dual [that is, $(\mathbb{Z}^n)^* \cong \mathbb{Z}^n$] for all n .

2.3. The checkerboard lattice D_n , its dual D_n^* , and the offset checkerboard packing D_n^+ . The *checkerboard lattice*, D_n , is an n -dimensional extension of the 3-dimensional *face-centered cubic (FCC, a.k.a. cubic close packed)* lattice. It is defined

$$D_n = \{(x_1, \dots, x_n) \in \mathbb{Z}^n : x_1 + \dots + x_n = \text{even}\}, \quad (2.3a)$$

and may be constructed via integer linear combination of the columns of the $n \times n$ basis matrix

$$B_{D_n} = \begin{pmatrix} -1 & 1 & & & 0 \\ -1 & -1 & 1 & & \\ & & & \ddots & \\ & & & & -1 & 1 \\ 0 & & & & & -1 \end{pmatrix}. \quad (2.3b)$$

The dual of the checkerboard lattice, denoted D_n^* and reasonably identified as the *offset Cartesian lattice*, is an n -dimensional extension of the 3-dimensional *body-centered cubic (BCC)* lattice. It may be written as

$$D_n^* = D_n \cup ([1] + D_n) \cup ([2] + D_n) \cup ([3] + D_n) \cong \mathbb{Z}^n \cup ([1] + \mathbb{Z}^n), \quad (2.4a)$$

where the *coset representatives* [1], [2], and [3] are defined in this case such that

$$[1] = \begin{pmatrix} 1/2 \\ \vdots \\ 1/2 \\ 1/2 \end{pmatrix}, \quad [2] = \begin{pmatrix} 0 \\ \vdots \\ 0 \\ 1 \end{pmatrix}, \quad [3] = \begin{pmatrix} 1/2 \\ \vdots \\ 1/2 \\ -1/2 \end{pmatrix}.$$

The D_n^* lattice may also be constructed via integer linear combination of the columns of the $n \times n$ basis matrix

$$B_{D_n^*} = \begin{pmatrix} 1 & & & 0 & 0.5 \\ & 1 & & & 0.5 \\ & & \ddots & & \vdots \\ & & & 1 & 0.5 \\ 0 & & & & 0.5 \end{pmatrix}. \quad (2.4b)$$

It is important to recognize that, for $n \geq 5$, the contact graph of the D_n^* lattice is simply two disjoint nets given by the contact graphs of the \mathbb{Z}^n and shifted \mathbb{Z}^n sets of lattice points upon which D_n^* may be built [see (2.4a)]. Thus, as suggested by Conway & Sloane (1997), we introduce, for $n \geq 4$, a *generalized net* formed by connecting each node of the unshifted \mathbb{Z}^n set to the 2^n nearest nodes on the shifted \mathbb{Z}^n set, and each node on the shifted \mathbb{Z}^n set to the 2^n nearest nodes on the unshifted \mathbb{Z}^n set. The resulting net, of coordination number 2^n , is uninodal, but is *not* a contact graph of the corresponding sphere packing.

The packing D_n^+ , reasonably identified as the *offset checkerboard packing*, is an n -dimensional extension of the 3-dimensional *diamond* packing, and is defined simply as

$$D_n^+ = D_n \cup ([1] + D_n); \quad (2.5)$$

note that D_n^+ is a lattice packing only for even n , and that D_3^+ is the *diamond packing* (for further discussion, see §3.4.1).

2.4. The zero-sum lattice A_n , its dual A_n^* , and the glued zero-sum lattices A_n^r . The *zero-sum lattice*, A_n , may be thought of as an n -dimensional extension of the 2-dimensional *triangular lattice*; in 3 dimensions, $A_3 \cong D_3$. It is defined

$$A_n = \{(x_0, \dots, x_n) \in \mathbb{Z}^{n+1} : x_0 + \dots + x_n = 0\}, \quad (2.6a)$$

and may be constructed via integer linear combination of the columns of the $(n+1) \times n$ basis matrix

$$B_{A_n} = \begin{pmatrix} -1 & & & & 0 \\ 1 & -1 & & & \\ & & \ddots & & \\ & & & 1 & -1 \\ 0 & & & & 1 \end{pmatrix}, \quad \text{with} \quad \mathbf{n}_{A_n} = \begin{pmatrix} 1 \\ 1 \\ \vdots \\ 1 \\ 1 \end{pmatrix}. \quad (2.6b)$$

Notice that A_n is constructed here via n basis vectors in $n+1$ dimensions. The resulting lattice lies in an n -dimensional subspace in \mathbb{R}^{n+1} ; this subspace is normal to the vector \mathbf{n}_{A_n} . An illustrative example is A_2 , the triangular 2D lattice, which may conveniently be constructed on a plane in \mathbb{R}^3 (see Figure 2.1).

Note that, starting from a (2D) triangular configuration of oranges or cannonballs (see Figure 1.1a), one can stack additional layers of oranges in a triangular configuration on top, appropriately offset from the base layer, to build up the (3D) FCC configuration mentioned previously (see Figure 1.3a). This idea is referred to as lamination, and will be extended further in §2.6 when considering the Λ_n family of lattices.

Also note that, in the special case of $n = 2$, the A_2 lattice may also be written as

$$A_2 \cong R_2 \cup (\mathbf{a} + R_2), \quad \text{where} \quad \mathbf{a} = \begin{pmatrix} 1/2 \\ \sqrt{3}/2 \end{pmatrix} \quad (2.6c)$$

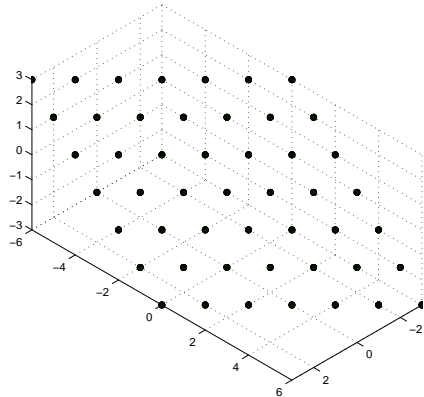


FIG. 2.1. A cloud of points on the A_2 lattice, defined on a plane in \mathbb{R}^3 . Note that the normal vector $\mathbf{n}_{A_2} = (1\ 1\ 1)^T$ points directly out of the page in this view.

and R_2 is the *rectangular grid* (not a lattice, nor even a nonlattice packing) obtained by stretching the \mathbb{Z}^2 lattice in the second element by a factor of $\sqrt{3}$.

The dual of the zero-sum lattice, denoted A_n^* , may be written as

$$A_n^* = \bigcup_{s=0}^n ([s] + A_n), \quad (2.7a)$$

where the $n+1$ coset representatives $[s]$, for $s = 0, \dots, n$, are defined such that the k 'th component of the vector $[s]$ is

$$[s]_k = \begin{cases} \frac{s}{n+1} & k \leq n+1-s, \\ \frac{s-n-1}{n+1} & \text{otherwise.} \end{cases} \quad (2.7b)$$

The A_n^* lattice may be constructed via integer linear combination of the columns of the $(n+1) \times n$ basis matrix

$$B_{A_n^*} = \begin{pmatrix} 1 & 1 & \cdots & 1 & \frac{-n}{n+1} \\ -1 & & & 0 & \frac{1}{n+1} \\ & -1 & & & \frac{1}{n+1} \\ & & \ddots & & \vdots \\ & & & -1 & \frac{1}{n+1} \\ 0 & & & & \frac{1}{n+1} \end{pmatrix}, \quad \text{with } \mathbf{n}_{A_n^*} = \mathbf{n}_{A_n}. \quad (2.7c)$$

A related family of lattice packings, developed in §12 of Coxeter (1951) and reasonably identified as the *glued zero-sum lattices* A_n^r , is a family of lattices somewhere between A_n and A_n^* [as given in (2.7a)] defined via the union of r translates of A_n for $n \geq 5$:

$$A_n^r = A_n \cup ([s] + A_n) \cup ([2s] + A_n) \cup \dots \cup [(r-1)s] + A_n, \quad \text{where } r \cdot s = n+1, \quad (2.8)$$

where the components of the “glue” vectors $[s]$ are specified in (2.7b), and where r and s are integer divisors of $(n+1)$ with $1 < s < n+1$ and $1 < r < n+1$, excluding the case $\{r=2, s=3\}$ for $n=5$. The lattices A_9^5 , A_{11}^4 , A_{13}^7 , A_{14}^5 , A_{15}^8 , A_{17}^9 , A_{19}^{10} , A_{20}^7 , and A_{21}^{11} are found to have especially good covering thickness, with the last four currently the thinnest coverings available in their respective dimensions (see Baranovskii 1994, Anzin 2002, and Sikirić, Schürmann, & Vallentin 2008). Note also that $A_7^2 \cong E_7$, $A_7^4 \cong E_7^*$, and $A_8^3 \cong E_8$, each of which is discussed further below.

Note finally that the contact graphs of some of the A_n^r lattices, such as A_9^5 and A_{11}^4 , are disjoint nets given by the contact graphs of the A_n and shifted A_n sets of lattice points upon which these glued zero-sum lattices are built [see (2.8)]. Thus, as in the case of D_n^* for $n > 4$ as discussed in §2.3, a *generalized net* may be formed by connecting each node of the unshifted A_n set to the nearest nodes on the shifted A_n set. Again, the resulting net is uninodal, but is not a contact graph of the corresponding sphere packing.

2.5. The Gosset lattice $E_8 \cong E_8^*$, E_7 , E_7^* , E_6 , and E_6^* . The Gosset lattice $E_8 \cong E_8^*$, which has a (remarkable) kissing number of $\tau = 240$, may be defined simply as

$$E_8 = D_8^+, \quad (2.9a)$$

and may be constructed via integer linear combination of the columns of the 8×8 basis matrix

$$B_{E_8} = \begin{pmatrix} 2 & -1 & & & & & 0 & 1/2 \\ & 1 & -1 & & & & & 1/2 \\ & & 1 & -1 & & & & 1/2 \\ & & & 1 & -1 & & & 1/2 \\ & & & & 1 & -1 & & -1/2 \\ & & & & & 1 & -1 & -1/2 \\ & & & & & & 1 & -1/2 \\ 0 & & & & & & & -1/2 \end{pmatrix}. \quad (2.9b)$$

The lattice E_7 is defined by restricting E_8 , as constructed above, to a 7-dimensional subspace,

$$E_7 = \{(x_1, \dots, x_8) \in E_8 : x_1 + \dots + x_8 = 0\}, \quad (2.10a)$$

and may be constructed directly via integer linear combination of the columns of the 8×7 basis matrix

$$B_{E_7} = \begin{pmatrix} -1 & & & & & & 0 & 1/2 \\ 1 & -1 & & & & & & 1/2 \\ & 1 & -1 & & & & & 1/2 \\ & & 1 & -1 & & & & 1/2 \\ & & & 1 & -1 & & & -1/2 \\ & & & & 1 & -1 & & -1/2 \\ & & & & & 1 & -1 & -1/2 \\ 0 & & & & & & 1 & -1/2 \\ & & & & & & & -1/2 \end{pmatrix}, \quad \text{with} \quad \mathbf{n}_{E_7} = \begin{pmatrix} 1/2 \\ 1/2 \\ 1/2 \\ 1/2 \\ 1/2 \\ 1/2 \\ 1/2 \\ 1/2 \end{pmatrix}. \quad (2.10b)$$

The dual of the E_7 lattice may be written as

$$E_7^* = E_7 \cup ([1] + E_7), \quad \text{where} \quad [1] = \begin{pmatrix} 1/4 \\ \vdots \\ 1/4 \\ -3/4 \\ -3/4 \end{pmatrix}, \quad (2.11a)$$

and may be constructed directly via integer linear combination of the columns of the 8×7 basis matrix

$$B_{E_7^*} = \begin{pmatrix} -1 & & & & & & 0 & -3/4 \\ 1 & -1 & & & & & & -3/4 \\ & 1 & -1 & & & & & 1/4 \\ & & 1 & -1 & & & & 1/4 \\ & & & 1 & -1 & & & 1/4 \\ & & & & 1 & -1 & & 1/4 \\ & & & & & 1 & & 1/4 \\ 0 & & & & & & & 1/4 \end{pmatrix}, \quad \text{with} \quad \mathbf{n}_{E_7^*} = \mathbf{n}_{E_7}. \quad (2.11b)$$

The lattice E_6 is defined by further restricting E_7 , as defined in (2.10), to a 6-dimensional subspace,

$$E_6 = \{(x_1, \dots, x_8) \in E_7 : x_1 + x_8 = 0\}, \quad (2.12a)$$

and may be constructed directly via integer linear combination of the columns of the 8×6 basis matrix

$$B_{E_6} = \begin{pmatrix} & & & & 0 & 1/2 \\ -1 & & & & & 1/2 \\ 1 & -1 & & & & 1/2 \\ & 1 & -1 & & & 1/2 \\ & & 1 & -1 & & -1/2 \\ & & & 1 & -1 & -1/2 \\ & & & & 1 & -1/2 \\ 0 & & & & & -1/2 \end{pmatrix}, \quad \text{with} \quad N_E = \begin{pmatrix} 1 & 1/2 \\ 0 & 1/2 \\ 0 & 1/2 \\ 0 & 1/2 \\ 0 & 1/2 \\ 0 & 1/2 \\ 0 & 1/2 \\ 1 & 1/2 \end{pmatrix} = \begin{pmatrix} | & | \\ \mathbf{n}_{E_6} & \mathbf{n}_{E_7} \\ | & | \end{pmatrix}. \quad (2.12b)$$

The dual of the E_6 lattice may be written as

$$E_6^* = E_6 \cup ([1] + E_6) \cup ([2] + E_6), \quad \text{where} \quad [1] = \begin{pmatrix} 0 \\ -2/3 \\ -2/3 \\ 1/4 \\ \vdots \\ 1/4 \\ 0 \end{pmatrix}, \quad [2] = -[1], \quad (2.13a)$$

and may be constructed directly via integer linear combination of the columns of the 8×6 basis matrix

$$B_{E_6^*} = \begin{pmatrix} & & & & 0 & 0 & 1/2 \\ -1 & & & & & 2/3 & 1/2 \\ 1 & -1 & & & & 2/3 & 1/2 \\ & 1 & -1 & & & -1/3 & 1/2 \\ & & 1 & -1 & & -1/3 & -1/2 \\ & & & 1 & -1 & -1/3 & -1/2 \\ & & & & 1 & -1/3 & -1/2 \\ 0 & & & & & -1/3 & -1/2 \\ & & & & & 0 & -1/2 \end{pmatrix}, \quad \text{with} \quad N_{E^*} = N_E. \quad (2.13b)$$

2.7. Some numerically-generated lattices for thin coverings in dimensions 6-15.

Recall from §2.1 that an n -dimensional real lattice may be defined as an integer linear combination of a set of n basis vectors \mathbf{b}^i defined in \mathbb{R}^{n+m} for $m \geq 0$; that is, any lattice point may be written as

$$\mathbf{x} = \xi_1 \mathbf{b}^1 + \xi_2 \mathbf{b}^2 + \dots + \xi_n \mathbf{b}^n = B \boldsymbol{\xi},$$

where the elements $\{\xi_1, \dots, \xi_n\}$ of the vector $\boldsymbol{\xi}$ are taken as integers. The square of the distance of any lattice point from the origin is thus given by $f(\boldsymbol{\xi}) = \boldsymbol{\xi}^T A \boldsymbol{\xi}$, where $A \triangleq B^T B$ is known as the *Gram matrix* associated with the lattice in question, and the function $f(\boldsymbol{\xi})$ is referred to as the corresponding *quadratic form* [note that each term of $f(\boldsymbol{\xi})$ is quadratic in the elements of $\boldsymbol{\xi}$]. All of the lattices studied thus far, when scaled appropriately, are characterized by Gram matrices with *integer elements*, and thus their corresponding quadratic forms $f(\boldsymbol{\xi})$ have integer coefficients (and are thus referred to as *integral quadratic forms*).

There is particular mathematical interest in discovering (or generating numerically) both lattice and non-lattice packings which minimize covering thickness and/or packing density. The numerical approach to this problem studied in Schürmann & Vallentin (2006) and Sikirić, Schürmann, & Vallentin (2008) has generated new lattices in dimensions 6-15 with the thinnest covering thicknesses known amongst all lattices. The lattice so generated in dimension 7 happens to correspond to an integral quadratic form, but the others, apparently, do not. Gram matrices A corresponding to these 10 lattices (denoted $L_6^c, L_7^c, L_8^c, \dots, L_{15}^c$) are available at http://fma2.math.uni-magdeburg.de/~latgeo/covering_table.html; (nonunique) basis matrices B corresponding to each of these lattices may be generated simply by taking the Cholesky decomposition of the corresponding Gram matrix, as $A = B^T B$.

2.8. Discussion. For all of the dense lattices described thus far, as well as for the rare packings and nets described in §3, Tables 2-3 list the known values of the packing density Δ , the covering thickness Θ , and the mean squared quantization error per dimension, G . Table 2 also lists the coordination sequence through $k = 10$ of the corresponding net, as well as its local topological density td_{10} . If this net is a contact graph, the coordination number (that is, the first element of the coordination sequence) is equal to the kissing number of the corresponding packing; if this net is *not* a contact graph, it is marked with a **G**, and the kissing number τ of the corresponding sphere packing is listed in parentheses.

The other information appearing in Table 2 is described further in §3. Note that Table 2 alone has 8 columns and over 100 rows, with those results which we believe to be new denoted in italics. The original source of each of the several hundred existing results reported can not feasibly be spelled out here. Suffice it to say that the vast majority of those existing results related to lattices are discussed in Conway & Sloane (1998) and in the On-Line Encyclopedia of Integer Sequences (on the web at <http://www.research.att.com/~njas/sequences/>), where a large number of the original references are listed in detail. The vast majority of those existing results related to 3D nets (see §3), *including clear drawings of each* as well as detailed lists of original references, are given in the Reticular Chemistry Structure Resource, available online at, e.g., <http://rcsr.anu.edu.au/nets/fcu>, where “fcu” may be replaced by any of the lowercase boldface three-letter identifiers given in Table 2 and §3; for further discussion of this database and others, see O’Keeffe et al. (2008), Treacy et al. (2004), Blatov (2006), and Hyde et al. (2006). Note also that there are hundreds of new results reported in Tables 2 and 3, as denoted in italics; most of these are the result of painstaking numerical simulation, some of which took weeks of CPU time (on a quad-core 3GHz Intel Xeon server) to complete.

Note finally that there are a variety of (lattice-specific) ways to quantize to the nearest lattice point; for an introduction, see §5.

n	packing	net	Δ	Θ	G	coordination sequence (through $k = 10$)	td_{10}	point symbol vertex symbol	
1	\mathbb{Z}, Λ_1	integer	<u>1</u>	<u>1</u>	<u>0.083333</u>	<u>2</u> , 2, 2, 2, 2, 2, 2, 2, 2	21	*	
2	A_2, A_2^*, Λ_2	triangular	<u>0.90690</u>	<u>1.2092</u>	<u>0.080188</u>	<u>6</u> , 12, 18, 24, 30, 36, 42, 48, 54, 60	331	$3^6.4^6.5^3$	
	$\mathbb{Z}^2, D_2, D_2^+, D_2^{++}$	square	0.78540	1.5708	0.083333	4, 8, 12, 16, 20, 24, 28, 32, 36, 40	221	4.4.4.4.*.*	
	$A_2^+, {}^T A_2^*$	honeycomb	0.60460	2.4184	0.09623	3, 6, 9, 12, 15, 18, 21, 24, 27, 30	166	6.6.6	
	$\hat{A}_2^+, {}^T \hat{A}_2^*$	augmented honeycomb	0.39067	5.832	0.1652	3, 4, 6, 8, 12, 14, 15, 18, 21, 22	124	3.12.12	
3	D_3, A_3, Λ_3	fcu	<u>0.74048</u>	2.0944	0.078745	<u>12</u> , 42, 92, 162, 252, 362, 492, 642, 812, 1002	3871	$3^{24}.4^{36}.5^6$	
		hcp	<u>0.74048</u>	2.0944	0.078745	<u>12</u> , 44, 96, 170, 264, 380, 516, 674, 852, 1052	4061	$3^{24}.4^{33}.5^9$	
	D_3^+, A_3^+	bcu	0.68017	<u>1.4635</u>	<u>0.078543</u>	8, 26, 56, 98, 152, 218, 296, 386, 488, 602	2331	$4^{24}.6^4$	
	\mathbb{Z}^3	pcu	0.52360	2.7207	0.083333	6, 18, 38, 66, 102, 146, 198, 258, 326, 402	1561	$4^{12}.6^3$	
		qtz , V_3^{60}	0.39270	2.0405	0.08534	4, 12, 30, 52, 80, 116, 156, 204, 258, 318	1231	6.6.6 ₂ .6 ₂ .8 ₇ .8 ₇	
	A_3^+, D_3^+	dia , V_3^{90}	0.34009	2.7207	0.09114	4, 12, 24, 42, 64, 92, 124, 162, 204, 252	981	6 ₂ .6 ₂ .6 ₂ .6 ₂ .6 ₂ .6 ₂	
		lon	0.34009	3.3068	0.09139	4, 12, 25, 44, 67, 96, 130, 170, 214, 264	1027	6 ₂ .6 ₂ .6 ₂ .6 ₂ .6 ₂ .6 ₂	
		sod	0.2777	8.781	0.1092	4, 10, 20, 34, 52, 74, 100, 130, 164, 202	791	4.4.6.6.6.6	
		\hat{A}_3^+	dia-a	0.12354	9.1723	0.1511	4, 6, 12, 18, 36, 48, 60, 78, 108, 126	497	3.12 ₂ .3.12 ₂ .3.12 ₂
		${}^T \hat{A}_3^*$	sod-a	0.1033	28.26	0.1943	4, 6, 12, 17, 28, 38, 52, 64, 84, 104	410	3.8.3.12.3.12
		(unstable)	qzd , T_3^{60}	0.6046	2.1549	0.08151	G : 4, 12, 36, 72, 122, 188, 264, 354, 456, 570 ($\tau = 8$)	2079	$7_2.*.7_3.7_3.7_3.7_3$
			cds , T_3^{90}	0.52360	2.7207	0.08333	G : 4, 12, 30, 58, 94, 138, 190, 250, 318, 394 ($\tau = 6$)	1489	6.6.6.6.6 ₂ .*
			nbo , S_3	0.39270	3.1416	0.08602	4, 12, 28, 50, 76, 110, 148, 194, 244, 302	1169	6 ₂ .6 ₂ .6 ₂ .6 ₂ .8 ₂ .8 ₂
			bto ($\alpha = 60^\circ$), Y_3^{60} ($\alpha \approx 70.5^\circ$)	0.2687 0.2551	3.0042 2.7251	0.09129 0.09217	3, 6, 12, 24, 43, 64, 91, 124, 160, 202	730	10.10 ₂ .10 ₂
			ths ($\alpha = 60^\circ$), Y_3^{90} ($\alpha \approx 70.5^\circ$)	0.2327 0.2207	4.3099 3.518	0.09706 0.09817			
			srs	0.1851	3.4281	0.1072	3, 6, 12, 24, 35, 48, 69, 86, 108, 138	530	10 ₅ .10 ₅ .10 ₅
	srs-a		0.0555	9.739	0.1882	3, 4, 6, 8, 12, 16, 24, 32, 48, 54	208	3.20 ₅ .20 ₅	

Table 2a. (Continued on next page.)

4	D_4, D_4^*, Λ_4	0.61685	2.4674	0.076603	<u>24</u> , 144, 456, 1056, 2040, 3504, 5544, 8256, 11736, 16080 G : 16, 80, 240, 544, 1040, 1776, 2800, 4160, 5904, 8080 ($\tau = 24$)	48,841	$3^{96} .4^{168} .5^{12}$	
	A_4	0.55173	3.1780	0.078020	20, 110, 340, 780, 1500, 2570, 4060, 6040, 8580, 11750	35,751	$4^{112} .6^8$	
	A_4^+	0.44138	1.7655	0.077559	10, 50, 150, 340, 650, 1110, 1750, 2600, 3690, 5050	15,401	$4^{40} .6^5$	
	\mathbb{Z}^4, D_4^+	0.30843	4.9348	0.08333	8, 32, 88, 192, 360, 608, 952, 1408, 1992, 2720	8361	$4^{24} .6^4$	
	A_4^+	0.17655	6.3558	0.08827	5, 20, 50, 110, 200, 340, 525, 780, 1095, 1500	4626	6^{10}	
	${}^T A_4^*$	0.10593	42.4	0.1221	5, 15, 35, 70, 125, 205, 315, 460, 645, 875	2751	$4^5 .6^5$	
	\hat{A}_4^+	0.03354	23.82	0.1398	5, 8, 20, 32, 80, 116, 170, 236, 380, 482	1530	$3^6 .12^4$	
	(unstable)	T_4^{90}	0.3084	4.935	0.08333	G : 4, 12, 36, 92, 200, 384, 664, 1056, 1576, 2240 ($\tau = 8$)	6265	$8_3 .8_3 .8_3 .8_3 .8_4 .*$
		S_4	0.1542	3.855	0.08692	4, 12, 36, 84, 172, 292, 468, 692, 988, 1348	4097	$8_2 .8_2 .8_5 .8_5 .8_5 .8_5$
		V_4^{90}	0.1187	5.814	0.09333	4, 12, 36, 74, 136, 228, 352, 518, 732, 994	3087	$8_6 .8_6 .8_7 .8_7 .8_7 .8_7$
Y_4^{90}		0.06793	6.458	0.09736	3, 6, 12, 24, 48, 90, 146, 230, 336, 478	1374	$12_2 .12_2 .12_2$	
5	D_5, Λ_5	0.46526	4.5977	0.075786	<u>40</u> , 370, 1640, 4930, 11752, 24050, 44200, 75010, 119720, 182002	463,715	$3^{240} .4^{520} .5^{20}$	
	A_5	0.37988	5.9218	0.077647	30, 240, 1010, 2970, 7002, 14240, 26070, 44130, 70310, 106752	272,755	$3^{120} .4^{300} .5^{15}$	
	D_5^*	0.32899	2.4982	0.075625	G : 32, 242, 992, 2882, 6752, 13682, 24992, 42242, 67232, 102002 ($\tau = 10$)	261,051	$4^{480} .6^{16}$	
	D_5^+	0.28736	5.2638	0.07784	16, 120, 480, 1410, 3296, 6712, 12256, 20770, 33056, 50232	128,349	$4^{80} .6^{40}$	
	A_5^*	0.25543	2.1243	0.076922	12, 72, 272, 762, 1752, 3512, 6372, 10722, 17012, 25752	66,241	$4^{60} .6^6$	
	\mathbb{Z}^5	0.16449	9.1955	0.083333	10, 50, 170, 450, 1002, 1970, 3530, 5890, 9290, 14002	36,365	$4^{40} .6^5$	
	A_5^+	0.08514	8.8223	0.08646	6, 30, 90, 240, 510, 1010, 1770, 2970, 4626, 7002	18,255	6^{15}	
	${}^T A_5^*$	0.035174	254.9	0.1349	6, 21, 56, 126, 252, 461, 786, 1266, 1946, 2877	7798	$4^9 .6^6$	
	\hat{A}_5^+	0.008055	35.81	0.1313	6, 10, 30, 50, 150, 230, 390, 570, 1050, 1420	3907	$3^{10} .12^5$	
	(unstable)	T_5^{90}	0.16449	9.1955	0.08333	G : 4, 12, 36, 100, 258, 610, ? ($\tau = 10$)	?	$8_2 .8_2 .8_2 .8_2 .10_6 .*$
		S_5	0.05140	9.310	0.08666	4, 12, 36, 100, 244, 514, 980, 1682, 2724, 4162	10,459	$8 .8 .8 .8 .8_2 .8_2$
		V_5^{60}	0.04786	8.4884	0.08753	4, 12, 36, 100, 248, 522, 988, 1724, 2800, 4324	10,759	$8 .8 .8 .8 .8_2 .8_2$
		Y_5^{60}	0.03516	254.8	0.1350	3, 6, 12, 24, 48, 90, 168, 312, 556, 914	2134	$12_2 .12_2 .12_2$
		T_5^{60}	0.02478	6.2578	0.09038	G : 4, 12, 36, 100, 268, ? ($\tau = 14$)	?	$8_2 .8_2 .8_2 .8_2 .11_{10} .*$
V_5^{90}		0.02478	6.016	0.09037	4, 12, 36, 100, 220, 428, 752, 1254, 1944, 2924	7675	$8 .8 .8 .8 .8_2 .8_2$	
Y_5^{90}		0.01858	11.19	0.09605	3, 6, 12, 24, 48, 90, 168, 312, 532, 872	2068	$12_2 .12_2 .12_2$	

Table 2b. (Continued on next page.)

n	packing	net	Δ	Θ	G	coordination sequence (through $k = 10$)	td_{10}	point symbol vertex symbol	
6	E_6, Λ_6		0.37295	7.0722	0.074347	72 , 1062, 6696, 26316, 77688, 189810, 405720, 785304, 1408104	2,900,773	$3^{720}.4^{1800}.5^{36}$	
	E_6^*		0.33151	2.6521	0.074244	54, 828, 5202, 20376, 60030, 146484, 312858, 605232, 1084806, 1830060	4,065,931	$3^{270}.4^{1134}.5^{27}$	
	D_6		0.32298	8.7205	0.075591	60, 792, 4724, 18096, 52716, 127816, 271908, 524640, 938652, 1581432	3,520,837	$3^{480}.4^{1260}.5^{30}$	
	D_6^+		0.27252	5.1677	0.07459	32, 332, 1824, 6776, 19488, 46980, 99680, 192112, 343584, 578876	1,289,685	$4^{480}.6^{16}$	
	A_6		0.24415	9.8401	0.077466	42, 462, 2562, 9492, 27174, 65226, 137886, 264936, 472626, 794598	1,775,005	$3^{210}.4^{630}.5^{21}$	
	D_6^*		0.16149	4.3603	0.075120	G : 64, 728, 4032, 14896, 42560, 102024, 215488, 413792, 737856, 1240120 ($\tau = 12$)	244,069	$4^{1984}.6^{32}$	
	A_6^*		0.13453	2.5511	0.076490	14, 98, 462, 1596, 4410, 10374, 21658, 41272, 73206, 122570	275,661	$4^{84}.6^7$	
	L_6^c		0.31853	2.4648	?	32, ?	?	?	
	\mathbb{Z}^6		0.08075	17.441	0.08333	12, 72, 292, 912, 2364, 5336, 10836, 20256, 35436, 58728	134,245	$4^{60}.6^6$	
	A_6^+		0.03844	19.681	0.08525	7, 42, 147, 462, 1127, 2562, 5047, 9492, 16317, 27174	62,378	6^{21}	
	\overline{A}_6^*		0.010459	1836.5	0.14712	7, 28, 84, 210, 462, 924, 1715, 2996, 4977, 7924	19,328	$4^{14}.6^7$	
	\hat{A}_6^+		0.001774	99.91	0.1259	7, 12, 42, 72, 252, 402, 777, 1182, 2457, 3492	6,496	$3^{15}.12^6$	
	(unstable)	T_6^{90}		0.08075	17.441	0.08333	G : 4, 12, 36, 100, ? ($\tau = 12$)	?	?
		S_6		0.01514	9.78	0.08601	4, 12, 36, 100, 276, 660, 1484, 2920, ?	?	8.8.8.8.8 ₂ .8 ₂
V_6^{90}			9.740e-3	19.79	0.09322	4, 12, 36, 100, 276, 610, 1284, 2346, 4152, 6792	15,613	8.8.8.8.8 ₂ .8 ₂	
Y_6^{90}			4.640e-3	24.15	0.09479	3, 6, 12, 24, 48, 90, 168, 312, 580, 1046	2290	12 ₂ .12 ₂ .12 ₂	
7	E_7, Λ_7		0.29530	13.810	0.073231	126 , 2898, 25886, 133506, 490014, 1433810, 3573054, 7902594, 15942206, 29896146	59,400,241	$3^{2016}.4^{5796}.5^{63}$	
	D_7^+		0.26170	4.7248	0.07273	64, 1092, 8064, 37842, 131328, 371940, 906816, 1976898, 3946048, 7344164	14,724,257	$4^{1792}.6^{224}$	
	E_7^*		0.21578	4.1872	0.073116	56, 938, 7688, 39746, 150248, 455114, 1171928, 2668610, 5521880, 10585514	20,601,723	$4^{1512}.6^{28}$	
	D_7		0.20881	16.749	0.075686	84, 1498, 11620, 55650, 195972, 559258, 1371316, 2999682, 6003956, 11193882	22,392,919	$3^{840}.4^{2604}.5^{42}$	
	A_7		0.14765	18.899	0.077396	56, 812, 5768, 26474, 91112, 256508, 623576, 1356194, 2703512, 5025692	10,089,705	$3^{336}.4^{1176}.5^{28}$	
	D_7^*		0.07382	4.5687	0.07493	G : 128, 2186, 16256, 75938, 263552, 745418, 1817216, 3959426, 7902848, 14704202 ($\tau = 14$)	29,487,171	$4^{8064}.6^{64}$	
	A_7^*		0.06542	3.0596	0.076187	16, 128, 688, 2746, 8752, 23536, 55568, 118498, 232976, 428752	871,661	$4^{112}.6^8$	
	L_7^c		0.11738	2.9000	?	?	?	?	
	\mathbb{Z}^7		0.03691	33.498	0.083333	14, 98, 462, 1666, 4942, 12642, 28814, 59906, 115598, 209762	433,905	$4^{84}.6^7$	
	A_7^+		0.01636	30.163	0.08442	8, 56, 224, 812, 2240, 5768, 12656, 26474, 49952, 91112	189,303	6^{28}	
	\overline{A}_7^*		2.839e-3	?	?	8, 36, 120, 330, 792, 1716, 3432, 6434, 11432, 19412	43,713	$4^{20}.6^8$	
	\hat{A}_7^+		3.586e-4	137.9	0.1214	8, 14, 56, 98, 392, 644, 1400, 2198, 5096, 7532	17,439	$3^{21}.12^7$	

Table 2c. (Continued on next page.)

7 (unstable)	T_7^{60}	0.05673	15.87	0.08076	G : 4, 12, 36, 100, 276, ? ($\tau = 20$)	?	?	
	T_7^{90}	0.03691	33.50	0.08333	G : 4, 12, 36, 100, 276, ? ($\tau = 14$)	?	?	
	S_7	4.035e-3	24.15	0.08525	4, 12, 36, 100, 276, ?	?	?	
	V_7^{60}	3.730e-3	15.00	0.08702	4, 12, 36, 100, 276, ?	?	?	
	V_7^{90}	2.424e-3	32.39	0.09267	4, 12, 36, 100, 276, 724, 1676, 3592, 7012, 12868	26,301	8.8.8.8.8 ₂ .8 ₂	
	Y_7^{60}	1.652e-3	18.95	0.08854	3, 6, 12, 24, 48, ?	?	?	
	Y_7^{90}	1.074e-3	36.73	0.09365	3, 6, 12, 24, 48, 90, 168, 312, 580, 1046	2290	12 ₂ .12 ₂ .12 ₂	
8	$E_8, E_8^*, D_8^+, \Lambda_8$	<u>0.25367</u>	4.0587	0.071682	240 , 9120, 121680, 864960, 4113840, 14905440, 44480400, 114879360, 265422960, 561403680	1,006,201,681	3 ⁶⁷²⁰ .4 ²¹⁸⁴⁰ .5 ¹²⁰	
	D_8	0.12683	32.470	0.075914	112, 2592, 25424, 149568, 629808, 2100832, 5910288, 14610560, 32641008, 67232416	123,302,609	3 ¹³⁴⁴ .4 ⁴⁸¹⁶ .5 ⁵⁶	
	A_8	0.08456	32.993	0.077391	72, 1332, 11832, 66222, 271224, 889716, 2476296, 6077196, 13507416, 27717948	51,019,255	3 ⁵⁰⁴ .4 ²⁰¹⁶ .5 ³⁶	
	D_8^*	0.03171	8.1174	0.074735	G : 256, 6560, 65280, 384064, 1614080, 5374176, 15097600, 37281920, 83222784, 171312160 ($\tau = 16$)	314,358,881	4 ³²⁵¹² .6 ¹²⁸	
	A_8^*	0.02969	3.6658	0.075972	18, 162, 978, 4482, 16722, 53154, 148626, 374274, 864146, 1854882	3,317,445	4 ¹⁴⁴ .6 ⁹	
	L_8^c	0.08253	3.1422	?	?	?	?	
	\mathbb{Z}^8	0.01585	64.939	0.083333	16, 128, 688, 2816, 9424, 27008, 68464, 157184, 332688, 658048	1,256,465	4 ¹¹² .6 ⁸	
	A_8^+	6.599e-3	65.99	0.0838	9, 72, 324, 1332, 4104, 11832, 28674, 66222, 136404, 271224	520,198	6 ³⁶	
	$^T A_8^*$	7.128e-4	?	?	9, 45, 165, 495, 1287, 3003, 6435, 12870, 24309, 43749	92,368	4 ²⁷ .6 ⁹	
	\hat{A}_8^+	6.759e-5	301.1	0.1178	9, 16, 72, 128, 576, 968, 2340, 3768, 9648, 14716	32,242	3 ²⁸ .12 ⁸	
	(unstable)	T_8^{90}	0.01585	64.94	0.08333	G : 4, 12, 36, 100, 276, 724, ? ($\tau = 16$)	?	?
		S_8	9.903e-4	28.28	0.08452	4, 12, 36, 100, 276, 724, ?	?	?
		V_8^{90}	5.590e-4	49.89	0.09206	4, 12, 36, 100, 276, 724, 1908, 4390, 9876, 19682	37,009	8.8.8.8.8 ₂ .8 ₂
Y_8^{90}		2.327e-4	87.31	0.09266	3, 6, 12, 24, 48, 90, 168, 312, 580, 1046	2290	12 ₂ .12 ₂ .12 ₂	

Table 2d. (Continued from previous pages.) Characteristics of some exemplary lattice and uninodal nonlattice packings and nets through $n = 8$, ordered from dense to rare in each section. Values in italics are (as far as we know) new. At each n , bold double underlined values are proven to be optimal (maximum or minimum) amongst all packings, and bold single underlined values are proven to be optimal amongst all lattices. Bold values (without underlines) are the best known values amongst all packings, and bold undertilded values are the best known values amongst all lattices. The point symbol is provided for those nets with $\tau \geq 5$; the vertex symbol is provided for those nets with $\tau \leq 4$. Nets whose coordination sequences are identified with a **G** are generalized nets, not contact graphs (see, e.g., the second-to-last paragraph of §2.3); in these cases, the kissing number τ is indicated in parentheses after the coordination sequence. In all other cases, the first element of the coordination sequence is the kissing number τ . Note also that the Y_n^{90} and Y_n^{60} nets are constructed with $\alpha = \cos^{-1}(1/n)$ for $n \geq 3$ (see §3.4.5); in addition, the barycentric constructions with $\alpha = 60$, corresponding to **bto** and **ths**, are also listed for $n = 3$.

n	packing	Δ	Θ	G	τ
9	Λ_9	0.14577	9.0035	<i>0.07206</i>	272
	D_9^+	0.14577	4.3331	0.07110	144
	D_9^*	0.01288	8.6662	0.07469	18
	A_9^*	0.01268	4.3889	0.07582	20
	A_9^5	<i>0.08447</i>	4.3402	<i>0.07207</i>	90
	L_9^c	<i>0.08149</i>	4.2686	?	?
	\mathbb{Z}^9	0.006442	126.81	0.08333	18
10	Λ_{10}	0.09202	12.409	<i>0.07150</i>	336
	D_{10}^+	0.07969	7.7825	0.07081	180
	A_{10}^*	0.005128	5.2517	0.07570	22
	L_{10}^c	<i>0.02995</i>	5.1545	?	?
	\mathbb{Z}^{10}	0.002490	249.04	0.08333	20
11	K_{11}	0.06043	?	?	432
	Λ_{11}^{\max}	0.05888	24.781	<i>0.07116</i>	438
	D_{11}^+	0.04163	8.4072	?	220
	A_{11}^*	0.001974	6.2813	0.07562	24
	A_{11}^4	<i>0.04740</i>	5.5983	<i>0.07025</i>	132
	L_{11}^c	<i>0.04124</i>	5.5056	?	?
	\mathbb{Z}^{11}	9.200e-4	491.40	0.08333	22
12	K_{12}, K_{12}^*	0.04945	17.783	0.07010	756
	Λ_{12}^{\max}	0.04173	30.419	<i>0.07058</i>	648
	D_{12}^+	0.02086	15.209	?	264
	A_{12}^*	7.271e-4	7.5101	0.07557	26
	L_{12}^c	<i>0.004306</i>	7.4655	?	?
	\mathbb{Z}^{12}	3.260e-4	973.41	0.08333	24
13	K_{13}	0.02921	?	?	918
	Λ_{13}^{\max}	0.02846	60.455	<i>0.07009</i>	906
	A_{13}^*	2.569e-4	8.9768	0.07553	28
	A_{13}^7	?	7.8641	?	368
	L_{13}^c	<i>0.002255</i>	7.7621	?	?
	\mathbb{Z}^{13}	1.112e-4	1934.6	0.08333	26
14	Λ_{14}	0.02162	98.876	<i>0.06946</i>	1422
	A_{14}^*	8.740e-5	10.727	0.07551	30
	A_{14}^5	?	9.0066	?	?
	L_{14}^c	<i>0.005221</i>	8.8252	?	?
	\mathbb{Z}^{14}	3.658e-5	3855.6	0.08333	28
15	Λ_{15}	0.01686	202.91	<i>0.06892</i>	2340
	A_{15}^*	2.870e-5	12.817	0.07549	32
	A_{15}^8	?	11.602	?	?
	L_{15}^c	<i>6.206e-5</i>	11.005	?	?
	\mathbb{Z}^{15}	1.164e-5	7703.1	0.08333	30

Table 3a. (Continued on next page.)

n	packing	Δ	Θ	G	τ
16	$\Lambda_{16}, \Lambda_{16}^*$	0.01471	96.500	0.06830	4320
	A_{16}^*	9.116e-6	15.311	0.07549	34
	\mathbb{Z}^{16}	3.591e-6	15,422	0.08333	32
17	Λ_{17}	0.008811	197.72	0.06822	5346
	A_{17}^*	2.807e-6	18.288	0.07549	36
	A_{17}^9	?	12.357	?	?
	\mathbb{Z}^{17}	1.076e-6	30,936	0.08333	34
18	Λ_{18}	0.005928	301.19	0.06792	7398
	A_{18}^*	8.396e-7	21.841	0.07550	38
	\mathbb{Z}^{18}	3.134e-7	62,158	0.08333	36
19	Λ_{19}	0.004121	607.62	0.06767	10668
	A_{19}^*	2.443e-7	26.082	0.07552	40
	A_{19}^{10}	?	21.229	?	?
	\mathbb{Z}^{19}	8.892e-8	125,077	0.08333	38
20	Λ_{20}	0.003226	889.86	0.06731	17400
	A_{20}^*	6.924e-8	31.143	0.07553	42
	A_{20}^7	?	20.367	?	?
	\mathbb{Z}^{20}	2.461e-8	252,020	0.08333	40
21	Λ_{21}	0.002466	1839.5	0.06701	27720
	A_{21}^*	1.914e-9	37.185	0.07555	44
	A_{21}^{11}	?	27.773	?	?
	\mathbb{Z}^{21}	6.651e-9	508,417	0.08333	42
22	Λ_{22}	0.002128	≤ 3426.8	?	49896
	Λ_{22}^*	2.952e-4	≤ 27.884	?	1782
	A_{22}^*	5.168e-10	44.395	0.07558	46
	\mathbb{Z}^{22}	1.757e-9	1,026,792	0.08333	44
23	Λ_{23}	0.001905	≤ 7609.0	?	93150
	Λ_{23}^*	2.788e-4	≤ 15.322	?	4600
	A_{23}^*	1.364e-10	53.000	0.07560	48
	\mathbb{Z}^{23}	4.543e-10	2,075,774	0.08333	46
24	$\Lambda_{24}, \Lambda_{24}^*$	0.001930	7.9035	0.06577	<u>196560</u>
	A_{24}^*	3.523e-11	63.269	0.07563	50
	\mathbb{Z}^{24}	1.150e-10	4,200,263	0.08333	48

Table 3b. (Continued from previous page.) Characteristics of some exemplary dense lattices for $n = 9$ to 24, with \leq denoting a bound, not an exact value; see Table 2 legend for description of notation. Note that the covering radii of Λ_{13} through Λ_{15} and Λ_{17} through Λ_{21} are, respectively, $\{\sqrt{26}, \sqrt{80/3}, \sqrt{28}\}$ and $\{\sqrt{26}, \sqrt{80/3}, \sqrt{28}, \sqrt{28}, \sqrt{29}\}$ (this was verified numerically in the present work; lower bounds on these values, which turn out to be sharp, are given in Conway & Sloane 1998).

3. Rare nonlattice packings and nets for $n \leq 8$. We now turn our attention to the problem of infinite *rare* sphere packings, with packing density *lower* than that of the corresponding Cartesian packing, and the closely related problem of infinite nets. For $n = 2$, this problem is essentially trivial. For $n = 3$, the richness of solutions to this problem is fascinating and, due to the intense interest in crystallographic structures with various desirable chemical properties, has been exhaustively studied and catalogued. For $n > 3$, relatively few regular constructions are known, and it appears as if what academic interest there has been has not yet led to any applications of significance in science and engineering; Part III of this work intends to change this, thus motivating the present study.

Interest in n -dimensional space groups and symmetries dates back to the nineteenth century, with the work of Hessel, Bravais, Gadolin, Frankenheim, Barlow, Rodrigues, Möbius, Jordan, Sohncke, Fedorov, Schönflies, Fricke, and Klein. Historical accounts of this early work, as well as several follow-on mathematical developments related to space groups and symmetries, are available in Brown et al. (1978) and Schwarzenberger (1980). Much of the related work in the field of geometry was developed by Coxeter (1970, 1973, 1974, 1987, 1989). Despite this intense interest, there are very few explicit constructions of regular rare sphere packings for $n > 3$ available today, outside of very short treatments of the subject by O’Keeffe (1991b) and Beukemann & Klee (1992), discussed below.

As mentioned in the abstract and explored in depth in Part III, certain emerging engineering applications now motivate the further development and deployment of quasi-infinite n -dimensional nets, with a particular focus on structured nets with low coordination number and high topological density. Such nets are well suited for the rapid spread of information in switchless computational interconnect systems with a reduced number of wires and, thus, reduced cost. In such systems, a logical network with $n > 3$ may easily be designed and built¹³ and, as we will see, there are significant potential benefits for so doing. We are thus motivated to revisit the problem of the design of structured nets with low coordination number. Note that none of the lattice alternatives to the Cartesian lattice discussed in §2 have a coordination number lower than that of the corresponding Cartesian lattice, $\tau = 2n$. However, for $n = 3$, there is a wide range of stable and unstable nonlattice packings that lead to such nets; as shown below, many of these packings and nets generalize naturally to higher dimensions.

3.1. Net terminology. The terminology used to discuss 3D nets, most of which generalizes readily to the discussion of n -dimensional nets, has been clarified significantly over the last decade, and is now quite precise.

Recall first the measures defined in §1, including the *coordination number*, the *coordination sequence*, and a k -hop measure of *local topological density* given by the cumulative sum of all nodes reached within k hops from origin, denoted td_k (Tables 1 and 2 list this quantity for $k = 10$). O’Keeffe (1991a) defines another, sometimes preferred (see, e.g., Grosse-Kunstleve et al. 1996) measure of *global topological density*, $td = \lim_{k \rightarrow \infty} td_k/k^n$, which reveals the rate of growth of td_k with k in the limit of large k . [For a uninodal n -dimensional net, td may be found by representing¹⁴ the coordination sequence as an $(n - 1)$ ’th-order polynomial in the number of hops k , then taking the leading coefficient of this polynomial and dividing by n .] Despite some impressive efforts in representing coordination sequences with such polynomials (see, e.g., Conway & Sloane 1997, and the references contained therein), the measure td is currently unknown for most of the nets discussed here. As a matter of computational tractability, we thus resort in the present paper to the tabulation of the local topological density measure, td_{10} , as this measure is much easier to compute.

¹³Recall, e.g., the “hypercube” computational interconnect system introduced several years ago; though designed with a logical network with $n > 3$, the hypercube, like most computational interconnect strategies deployed today, is significantly hampered by its inherent dependence on a Cartesian topology.

¹⁴Or by *approximating* this coordination sequence as an $(n - 1)$ ’th-order polynomial for large k , if such a polynomial does not fit exactly.

Our attention in this paper is focused almost exclusively on *equilibrium packings* (that is, on sphere packings which, if unperturbed, can bear compressive loads applied at the edges of a packing that is built out to fill a finite convex domain) and their corresponding *equilibrium nets* (which are constructed with tensile members connecting nearest-neighbor nodes, and can bear tensile loads applied at the edges of a finite convex domain)^{15,16}. Equilibrium packings fall into two categories: stable (that is, sphere packings which, if perturbed, oscillate about their equilibrium configurations, and return to these configurations if there is damping present in the system) and unstable (that is, sphere packings which depart from equilibrium if perturbed); we consider both.

After years of conflicting terminology in the literature on nets, the concepts of *cycles*, *rings*, *strong rings*, *tilings*, *natural tilings*, *point symbols*, and *vertex symbols* have, in 3D, finally crystallized. The reader is referred to Blatov et al. (2009) and the references contained therein for description of this modern terminology, as well as numerous cautions concerning the conflicting nomenclatures adopted elsewhere in the published literature. In short:

- A *cycle* is a sequence of nodes in a net, connected by edges, such that the first and last nodes of the sequence coincide, while none of the other nodes in the sequence appears more than once.
- A *cycle sum*, of cycles A and B, is the union of those edges in either A or B but not both.
- A *ring* is a cycle that is not the sum of two smaller cycles.
- A *strong ring* is a cycle that is not the sum of any number of smaller cycles.
- A *tiling* of \mathbb{R}^3 by a 3D net is simply the dissection of 3D space into volumes whose faces, which in general may be curved (as *minimal surfaces*, like soap bubbles; see, e.g., Sadoc & Rivier 1999), are bounded by cycles of the net. A 3D net generally admits many tilings.
- The *dual* of a tiling is the unique new tiling obtained by placing a new vertex inside each original tile and connecting the vertices of adjacent tiles (that is, with shared faces) in the original tiling with edges. If a tiling and its dual are identical, the tiling is said to be *self-dual*. The dual of a dual is the original tiling.
- A *natural tiling* of \mathbb{R}^3 by a 3D net is a tiling with the smallest possible tiles such that the tiles have the maximum combinatorial symmetry and all the faces of the tiles are strong rings. A 3D net often¹⁷ admits a unique natural tiling. If a tiling and its dual are both natural, the pair is referred to as *natural duals*. If a natural tiling is self-dual, it is said to be *naturally self-dual*.
- The *point symbol* of a uninodal net, of the form $A^a.B^b.C^c \dots$, indicates that there are a pairs of edges touching the node at the origin with shortest cycles of length A , b pairs of edges touching the node at the origin with shortest cycles of length B (with $B > A$), etc. Note that the sum of the superscripts in a point symbol totals $\tau(\tau - 1)/2$.
- The *vertex symbol* of a uninodal net, of the form $A_a.B_b.C_c \dots$, indicates that the first pair of edges touching the node at the origin has a shortest rings of length A , the second pair of edges touching the node at the origin has b shortest rings of length B , etc. If for any entry there is only 1 such shortest ring, the subscript is suppressed; if for any entry there is no ring, a subscript $*$ is used. The entries are sorted such that smaller rings are listed first, and when two rings of the same size appear, the entry with the smaller subscript is listed first. In the special case of $\tau = 4$, the six entries of the vertex symbol are listed as three

¹⁵A family of structures with both tensile and compressive members, known as *tensegrity*, might be said to cover the gap between purely compressive sphere packings and purely tensile nets. The mathematical characterization of tensegrity systems in 3D is now precise, due largely to the work of Skelton & de Oliveira (2009). An interesting extension of the present study would be to generalize such tensegrity systems to $n > 3$ dimensions.

¹⁶For the purpose of the applications studied in Parts II and III, we do not actually use the property of mechanical equilibrium of the corresponding structure; this property may rather be considered as a convenient means to an end when designing a regular packing or net. Several nets discussed in the literature (see, e.g., Wells 1977, page 80) are not equilibrium sphere packings, and might be interesting to consider further.

¹⁷Unfortunately, not all 3D nets have natural tilings, and some have multiple natural tilings; §3 of Blatov et al. (2007) discusses this issue further.

pairs of entries, with each pair of entries corresponding to opposite pairs of edges, and are otherwise again sorted from smallest to largest. Note that the number of entries in a vertex symbol is $\tau(\tau - 1)/2$.

The concepts of *cycles*, *rings*, *strong rings*, *point symbols*, and *vertex symbols* extend immediately to n dimensions; for practical considerations (specifically, because the number of entries in a vertex symbol gets unmanageable for large τ), we list the point symbol in Table 2 wherever $\tau \geq 5$, and the vertex symbol where $\tau \leq 4$. The extension of the tiling concept to n dimensions is more delicate, and is discussed further in §3.5.

Following Delgado-Friedrichs et al. (2003a,b), the *regularity* of a 3D net may now be characterized precisely. In short, consider a 3D net with p kinds of vertex and q kinds of edge and whose natural tiling is characterized by r kinds of face and s kinds of tile. Delgado-Friedrichs & Huson (2000) introduced a clear and self-consistent method for characterizing the regularity of such a net simply by forming the array $pqrs$: examining the 4-digit number so formed, referred to as the *transitivity* of the net, the most “regular” 3D nets are generally those with the smallest transitivity.

Finally, a *minimal net* is a net with the minimum possible number of vertices and edges in its primitive cell¹⁸; that is, upon deletion of any further edges in the primitive cell, the resulting net breaks into multiple disconnected structures. Beukemann & Klee (1992) establish that there are only 15 such minimal nets in 3D. Delgado-Friedrichs & O’Keeffe (2003) define a 3D net as *barycentric* if every vertex is placed in the center of gravity of its neighbors (to which it is connected by edges). Bonneau et al. (2004), in turn, establish that 7 of the 15 such minimal nets in 3D have *collisions*; that is, when arranged in barycentric fashion, the location of two or more vertices coincide (and, thus, the net is in a sense degenerate). Of the 8 remaining minimal nets without collision, five are uninodal.

3.2. 2D nets. Consider first the development of uninodal 2D nets with low coordination number. Start from the triangular ($A_2^* \cong A_2$) lattice (see §1) and perform a red/black/blue coloring of the nodes such that no two nearest-neighbor nodes are the same color. If we retain only the red and black nodes, we are left with the *honeycomb packing* (see Figure 1.1e), and the corresponding net is an array of hexagons. The coordination number of this stable sphere packing is $\tau = 3$, which is less than that of the 2D square packing ($\tau = 4$); this implies fewer wires in the corresponding computational interconnect application. Unfortunately, the topological density of this net is quite poor, with $td_{10} = 166$ (that is, with information spreading from one node to only 165 others after a message progresses 10 hops in the network application). We are thus motivated to explore other ways of constructing structured (that is, easy-to-build and easy-to-navigate) nets with low coordination number (that is, with low cost) but high topological density (that is, with a fast spread of information).

Note that the honeycomb packing has a packing density which is less than that of the corresponding triangular and square lattices discussed previously (see Table 2). If minimization of packing density is the goal¹⁹, then the honeycomb packing may be *augmented* by replacing every sphere with a set of three spheres in contact, each such set forming an equilateral triangle which touches the neighbors in exactly the same locations as the single sphere which it replaces in the original (unaugmented) packing (see, e.g., Heesch & Laves 1933, Figure 13). The packing density of the resulting stable *augmented honeycomb* packing is less than 2/3 that of the original honeycomb packing (see Table 2), and is the rarest uninodal sphere packing available in 2D.

3.3. A List of Twelve “highly regular” uninodal 3D nets. There are far too many 3D nets to review them all here. We thus identify a List of Twelve highly “regular” (as defined in §3.1, via their transitivity) uninodal 3D nets upon which we will focus our attention and

¹⁸A *primitive cell* of a net is the smallest fundamental volume (e.g., hypercube) that, when repeated as an infinite array in all directions with zero spacing, generates the net.

¹⁹Note that, for $n > 3$, the authors are actually unaware of any practical application, other than mathematical curiosity, for which minimization of packing density is a significant goal.

which, following Delgado-Friedrichs et al. (2003a,b), we denote (listing from dense to rare):

- | | | |
|--|------------------------------|--|
| 1. fcu : face-centered cubic (FCC), | 5. nbo : NbO, | 9. cds : CdSO ₄ , |
| 2. bcu : body-centered cubic (BCC), | 6. dia : diamond, | 10. bto : B ₂ O ₃ , |
| 3. pcu : cubic, | 7. sod : sodalite, | 11. ths : ThSi ₂ , |
| 4. qtz : quartz, | 8. qzd : quartz dual, | 12. srs : SrSi ₂ . |

See Table 2 for the common names, associated packings, and key characteristics of each²⁰. These twelve nets have been studied thoroughly in the literature, including the landmark work of Wells (1977, 1979, 1983, 1984) and scores of important publications since, including Koch & Fischer (1995, 2006) and the numerous references contained therein; space does not allow a comprehensive review of this broad body of literature here, nor even a comprehensive analysis of these twelve well-studied nets. Suffice it to say here that included in our List of Twelve are the 5 *regular* nets (that is, of transitivity 1111), **bcu**, **pcu**, **nbo**, **dia**, and **srs**, and the 1 *quasiregular* net (of transitivity 1112), **fcu**, as well as 2 of the 14 *semiregular* nets (of transitivity 11rs), **qtz** and **sod** (both of which have transitivity 1121), as discussed in O’Keeffe et al. (2000) and Delgado-Friedrichs et al. (2003a,b). Also included in this list are the 5 uninodal minimal nets without collision, **pcu**, **dia**, **cds**, **srs**, and **ths**, the first 4 of which are naturally self-dual, as discussed in Bonneau et al. (2004, Table 1); note that **cds** is of transitivity 1221, and **ths** is of transitivity 1211²¹. The remaining 2 nets on our List of Twelve, **qzd** (transitivity 1211; see Delgado-Friedrichs et al. 2003c) and **bto** (transitivity 1221; see Blatov 2007), are included because of their close structural relationship to the others, as discussed further in §3.4. We also note that four on our List of Twelve, **qtz**, **qzd**, **bto**, and **srs**, are *chiral* (that is, these nets twist in such a way that the nets and their reflections are not superposable).

The 12 remaining semiregular nets (of transitivity 11rs) of Delgado-Friedrichs et al. (2003b, Table 1) are the next natural candidates in this taxonomy (**hxx**, **crs**, **reo**, and **rhr** might be of particular interest), perhaps followed by the 28 binodal edge-transitive nets (of transitivity 21rs) of Delgado-Friedrichs et al. (2006, Table 1) and the 3 binodal minimal nets without collision (of transitivity 2222, 2211, and 2321) of Bonneau et al. (2004, Table 1) [see also Delgado-Friedrichs & O’Keeffe (2007)]. Note that just half of the List of Twelve considered here (specifically, in order of frequency, **dia**, **pcu**, **srs**, **ths**, **nbo**, and **cds**) account for 66% of the 774 uninodal metal-organic frameworks (MOFs) tabulated in the Cambridge Structural Database (CSD), as reviewed by Ockwig et al. (2005), thus indicating the prevalence in nature of several of the structures considered here.

The idea of augmentation, introduced in §3.2, extends directly to many 3D nets in order to reduce packing density. For example, in the (stable) packings related to the **dia** and **sod** nets (discussed further in §3.4.1 and §3.4.3 respectively), both of which have coordination number 4, we may replace each sphere with a set of four spheres in contact, each such set of spheres forming a tetrahedron, creating what is referred to as the *augmented diamond* (**dia-a**) and *augmented sodalite* (**sod-a**) nets. In the case of the augmentation of the packing related to the **dia** net, each tetrahedral set touches the neighbors in exactly the same locations as the single sphere which it replaces in the original (unaugmented) packing (see Heesch & Laves 1933, Figure 12). In the case of the augmentation of the packing related to the **sod** net, as the angles between the 4 nearest neighbors of any node are not uniform in the **sod** net, each tetrahedral set is slightly larger than the single sphere which they replace in the original (unaugmented) packing, and the contact points are slightly shifted (O’Keeffe 1991b); note that the packing associated with the **sod-a** net is the rarest uninodal stable 3D packing currently known. On the other hand, in the augmentation of the (unstable) packing related to the **srs** net, which has coordination number 3, we may replace each sphere with a set of three spheres in contact, each such set of spheres, as in the augmentation of the honeycomb packing, forming an

²⁰Again, clear drawings of each of these nets are available at <http://rcsr.anu.edu.au/nets/fcu>, where “fcu” may be replaced by any of the lowercase boldface three-letter identifiers given here.

²¹As illustrated in Bonneau et al. (2004, Figure 3), a self-dual tiling of **ths** may in fact be constructed; this tiling has transitivity 1221.

equilateral triangle and touching the neighbors in exactly the same locations as the single sphere which it replaces in the original (unaugmented) packing (see Heesch & Laves 1933, Figure 10); note that the packing associated with the resulting **srs-a** net is the rarest uninodal unstable 3D packing known.

Comparing augmented honeycomb to honeycomb, **dia-a** (transitivity 1222) to **dia**, **sod-a** (transitivity 1332) to **sod**, and **srs-a** (transitivity 1221) to **srs**, it is seen that augmentation, while reducing the packing density Δ (see Table 2), also significantly reduces both the topological density, td_{10} , and the regularity of the resulting net. Thus, the process of augmentation appears to be of little interest for the purpose of developing efficient computational interconnects. Note that Fischer (2005) and Dorozinski & Fischer (2006) show that the process of augmentation can be repeated indefinitely in order to obtain (non-uninodal) sphere packings of arbitrarily low packing density.

Finally, there are two other 3D nets which, though less regular than our List of Twelve, are worthy of “honorable mention”: *hexagonal close packing* (**hcp**, transitivity 1232) and *lonsdaleite* (**lon**, transitivity 1222). As hinted by their identical packing densities (see Table 2a), **hcp** is closely related to **fcu**, and **lon** is closely related to **dia**; curiously, both have slightly *higher* values of td_{10} than do their more regular cousins. The relations between these two pairs of packings is readily evident when they are considered as built up in layers, as introduced in the second paragraph of §2.4 and discussed further below.

The A_3 lattice (a.k.a. FCC, corresponding to the **fcu** net) may be built up as an alternating series of three 2D triangular (A_2) layers, offset from each other in the form *abcabc* . . . , with the nodes in one layer over the holes in the layer below; **hcp** is built up similarly, but with two alternating layers, offset from each other in the form *abab* . . .

Similarly, the sphere packings corresponding to the **dia** and **lon** nets may be built up as alternating series of approximately 2D honeycomb layers offset from each other. These honeycomb “layers” are in fact not quite 2D; if the nodes in a single layer are marked with an alternate red/black coloring, the red nodes are raised a bit and the black nodes lowered a bit. In both packings, the layers are offset from each other, with the lowered nodes in one layer directly over the raised nodes in the other. In the packing corresponding to the **dia** net, there are three such alternating layers stacked in the form *abcabc* . . . ; in the packing corresponding to the **lon** net, there are two such alternating layers stacked in the form *abab* . . .

3.4. Uninodal extension of several regular 3D nets to higher dimensions. The **fcu** net is based on the $D_3 \cong A_3$ lattice, and thus may be extended to n dimensions in two obvious ways (that is, via A_n or D_n). The **bcu** net is based on the $D_3^* \cong A_3^*$ lattice, and thus may also be extended to n dimensions in two obvious ways (via A_n^* or D_n^*). The **pcu** net is based on the \mathbb{Z}^3 lattice, and thus extends to n dimension via \mathbb{Z}^n . This section explores how most of the other nets on the List of Twelve described above extend naturally to higher dimensions.

It is important to recall that the nets in the D_n^* case for $n > 4$ turn out to be a bit peculiar, as discussed further in §2.3; the T_n^{90} and T_n^{60} nets encountered in §3.4.7 are similar.

3.4.1. Extending dia: the A_n^+ and D_n^+ packings. The **dia** net may be obtained from the well-known D_3^+ packing defined in (2.5) (see also Sloane 1987), and thus extends naturally to n dimensions as D_n^+ . However, there is an alternative construction of the **dia** net, described below and denoted A_n^+ , which is equivalent to D_n^+ for $n = 3$ but extends to n dimensions differently. In fact, a third extension of the **dia** net to n dimensions, the V_n^{90} construction, is introduced in §3.4.6. These alternative extensions of the **dia** net to n dimensions, with low coordination number, are perhaps better suited than D_n^+ for many practical applications. We thus stress that names such as “ n -dimensional diamond” are parochial, as there are sometimes multiple “natural” n -dimensional extensions of a net related to a given three-dimensional crystalline structure (e.g., D_n^+ , A_n^+ , and V_n^{90}). For n -dimensional nets in general, we thus strongly prefer names derived from a corresponding well-defined n -dimensional lattice or, when such a name is not available, names evocative of their n -dimensional construction; this

preference is in sharp contrast with the names suggested by O’Keeffe (1991b).

Recall the first paragraph of §3.2. Now start from a BCC ($A_3^* \cong D_3^*$) lattice and perform a red/black/blue/yellow coloring of the points such that no two nearest-neighbor points are the same color. If we retain only the red and black points, we are left with the diamond packing. The coordination number of this packing is $\tau = 4$, which is less than that of the 3D cubic packing ($\tau = 6$), but also has a reduced topological density, as quantified by td_{10} (see Table 2). The diamond packing also has a packing density which is less than that of the corresponding FCC, BCC, and cubic lattices.

Note in general [see (2.7a)] that A_n^* may be defined as the union of $n + 1$ shifted A_n lattices, which is analogous to the property [see (2.4a)] that D_n^* may be defined as the union of 4 shifted D_n lattices. Recall from (2.5) that D_n^+ , which we referred to the *offset checkerboard packing*, was defined as the union of just 2 shifted D_n lattices, and generates the diamond packing in 3D (where $D_3 \cong A_3$). Motivated by the previous paragraph and the first paragraph of §3.2, we are thus also keenly interested in the nonlattice packing considered in Table 1 of O’Keeffe (1991b), denoted here A_n^+ and referred to as the *offset zero-sum packing*, and which is defined as the union of just 2 shifted A_n lattices [cf. (2.5), (2.7)]:

$$A_n^+ = A_n \cup ([1] + A_n), \quad \text{where} \quad [1]_k = \begin{cases} \frac{1}{n+1} & k \leq n, \\ \frac{-n}{n+1} & k = n + 1. \end{cases} \quad (3.1)$$

The coordination number of the regular uninodal nonlattice packing A_n^+ is $n + 1$, with these $n + 1$ nearest neighbors forming a regular n -dimensional *simplex* [that is, a regular n -dimensional polytope with $n + 1$ vertices—e.g., in $n = 3$ dimensions, a tetrahedron]. The generalization of the honeycomb and diamond packings to higher dimensions given by A_n^+ is significant, as it illustrates how a highly regular stable packing with coordination number lower than that of the Cartesian lattice may be extended to dimension $n > 3$. Note also that the nonlattice packings A_n^+ are distinct from the lattice packings A_n^r defined in (2.8), which are generated in a similar manner.

3.4.2. Augmenting the A_n^+ packing: \hat{A}_n^+ . The third paragraph of §3.3 discusses the augmentation of the A_3^+ packing, replacing each sphere with a tetrahedral set of 4 smaller spheres. This idea extends immediately to the augmentation, in n dimensions, of the A_n^+ packing discussed above, replacing each (n -dimensional) sphere with a regular n -dimensional simplex of $n + 1$ smaller spheres.

3.4.3. Extending sod: the ${}^T A_n^*$ packing. The familiar **sod** net is formed by the edges of the Voronoï tessellation of space formed by the A_3^* (that is, BCC) packing, with the nodes of the net located at the *holes* of the packing rather than at the centers of the spheres of the packing. As noted by O’Keeffe (1991b), this construction extends immediately to the n -dimensional net formed by the Voronoï tessellation of space via the A_n^* packing. Constructing the A_n^* packing as defined in §2.4, the holes of this packing that are nearest to the origin (that is, in its Voronoï tessellation, the corners of the Voronoï cell which contains the origin) are given by the $(n + 1)!$ permutations of the vector (see Conway & Sloane, 1998, page 474):

$$\frac{1}{2(n+1)} (-n \quad -n+2 \quad -n+4 \quad \dots \quad n)^T.$$

These nodal points [which, like the lattice points of A_n^* itself, are defined in an $(n + 1)$ -dimensional space, but all lie in the n -dimensional subspace orthogonal to the vector \mathbf{n}_{A_n} defined in (2.6b)] are equidistant from their $n + 1$ nearest neighbors, and form *permutohedra* (in 3D, *truncated octahedra*) which tile n -dimensional space. Note that these nodal points themselves form a uninodal sphere packing with coordination number $\tau = n + 1$; due to its relationship to the *tessellation* of space via the points of the A_n^* packing, we thus introduce the notation ${}^T A_n^*$ for this packing.

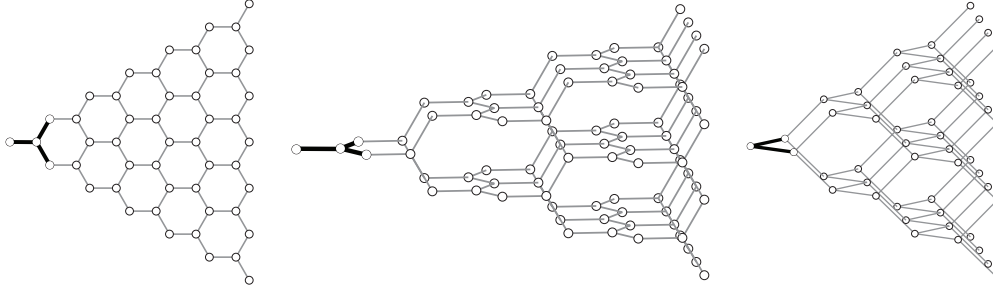


FIG. 3.1. Construction of three rare packings: (left) the Y_2 (honeycomb) net, (center) the Y_3^{90} (**ths**) net, and (right) the V_3^{90} (**dia**) net. All three constructions build from left to right in the above figures from a basic “Y” or “V” stencil, and have obvious extensions to higher dimensions.

3.4.4. Extending nbo: the S_n construction. The **nbo** net, a subset of the **pcu** net, has an obvious uninodal extension to n dimensions with $\tau = 4$, which may be visualized as the contact graph formed by repeating a unit hypercube pattern as an infinite array with unit spacing (see Figure 4.3), where each hypercube itself has two paths which “snake” along the edges from the $(0, 0, \dots, 0, 0)$ node to the $(1, 1, \dots, 1, 1)$ node, one coordinate direction at a time; we thus suggest the symbol S_n to denote this construction. These two paths touch at the opposite corners of the unit hypercube:

path A: $(0, 0, \dots, 0, 0), (0, 0, \dots, 0, 1), (0, 0, \dots, 1, 1), \dots, (0, 1, \dots, 1, 1), (1, 1, \dots, 1, 1)$, and
 path B: $(0, 0, \dots, 0, 0), (1, 0, \dots, 0, 0), (1, 1, \dots, 0, 0), \dots, (1, 1, \dots, 1, 0), (1, 1, \dots, 1, 1)$.

3.4.5. Extending ths and bto: the Y_n^{90} and Y_n^{60} constructions. The honeycomb packing A_2^+ , of coordination number $\tau = 3$, contains a fundamental Y-shaped stencil. As illustrated in Figure 3.1a, starting with this Y stencil and adjoining translates of itself, tip to tip, builds up the honeycomb packing in 2D. Extending this idea to 3D, as illustrated in Figure 3.1b, we may “twist” the Y stencil by 90° at each level: starting with the basic Y stencil in, say, the \mathbf{e}^1 - \mathbf{e}^2 plane, we can shift to the right (in \mathbf{e}^1) and adjoin Y stencils twisted by 90° (that is, aligned in the \mathbf{e}^1 - \mathbf{e}^3 plane), then shift to the right again and adjoin Y stencils twisted again (aligned in the \mathbf{e}^1 - \mathbf{e}^2 plane), etc. This construction forms the **ths** net in 3D, and extends immediately to dimension $n > 3$; we thus denote this construction Y_n^{90} .

Instead of twisting the Y stencil by 90° at each step, we may instead twist it by 60° . This forms the **bto** net in 3D. As with the **hcp** versus **fcu** and **lon** versus **dia** nets in 3D, as described at the end of §3.3, there is a bit of flexibility in terms of the ordering of the successive twists for $n > 3$. A highly regular net for odd n , which we denote Y_n^{60} , is formed by pairing off the dimensions after the first and alternating the twists as follows: starting with the basic Y stencil in, say, the \mathbf{e}^1 - \mathbf{e}^2 plane, we continue by adjoining Y stencils in the \mathbf{e}^1 - \mathbf{e}^4 plane, then in the \mathbf{e}^1 - \mathbf{e}^6 plane, etc. We then adjoin Y stencils in the \mathbf{e}^1 - \mathbf{z}_{23}^{60} plane, where \mathbf{z}_{23}^{60} is the vector formed by rotating the \mathbf{e}^2 unit vector 60° in the direction towards \mathbf{e}^3 ; we continue by adjoining Y stencils in the \mathbf{e}^1 - \mathbf{z}_{45}^{60} plane, then in the \mathbf{e}^1 - \mathbf{z}_{67}^{60} plane, etc. Next, we adjoin Y stencils in the \mathbf{e}^1 - \mathbf{z}_{23}^{120} plane, where \mathbf{z}_{23}^{120} is the vector formed by rotating the \mathbf{z}_{23}^{60} vector 60° further in the \mathbf{e}^2 - \mathbf{e}^3 plane; we continue by adjoining Y stencils in the \mathbf{e}^1 - \mathbf{z}_{45}^{120} plane, then in the \mathbf{e}^1 - \mathbf{z}_{67}^{120} plane, etc., and repeat (that is, with stencils again aligned in the \mathbf{e}^1 - \mathbf{e}^2 plane).

The Y_n^{90} and Y_n^{60} constructions have a parameter, denoted α and defined as half of the angle between the two top branches of the Y stencil (thus, $\alpha \rightarrow 0^\circ$ closes down the Y to an I, whereas $\alpha \rightarrow 90^\circ$ opens up the Y to a T). The Voronoï volume of the Y_n^{90} and Y_n^{60} constructions may be written as simple functions of α as follows:

$$\left. \begin{aligned} \mathcal{V}_{Y_n^{90}}(\alpha) &= f_{Y_n}(\alpha) \mathcal{V}_{Y_n^{90}}(\bar{\alpha}) \\ \mathcal{V}_{Y_n^{60}}(\alpha) &= f_{Y_n}(\alpha) \mathcal{V}_{Y_n^{60}}(\bar{\alpha}) \end{aligned} \right\} \text{ with } \bar{\alpha} = 45^\circ, \quad f_{Y_n}(\alpha) = (2 - \sqrt{2})(1 + \cos \alpha)(\sqrt{2} \sin \alpha)^{n-1}.$$

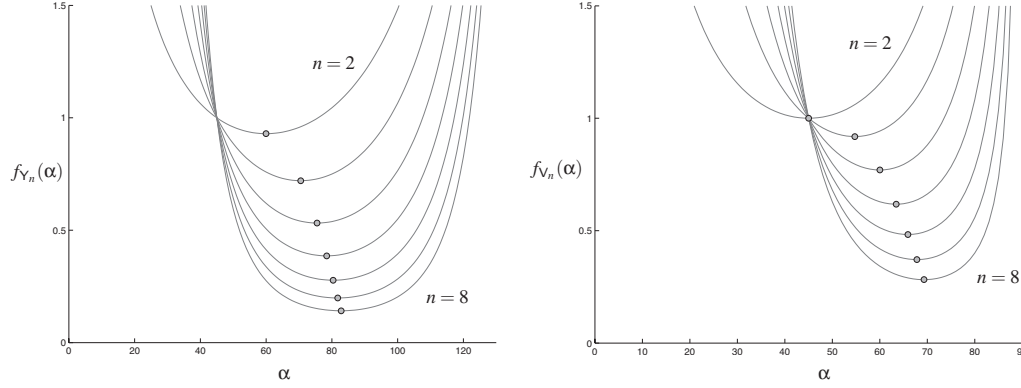


FIG. 3.2. Variation of the Voronoi volume of the (left) Y_n^{90} & Y_n^{60} and (right) V_n^{90} & V_n^{60} packings as a function of α for $n = 2$ to $n = 8$.

This relation is plotted in Figure 3.2a. The characteristics of Y_n^{90} and Y_n^{60} reported in Table 2 are computed for $\alpha = \cos^{-1}(1/n)$, as marked with circles in Figure 3.2a, which maximizes the Voronoi volume and, thus, minimizes the packing density. An alternative natural choice is $\alpha = 60^\circ$, which results in barycentric constructions of Y_n^{90} and Y_n^{60} .

3.4.6. Extending dia and qtz: the V_n^{90} and V_n^{60} constructions. The V_n^{90} and V_n^{60} constructions are defined in an identical manner as their Y_n^{90} and Y_n^{60} counterparts, with a V stencil replacing the Y stencil (see, e.g., Figure 3.1c), thus resulting in nets with coordination number $\tau = 4$ instead of $\tau = 3$. These constructions lead to the **dia** and **qtz** nets in 3D.

As with the Y_n^{90} and Y_n^{60} construction, the V_n^{90} and V_n^{60} constructions have a parameter, denoted α and defined as half of the angle between the two top branches of the V stencil. The Voronoi volume of the V_n^{90} and V_n^{60} constructions may be written as simple functions of α as follows:

$$\left. \begin{aligned} \mathcal{V}_{V_n^{90}}(\alpha) &= f_{V_n}(\alpha) \mathcal{V}_{V_n^{90}}(\bar{\alpha}) \\ \mathcal{V}_{V_n^{60}}(\alpha) &= f_{V_n}(\alpha) \mathcal{V}_{V_n^{60}}(\bar{\alpha}) \end{aligned} \right\} \text{ with } \bar{\alpha} = 45^\circ, \quad f_{V_n}(\alpha) = 2^{n/2} \cos \alpha (\sin \alpha)^{n-1}.$$

This relation is plotted in Figure 3.2b. The characteristics of V_n^{90} and V_n^{60} reported in Table 2 are computed for $\alpha = \cos^{-1}(1/\sqrt{n})$, as marked with circles in Figure 3.2a, which maximize the Voronoi volumes and, thus, minimize the packing density. Note that the V_n^{90} and V_n^{60} constructions are barycentric for any α in the range $0 < \alpha < 90^\circ$.

3.4.7. Extending cds and qzd: the T_n^{90} and T_n^{60} constructions. The T_n^{90} and T_n^{60} constructions are defined in an analogous manner as their Y_n^{90} , V_n^{90} , Y_n^{60} , and V_n^{60} counterparts, and lead to the **cds** and **qzd** nets in 3D. The only difference now is that, instead of adjoining two new Y or V symbols on the tips of each Y or V symbol in the previous layer, we now adjoin a single new T symbol centered atop each T symbol in the previous layer, appropriately twisted; these constructions thus result in nets with coordination number $\tau = 4$. Note that the “horizontal” and “vertical” distances between nodes in these constructions are equal, and that these constructions are parameter free and barycentric.

Note that the x_1 direction is special in the Y_n^{90} , Y_n^{60} , V_n^{90} , V_n^{60} , T_n^{90} , and T_n^{60} constructions. These constructions are configured in this way intentionally, in order to construct equilibrium packings; however, other variations are certainly possible. Note also that the Y_n^{60} , V_n^{60} , and T_n^{60} constructions involve pairing off the dimensions after the first and rotating in each pair of dimensions 60° at a time, in the manner described in §3.4.5. If we follow the same procedure but rotate 90° at a time, we recover nets equivalent to the corresponding Y_n^{90} , V_n^{90} , and T_n^{90} nets, respectively, as defined previously.

Note also that the Y_n^{90} , V_n^{90} , and T_n^{90} constructions form square layers in the e_2 - e_3 plane, the e_4 - e_5 plane, the e_6 - e_7 plane, etc., whereas the Y_n^{60} , V_n^{60} , and T_n^{60} constructions form triangular layers in these planes. In the resulting Y_n^{90} , Y_n^{60} , V_n^{90} , and V_n^{60} nets, there are, in fact, no edges of the net within these layers (that is, all of the edges connect nodes in different layers). On the other hand, in the resulting T_n^{90} and T_n^{60} nets, each node is connected via edges of the net to exactly two others (note: *not* four or six) within these layers. As with the peculiar D_n^* net discussed previously, the T_n^{90} and T_n^{60} constructions are, in fact, *not* contact graphs of the corresponding sphere packings²²; some bonds must be cut in the corresponding contact graphs (which, in the case of T_n^{90} , is simply \mathbb{Z}^n) in order to form the T_n^{90} and T_n^{60} nets.

3.4.8. Other extensions. Sections 3.4.1 through 3.4.7 summarize several uninodal families of n -dimensional extrapolations of some common 3D nets; most of these (unless indicated otherwise, via references to existing literature) are new. Note that O’Keeffe (1991b) mentions two other such extensions, one corresponding to the **lon** net and one corresponding to the **sod-a**, the latter of which is currently the rarest uninodal stable packing known for $n > 3$ (and which, consistent with the above developed naming conventions, we might suggest to identify as T_n^*). Beukemann & Klee (1992, page 50) mentions two extensions of their own (at least, to $n = 4$), both related to the **dia** net. Judging from the vast assortment of distinct rare sphere packings and related nets available in 3D, there are certainly *many* more uninodal extensions to higher dimensions of regular rare 3D packings that are still awaiting discovery; we have focused our attention here on what appear to be several of the most regular. The regularity of n -dimensional nets for $n > 3$ is discussed further below.

3.5. Regularity and transitivity of n -dimensional nets for $n > 3$. As reviewed in §3.1, the regularity of a 3D net is defined based on its transitivity, which in turn is based on the so-called natural tiling of the 3D net. The natural tiles of 3D nets have been thoroughly characterized in the literature for all of the most regular 3D nets available. In §3.4, we described uninodal extensions of several regular 3D nets to higher dimensions, and mentioned that many more such uninodal nets with $n > 3$ most certainly exist. The natural question to ask, then, is how the concepts of regularity and transitivity can be extended to higher dimensions, so that we may differentiate between these nets and identify those which are the most regular.

This question is difficult to visualize in dimensions higher than three, and requires a symbolic/numerical description of the net to proceed. The net arising from the \mathbb{Z}^n lattice for $n = 4, 5, \dots$, which is naturally tiled by n -dimensional hypercubes, is by far the easiest starting point. Denote first the symbols $\{v, w, x, y, z\}$ as variables that range from 0 to 1. The 3D unit cube, denoted $\{xyz\}$, has six faces, $\{xy0, xy1, x0z, x1z, 0yz, 1yz\}$. Each face, in turn, has four edges; e.g., $\{0yz\}$ has edges $\{0y0, 0y1, 00z, 01z\}$. Finally, each edge connects two nodes; e.g., $\{00z\}$ connects nodes $\{000, 001\}$. The 4D unit hypercube, $\{wxyz\}$, has eight 3-faces, $\{wxy0, wxy1, wx0z, wx1z, w0yz, w1yz, 0xyz, 1xyz\}$, each 3-face has six 2-faces, each 2-face has four edges, and each edge connects two nodes. The 5D unit hypercube, $\{vwxyz\}$, has ten 4-faces, each 4-face has eight 3-faces, each 3-face has six 2-faces, each 2-face has four edges, and each edge connects two nodes; etc.

In 3D, as reviewed in §3.1, the transitivity is based on the number of distinct nodes, edges, (two-dimensional) faces, and (three-dimensional) tiles. By analogy, then, in 4D we may define the transitivity of a net based on the number of distinct nodes, edges, 2-faces, 3-faces, and (4-dimensional) tiles in the natural tiling. Similarly, in 5D, we may define the transitivity based on the number of distinct nodes, edges, 2-faces, 3-faces, 4-faces and (5-dimensional) tiles in the natural tiling; etc. Via this definition, the net derived from the \mathbb{Z}^4 lattice has transitivity 11111, the net derived from the \mathbb{Z}^5 lattice has transitivity 111111, etc.

²²Note that there is a lower-symmetry form of **cds** in 3D with four nearest neighbors per node whose contact graph does generate the **cds** net; see Delgado-Friedrichs et al. (2005, Figure 1). Lower symmetry forms of other T_n^{90} and T_n^{60} constructions, whose nets are contact graphs, might also exist.

For all of the other nets with $n > 3$ listed in Table 2, the computation of the transitivity remains an important unsolved problem. Note that, in a tiling corresponding to a 3D net, the (two-dimensional) faces of the (three-dimensional) tiles are, in general, minimal surfaces stretched over non-planar frames built from (one-dimensional) edges between several nodal points defined in 3D. In a tiling corresponding to an n -dimensional net for $n > 3$, the 2-faces of the tiles are, in general, minimal surfaces stretched over nonplanar frames between several nodes defined in n dimensions. [Note that the computation of such minimal surfaces in n dimensions is straightforward using standard level set methods; see, e.g., Cecil (2005).] Several of these nonplanar 2-faces combine to form the boundaries of each 3-face, which itself is not confined to lie within a 3D subspace of the n -dimensional domain. Several of these 3-faces then combine to form the boundaries of each 4-face; etc.

Identification of such high-dimensional natural tilings is apparently a task that could be readily accomplished numerically, but is, in general, expected to be difficult to visualize.

4. Coding theory. Though the lattices that arise from n -dimensional sphere packings have connections that permeate many foundational concepts in number theory and pure geometry, the list of successful direct applications in science and engineering of n -dimensional sphere packings with $n > 3$ is currently surprisingly short²³; this list includes

- the numerical evaluation of integrals (Sloan & Kachoyan 1987),
- the solution of the linear Diophantine inequalities that arise in integer linear programming (Schrijver 1986),
- the characterization of crystals with curious five-fold symmetries (Janssen 1986),
- attempts at unifying the 4 fundamental forces (in 10, 11, or 26 dimensions) via superstring theory (Kaku 1999), and
- the development of maximally effective numerical schemes to address an information-theoretic interference suppression problem known as the Witsenhausen counterexample (Grover, Sahai, & Park 2010).

Far and away the most elegant and practical application of n -dimensional sphere packings, however, is in the framing and understanding of *error correcting codes (ECCs)*. *The reader is referred to MacWilliams & Sloane (1977), Thompson (1983), Pless (1998), Conway & Sloane (1998), and Morelos-Zaragoza (2006) for some comprehensive reviews of this fascinating subject.* A brief overview of this field is given here to emphasize the existing practical relevance of n -dimensional sphere packings with $n > 3$; we aim to augment this list of practical applications significantly in Parts II and III of the present work, based heavily on the various extensions of n -dimensional sphere packing theory developed in this paper.

To proceed, define \mathbf{F}_q [also denoted $GF(q)$] as the set of symbols in a *finite field* (a.k.a. *Galois field*) of order q , where $q = p^a$ with p prime, and define \mathbf{F}_q^n as the set of all vectors of order n with elements selected from \mathbf{F}_q . The cases of particular interest in this work are the *binary field* $\mathbf{F}_2 = \{0, 1\}$, the *ternary field* $\mathbf{F}_3 = \{0, 1, 2\}$, and the *quaternary field*²⁴ $\mathbf{F}_4 = \{0, 1, \omega, \bar{\omega}\}$, where, as in §2.1, $\omega = (-1 + i\sqrt{3})/2$ [note that $\omega^2 = \bar{\omega}$, $\bar{\omega}^2 = \omega$, and $\bar{\omega} \cdot \omega = 1$]. In a finite field \mathbf{F}_q , addition (+) and multiplication (\cdot) are closed (that is, they map to elements within the field) and satisfy the usual rules: they are associative, commutative, and distributive, there is a 0 element such that $a + 0 = a$, there is a 1 element such that $a \cdot 1 = a$, for each a there is an element $(-a)$ such that $a + (-a) = 0$, and for each $a \neq 0$ there is an element a^{-1} such that $a \cdot a^{-1} = 1$. If q is itself prime (e.g., if $q = 2$ or $q = 3$), then standard integer addition and

²³Notably, Conway & Sloane (1998, page 12) state: “A related application that has not yet received much attention is the use of these packings for solving n -dimensional *search* or *approximation* problems”; this is exactly the problem focused on in our Part II.

²⁴We limit our attention in the quaternary case to codes designed over the finite field \mathbf{F}_4 ; though there is some attention in the literature to codes defined over \mathbb{Z}_4 [that is, over the integers mod 4], codes defined over finite fields turn out to be, in a sense, more natural.

multiplication mod q forms a finite field. If not (e.g., if $q = 4$), a bit more care is required in order to obtain closure within the finite field while respecting these necessary rules on addition and multiplication. For the cases considered in this section (specifically, \mathbf{F}_2 , \mathbf{F}_3 , and \mathbf{F}_4), addition and multiplication on \mathbf{F}_q are thus defined as follows:

$$\mathbf{F}_2: \begin{array}{c|c|c|c} + & 0 & 1 & \\ \hline 0 & 0 & 1 & \\ \hline 1 & 1 & 0 & \end{array} \quad \begin{array}{c|c|c|c} \cdot & 0 & 1 & \\ \hline 0 & 0 & 0 & \\ \hline 1 & 0 & 1 & \end{array} \quad \mathbf{F}_3: \begin{array}{c|c|c|c|c} + & 0 & 1 & 2 & \\ \hline 0 & 0 & 1 & 2 & \\ \hline 1 & 1 & 2 & 0 & \\ \hline 2 & 2 & 0 & 1 & \end{array} \quad \begin{array}{c|c|c|c|c} \cdot & 0 & 1 & 2 & \\ \hline 0 & 0 & 0 & 0 & \\ \hline 1 & 0 & 1 & 2 & \\ \hline 2 & 0 & 2 & 1 & \end{array}$$

$$\mathbf{F}_4: \begin{array}{c|c|c|c|c|c} + & 0 & 1 & \omega & \bar{\omega} & \\ \hline 0 & 0 & 1 & \omega & \bar{\omega} & \\ \hline 1 & 1 & 0 & \bar{\omega} & \omega & \\ \hline \omega & \omega & \bar{\omega} & 0 & 1 & \\ \hline \bar{\omega} & \bar{\omega} & \omega & 1 & 0 & \end{array} \quad \begin{array}{c|c|c|c|c|c} \cdot & 0 & 1 & \omega & \bar{\omega} & \\ \hline 0 & 0 & 0 & 0 & 0 & \\ \hline 1 & 0 & 1 & \omega & \bar{\omega} & \\ \hline \omega & 0 & \omega & \bar{\omega} & 1 & \\ \hline \bar{\omega} & 0 & \bar{\omega} & 1 & \omega & \end{array}$$

A vector in \mathbf{F}_q^n is a vector of length n with each element in \mathbf{F}_q . The *Hamming distance* between two such vectors is the number of elements that differ between them.

An $[n, k]_q$ (if d is specified, $[n, k, d]_q$) q -ary linear²⁵ code (LC) is defined via a set of $k < n$ independent *basis vectors* $\mathbf{v}^i \in \mathbf{F}_q^n$. The q^k distinct *codewords* $\mathbf{w}^i \in \mathbf{F}_q^n$ of the LC are given by all q -ary *linear combinations* of the basis vectors \mathbf{v}^i (that is, by all linear combinations with coefficients selected from \mathbf{F}_q , with addition and multiplication defined elementwise on \mathbf{F}_q). The basis vectors \mathbf{v}^i are generally selected such the *minimum distance* d of the LC (that is, the minimum Hamming distance between any two resulting codewords) is maximized.

This work focuses on cases with $q = 2$ [termed a *linear binary code (LBC)*], $q = 3$ [termed a *linear ternary code (LTC)*], and $q = 4$ [termed a *linear quaternary code (LQC)*]. In cases with $q = 2$, which are common, we frequently write simply $[n, k]$ or $[n, k, d]$, dropping the q subscript. We denote by $V_{[n, k]_q}$ (or $V_{[n, k, d]_q}$) the $n \times k$ *basis matrix* with the k basis vectors \mathbf{v}^i as columns, and by $W_{[n, k]_q}$ (or $W_{[n, k, d]_q}$) the $n \times q^k$ *codeword matrix* with the q^k codewords \mathbf{w}^i as columns. Without loss of generality, we write $V_{[n, k]_q}$ and a companion $(n - k) \times n$ *parity-check matrix* $H_{[n, k]_q}$ in the standard (a.k.a. *systematic*) form²⁶

$$H_{[n, k]_q} = \begin{bmatrix} -P_{(n-k) \times k} & I_{(n-k) \times (n-k)} \end{bmatrix}, \quad V_{[n, k]_q} = \begin{bmatrix} I_{k \times k} \\ P_{(n-k) \times k} \end{bmatrix}, \quad \mathbf{w}^i = \begin{bmatrix} \mathbf{d}^i \\ \mathbf{b}^i \end{bmatrix}. \quad (4.1)$$

When written in systematic form, each of the data vectors \mathbf{w}^i block decomposes into its k *data symbols*²⁷ \mathbf{d}^i and its $r = n - k$ *parity symbols* \mathbf{b}^i ; note that r is sometimes called the *redundancy* of the code. Note also that $H_{[n, k]_q} V_{[n, k]_q} = 0$ (on \mathbf{F}_q)²⁸, which establishes that the basis vectors \mathbf{v}^i so constructed [and, thus, all of the resulting codewords \mathbf{w}^i] each satisfy the *parity-check equations*, $H_{[n, k]_q} \mathbf{w}^i = 0$ (on \mathbf{F}_q), as implied by the rows of $H_{[n, k]_q}$ and illustrated by the several examples given in systematic form in §4.1, §4.2, and §4.3. Note further that, for LBCs and LQCs, $P = -P$.

The key to designing a “good” $[n, k]_q$ LC is to construct the *parity submatrix* $P_{(n-k) \times k}$ in (4.1) in such a way that the minimum distance d of the resulting code is maximized for given values of n , k , and q . Indeed, the problem of designing a good binary error correcting code is essentially a finite sphere packing problem on \mathbf{F}_2 ; thus the very close relationship

²⁵Nonlinear q -ary codes also appear in the literature, in which the valid codewords are *not* simply linear combinations of a set of basis vectors and must be enumerated differently. Such codes, which are related to nonlattice packings, are in general more difficult to decode than LCs, and are not considered further here.

²⁶In the literature on this subject, it is more common to use a “generator matrix” G to describe the construction of linear codes. The “basis matrix” convention V used here is related simply to the corresponding generator matrix such that $V = G^T$; we find the basis matrix convention to be more natural in terms of its linear algebraic interpretation.

²⁷The word “bit”, a portmanteau word for “binary digit”, is generally reserved for the case with $q = 2$; in the general case, we use the word “symbol” in its place.

²⁸The qualifiers “(on \mathbf{F}_q)” and “(mod q)” are used, as appropriate, to remind the reader that multiplication and addition in the equation indicated are performed elementwise on the finite field \mathbf{F}_q , as discussed above.

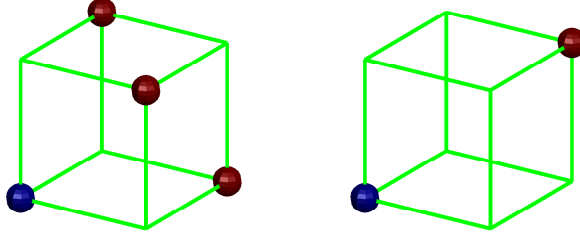


FIG. 4.1. Valid codewords of (left) the (SED) $[3,2,2]_2$ LBC, and (right) its dual, the (perfect, SEC) $[3,1,3]_2$ LBC. The blue sphere denotes the origin, and d specifies the number of edges between any two codewords.

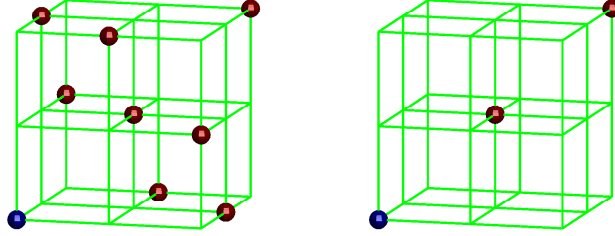


FIG. 4.2. Valid codewords of (left) the (SED) $[3,2,2]_3$ LTC, and (right) its dual, the (SEC) $[3,1,3]_3$ LTC.

between the design of error-correcting codes and the design of infinite sphere packings in \mathbb{R}^n , as discussed in §2.

For $q = p^a$ with p prime, *conjugation* in \mathbf{F}_q (that is, for a scalar $v \in \mathbf{F}_q$) is defined such that $\bar{v} = v^p$; conjugation in \mathbf{F}_q^n (that is, for vectors $\mathbf{v} \in \mathbf{F}_q^n$), as well as for matrices formed with a number of such vectors as columns, is performed elementwise. Any $[n, k]_q$ linear code C has associated with it an $[n, n-k]_q$ dual code C^\perp defined [cf. (2.1)] such that

$$C^\perp = \{ \mathbf{w} \in \mathbf{F}_q^n : \mathbf{w} \cdot \mathbf{u} = 0 \text{ for all } \mathbf{u} \in C \}. \quad (4.2)$$

The parity-check and codeword matrices of C^\perp may be written in systematic form as

$$H_{[n, n-k]_q}^\perp = \begin{bmatrix} \bar{P}^T & I_{(n-k) \times (n-k)} \end{bmatrix}, \quad V_{[n, n-k]_q}^\perp = \begin{bmatrix} I_{(n-k) \times (n-k)} \\ -\bar{P}^T \end{bmatrix}. \quad (4.3)$$

where \bar{P} denotes conjugation in \mathbf{F}_q of each element of the parity submatrix P of the original $[n, k]_q$ linear code C . Note that \bar{P}^T is of order $k \times (n-k)$, and, of course, that $H_{[n, n-k]_q}^\perp V_{[n, n-k]_q}^\perp = 0$ (on \mathbf{F}_q). Note further that, for LBCs and LTCs, $\mathbf{u} = \bar{\mathbf{u}}$ and $P = \bar{P}$.

A *self-dual* code C is a code for which the the transpose of the codeword matrix V results in a new matrix H which is itself the parity-check matrix of a code which is equivalent to C , albeit not in systematic form.

Graphically, the codewords of an $[n, k, d]_2$ LBC may be thought of as a carefully chosen subset of 2^k of the 2^n corners on a single n -dimensional unit hypercube, as illustrated for $n = 3$ in Figure 4.1, whereas an $[n, k, d]_3$ LTC may be thought of as a subset of 3^k of the 3^n gridpoints in a cluster of 2^n unit hypercubes in n -dimensions, as illustrated for $n = 3$ in Figure 4.2. For any q , d quantifies the minimum number of symbols which differ between any two codewords. It follows that:

- An LC with $d = 2$ is *single error detecting* (SED) [see, e.g., Figures 4.1a and 4.2a]. In this case, the sum (on \mathbf{F}_q) of the symbols in each transmitted codeword is zero, so if it is assumed that at most one symbol error occurred and this sum is nonzero, then a symbol error in transmission occurred, whereas if it is zero, then a symbol error did not occur. However, if a symbol error in transmission occurred, the received (invalid) message is generally equidistant from multiple codewords, so it is not possible to correct the symbol error. Two or more symbol errors generally cause the codeword to be misinterpreted.

- An LC with $d = 3$ is *single error correcting (SEC)* [see, e.g., Figures 4.1b and 4.2b]. In this case, if it is again assumed that at most one symbol error in transmission occurred, then if the received codeword is not a codeword, there is only one codeword that is unit Hamming distance away, so the single symbol error may in fact be *corrected*. Again, 2 or more symbol errors generally cause the codeword to be misinterpreted.
- An LC with $d = 4$ is *single error correcting and double error detecting (SECDED)*. In this case, if a single symbol error occurs, the received codeword will be unit Hamming distance away from a single codeword, and thus single symbol errors can be corrected. On the other hand, if two symbol errors occur, the received codeword is generally Hamming distance 2 away from multiple codewords, so double symbol errors can be detected but *not* corrected. Now, 3 or more symbol errors generally cause the codewords to be misinterpreted.
- An LC with $d = 5$ is *double error correcting (DEC)*, with 3 or more symbol errors generally causing misinterpretation.
- An LC with $d = 6$ is *double error correcting and triple error detecting (DECTED)*, with 4 or more symbol errors generally causing misinterpretation.
- An LC with $d = 7$ is *triple error correcting (TEC)*, with 4 or more symbol errors generally causing misinterpretation.
- An LC with $d = 8$ is *triple error correcting and quadruple error detecting (TECQED)*, with 5 or symbol errors generally causing misinterpretation.
- An LC with $d = 9$ is *quadruple error correcting (QEC)*, with 5 or more symbol errors generally causing misinterpretation.

The labels defined above are frequently used to quantify the error correction capability of an LC. Alternatively, if error correction is *not* attempted, then:

- An LC with $d = 2$ is single error detecting, with 2 or more symbol errors generally causing misinterpretation.
- An LC with $d = 3$ is double error detecting, with 3 or more symbol errors generally causing misinterpretation.
- An LC with $d = 4$ is triple error detecting, with 4 or more symbol errors generally causing misinterpretation.
- An LC with $d = 5$ is quadruple error detecting, with 5 or more symbol errors generally causing misinterpretation.

Error correcting algorithms are useful for a broad range of data transmission or data storage applications in which it is difficult or impossible to request that a corrupted codeword be retransmitted; algorithms which use such LCs for error detection only, on the other hand, may be used only when efficient handshaking is incorporated in a manner which makes it easy to request and resend any messages that might be corrupted during transmission.

An $[n, k, d]_q$ LC is *perfect* if, for some integer $t > 0$, each possible n -dimensional q -ary codeword is of Hamming distance t or less from a single codeword (that is, there are no “wasted” codewords that are Hamming distance $t + 1$ or more from the codewords, and thus may not be corrected under the assumption that at most t symbol errors have occurred); note that a perfect code has odd $d = 2t + 1 > 1$. A remarkable proof by Tietäväinen (1973), which was based on related work by Van Lint, establishes that the *only* nontrivial perfect LCs are the $[(q^m - 1)/(q - 1), (q^m - 1)/(q - 1) - m, 3]_q$ perfect q -ary Hamming codes and the $[23, 12, 7]_2$ and $[11, 6, 5]_3$ binary and ternary Golay codes, described further in §4.1 and §4.2.

An $[n, k, d]$ LC is *quasi-perfect* if, for some integer $t > 1$, each possible n -dimensional q -ary codeword is either (a) of Hamming distance $t - 1$ or less from a single codeword, and thus up to $t - 1$ symbol errors may be corrected, or (b) of Hamming distance t from at least one codeword, and thus codewords with t symbol errors may be detected but not necessarily corrected (that is, there are no “wasted” codewords that are Hamming distance $t + 1$ or more from a codeword, and thus may not be reconciled under the assumption that at most t symbol errors have occurred); note that a quasi-perfect code has even $d = 2t > 2$.

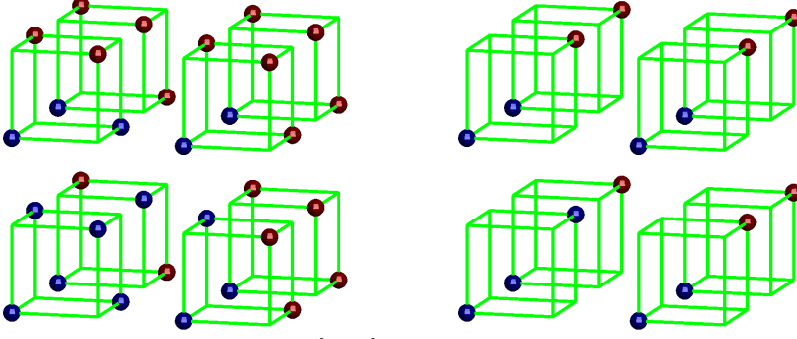


FIG. 4.3. The lattice corresponding to an $[n, k, d]$ LBC is formed by repeating the unit hypercube pattern given by the LBC (see, e.g., Figure 4.1) as an infinite array with unit spacing. In the above example, we illustrate this extension for (left) the face-centered cubic (FCC) lattice generated by the $[3, 2, 2]$ LBC, $D_3 = \bigcup_{i=1}^4 (\mathbf{w}_{[3,2,2]}^i + 2\mathbb{Z}^3)$, and (right) the body-centered cubic (BCC) lattice generated by the $[3, 1, 3]$ LBC, $D_3^* = \bigcup_{i=1}^2 (\mathbf{w}_{[3,1,3]}^i + 2\mathbb{Z}^3)$. The blue spheres, taken together, form a primitive cell that, repeated as an infinite array with zero spacing, tile (that is, fill) the domain.

Note finally, as illustrated for $n = 3$ in Figure 4.3, that a real lattice corresponding to an $[n, k, d]_2$ LBC may often be constructed by forming a union of 2^k cosets:

$$\text{Construction A: } \bigcup_{i=1}^{2^k} (\mathbf{w}_{[n,k,d]_2}^i + 2\mathbb{Z}^n), \quad (4.4a)$$

where the *coset representatives* in this construction, $\mathbf{w}_{[n,k,d]_2}^i$ for $i = 1, \dots, 2^k$, are the codewords of the $[n, k, d]_2$ LBC under consideration and $(\mathbf{w} + 2\mathbb{Z}^n)$ denotes a \mathbb{Z}^n lattice scaled by a factor of 2 with all nodal points shifted by the vector \mathbf{w} ; thus, Construction A denotes the union of the nodal points in several such scaled and shifted \mathbb{Z}^n lattices. An alternative real lattice may sometimes be constructed via:

$$\text{Construction B: } \bigcup_{i=1}^{2^k} (\mathbf{w}_{[n,k,d]_2}^i + 2J) \quad \text{where } J = \left\{ \mathbf{x} \in \mathbb{Z}^n \left| \left[\sum_{i=1}^n x_i \right] \in 2\mathbb{Z} \right. \right\}, \quad (4.4b)$$

where $(2\mathbb{Z})$ denotes the even integers, and thus the last condition is sometimes written $\sum_{i=1}^n x_i = 0 \pmod{2}$.

In an analogous fashion, a complex lattice corresponding to an $[n, k, d]_q$ LC may often be constructed by forming a union of q^k shifted and scaled n -dimensional \mathcal{E} lattices $\mathbb{Z}[\omega]^n$ (see §2.1) such that

$$\text{Construction } A_{\mathcal{E}}^{\pi}: \bigcup_{i=1}^{q^k} (\mathbf{w}_{[n,k,d]_q}^i + \pi\mathbb{Z}[\omega]^n), \quad (4.5a)$$

where, in the sequel, the multiplicative factor π takes two possible values (2 and $\theta = \omega - \bar{\omega} = i\sqrt{3}$) and the coset representatives in this construction, $\mathbf{w}_{[n,k,d]_q}^i$ for $i = 1, \dots, q^k$, are the codewords of the $[n, k, d]_q$ LC under consideration. An alternative complex lattice may sometimes be constructed via:

$$\text{Construction } B_{\mathcal{E}}^{\pi}: \bigcup_{i=1}^{q^k} (\mathbf{w}_{[n,k,d]_q}^i + \pi J) \quad \text{where } J = \left\{ \mathbf{x} \in \mathbb{Z}[\omega]^n \left| \left[\sum_{i=1}^n x_i \right] \in \pi\mathcal{E} \right. \right\}, \quad (4.5b)$$

where $(\pi\mathcal{E})$ denotes the lattice of Eisenstein integers in the complex plane multiplied (that is, rotated and scaled) by the (possibly complex) factor π . Note the remarkable similarity in structure between the real constructions in (4.4a)-(4.4b) and the complex constructions in (4.5a)-(4.5b). Note also that real lattices corresponding to any of the complex lattices so constructed may easily be generated via (2.2).

4.1. Exemplary linear binary codes (LBCs). We now summarize some of the families of LBCs available, presenting each in systematic form (4.1).

4.1.1. Binary single parity-check codes. The simple²⁹ $[n, n-1, 2]$ *binary single parity-check codes* are SED, and include $[2, 1, 2]$ (self-dual), $[3, 2, 2]$, $[4, 3, 2]$, $[5, 4, 2]$, etc. Using such a code, for each $(n-1)$ data bits to be transmitted, a *parity bit* is generated such that the sum (mod 2) of the data bits plus the parity bit is 0; when decoding, an error is flagged if this sum (mod 2) is 1. The $[3, 2, 2]$ code illustrated in Figure 4.1a is given by

$$H_{[3,2,2]} = (1 \ 1 \ 1), \quad V_{[3,2,2]} = \begin{pmatrix} 1 & 0 \\ 0 & 1 \\ 1 & 1 \end{pmatrix}, \quad W_{[3,2,2]} = \begin{pmatrix} 0 & 1 & 0 & 1 \\ 0 & 0 & 1 & 1 \\ 0 & 1 & 1 & 0 \end{pmatrix}. \quad (4.6)$$

Other binary single parity-check codes have a parity submatrix P [see (4.3)] of similar form (a row of 1's). As seen for $n = 3$ in Figure 4.3a, via Construction A, the $[n, n-1, 2]$ binary single parity-check code generates the D_n lattice (see §2.3), which for $n = 3$ is FCC.

A single parity-check code (binary or otherwise), with $d = 2$, can detect but not correct an error in an unknown position. However, it can correct an *erasure*; that is, the loss of data from a known position. A common application of this capability is in a RAID 5 system, a popular configuration for a relatively small *Redundant Array of Independent Disks*. In such a system, data is striped across n drives using a single parity check code; if any single drive fails, the data on it can be recovered simply by achieving parity with the other disks.

4.1.2. Binary repetition codes. The dual of the binary single parity-check codes are the simple $[n, 1, n]$ *binary repetition codes*, which include $[2, 1, 2]$ (SED, self-dual), $[3, 1, 3]$ (SEC, perfect), $[4, 1, 4]$ (SECDED), $[5, 1, 5]$ (DEC), etc. This family of codes just repeats any given data bit n times; when decoding, one simply needs to determine which of the two codewords that the received code is nearest to. The $[3, 1, 3]$ code illustrated in Figure 4.1b is given by

$$H_{[3,1,3]} = \begin{pmatrix} 1 & 1 & 0 \\ 1 & 0 & 1 \end{pmatrix}, \quad V_{[3,1,3]} = \begin{pmatrix} 1 \\ 1 \\ 1 \end{pmatrix}, \quad W_{[3,1,3]} = \begin{pmatrix} 0 & 1 \\ 0 & 1 \\ 0 & 1 \end{pmatrix}. \quad (4.7)$$

Other binary repetition codes have a parity submatrix of similar form (a column of 1's). As seen for $n = 3$ in Figure 4.3b, via Construction A, the $[n, 1, n]$ binary repetition code generates the D_n^* lattice (see §2.3), which for $n = 3$ is BCC. Via Construction B, on the other hand, the $[8, 1, 8]$ binary repetition code generates the E_8 lattice (see §2.5). Note also that the $[3, 2, 2]$ binary single parity-check code with each bit in V repeated vertically m times leads to a $[3m, 2, 2m]$ code, which may subsequently be rearranged into systematic form; taking $m = 4$ and applying Construction B, the resulting $[12, 2, 8]$ code, which is TECQED, generates the Λ_{12}^{\max} lattice (see §2.6).

4.1.3. Binary Hamming codes. The $[2^m - 1, 2^m - 1 - m, 3]$ *binary Hamming codes* are perfect and SEC, and include $[3, 1, 3]$, $[7, 4, 3]$, $[15, 11, 3]$, $[31, 26, 3]$, $[63, 57, 3]$, $[127, 120, 3]$, etc. For a given $(2^m - 1 - m)$ data bits to be transmitted, each parity bit is generated such that the sum (mod 2) of a particular subset of the data bits plus that parity bit is 0. Note that, when decoding, the m parity bits may be used in a simple fashion to determine not only whether or not a single bit error occurred (which is true if one or more of these parity bits is nonzero), but if it did, *which* bit contains the error, as discussed further in §4.4. To illustrate, the venerable $[7, 4, 3]$ code, with four data bits $\{d_1, d_2, d_3, d_4\}$ and three parity bits $\{b_1, b_2, b_3\}$, is given by

²⁹As mentioned previously, when $q = 2$, we suppress the q subscript for notational clarity; we thus do this throughout §4.1.

$$H_{[7,4,3]} = \begin{pmatrix} 0 & 1 & 1 & 1 & 1 & 0 & 0 \\ 1 & 0 & 1 & 1 & 0 & 1 & 0 \\ 1 & 1 & 0 & 1 & 0 & 0 & 1 \end{pmatrix}, \quad V_{[7,4,3]} = \begin{pmatrix} 1 & 0 & 0 & 0 \\ 0 & 1 & 0 & 0 \\ 0 & 0 & 1 & 0 \\ 0 & 0 & 0 & 1 \\ 0 & 1 & 1 & 1 \\ 1 & 0 & 1 & 1 \\ 1 & 1 & 0 & 1 \end{pmatrix}, \quad \mathbf{w} = \begin{pmatrix} d_1 \\ d_2 \\ d_3 \\ d_4 \\ b_1 \\ b_2 \\ b_3 \end{pmatrix}, \quad (4.8a)$$

$$W_{[7,4,3]} = \begin{pmatrix} 0 & 1 & 0 & 1 & 0 & 1 & 0 & 1 & 0 & 1 & 0 & 1 & 0 & 1 & 0 & 1 \\ 0 & 0 & 1 & 1 & 0 & 0 & 1 & 1 & 0 & 0 & 1 & 1 & 0 & 0 & 1 & 1 \\ 0 & 0 & 0 & 0 & 1 & 1 & 1 & 1 & 0 & 0 & 0 & 0 & 1 & 1 & 1 & 1 \\ 0 & 0 & 0 & 0 & 0 & 0 & 0 & 0 & 1 & 1 & 1 & 1 & 1 & 1 & 1 & 1 \\ 0 & 0 & 1 & 1 & 1 & 1 & 0 & 0 & 1 & 1 & 0 & 0 & 0 & 0 & 1 & 1 \\ 0 & 1 & 0 & 1 & 1 & 0 & 1 & 0 & 1 & 0 & 1 & 0 & 0 & 1 & 0 & 1 \end{pmatrix}. \quad (4.8b)$$

The parity-check matrix H of the $[7,4,3]$ code has as columns all nonzero binary vectors of length $(n-k) = 3$; when expressed in systematic form, the $(n-k)$ columns of H corresponding to the identity matrix are shifted to the end, and the remaining k columns of H , in arbitrary order, make up the parity submatrix P . Other binary Hamming codes may be built up similarly. Via Construction A, the $[7,4,3]$ binary Hamming code generates the E_7^* lattice (see §2.5).

A Hamming code (binary or otherwise), with $d = 3$, can only correct a single error in an unknown position. However, it can correct up to two *erasures* (cf. §4.1.1). A common application of this capability is in a RAID 6 system, a popular RAID configuration for very large storage systems in data critical applications. In such a system, data may be striped across n drives using a Hamming code; if any single drive fails, the data on it can be recovered using an appropriate parity check equation (that is, one of the parity check equations that takes that bit into account). If (while rebuilding the information on that disk, which might take a while if the disk is large) a *second* drive fails, then two useful equations may be derived from the $(n-k)$ parity check equations: one that takes failed disk A into account but not failed disk B, and one that takes failed disk B into account but not failed disk A. By restoring parity in these two derived equations, the information on *both* drives may be rebuilt.

4.1.4. Binary simplex codes. The dual of the binary Hamming codes are the $[2^m - 1, m, 2^{m-1}]$ *binary simplex codes* [a.k.a. the binary *maximum-length-sequence (MLS)* codes], which include $[3, 2, 2]$ (SED), $[7, 3, 4]$ (SECCED), $[15, 4, 8]$ (TECCQED), etc. These codes are remarkable geometrically, as their codewords form a regular simplex. The $[3, 2, 2]$ code is illustrated in Figure 4.1a; the $[7, 3, 4]$ code is given by

$$H_{[7,3,4]} = \begin{pmatrix} 0 & 1 & 1 & 1 & 0 & 0 & 0 \\ 1 & 0 & 1 & 0 & 1 & 0 & 0 \\ 1 & 1 & 0 & 0 & 0 & 1 & 0 \\ 1 & 1 & 1 & 0 & 0 & 0 & 1 \end{pmatrix}, \quad V_{[7,3,4]} = \begin{pmatrix} 1 & 0 & 0 \\ 0 & 1 & 0 \\ 0 & 0 & 1 \\ 0 & 1 & 1 \\ 1 & 0 & 1 \\ 1 & 1 & 0 \\ 1 & 1 & 1 \end{pmatrix}. \quad (4.9)$$

Other binary simplex codes have a parity submatrix given similarly by the transpose of the corresponding binary Hamming code. Via Construction A, the $[7, 3, 4]$ binary simplex code generates the E_7 lattice (see §2.5). Via Construction B, on the other hand, the $[15, 4, 8]$ binary simplex code generates the Λ_{15} lattice (see §2.6).

4.1.5. Extended binary Hamming codes. The $[2^m, 2^m - 1 - m, 4]$ *extended binary Hamming codes* are quasi-perfect and SECCED, and include $[4, 1, 4]$, $[8, 4, 4]$ (self-dual), $[16, 11, 4]$, etc. These codes are just binary Hamming codes (see §4.1.3) with an additional overall parity bit (see §4.1.1), and thus, assuming no more than 2 bit errors have occurred, may be decoded similarly, as discussed further in §4.4. To illustrate, the venerable $[8, 4, 4]$ code is given by

$$H_{[8,4,4]} = \begin{pmatrix} 0 & 1 & 1 & 1 & 1 & 0 & 0 & 0 \\ 1 & 0 & 1 & 1 & 0 & 1 & 0 & 0 \\ 1 & 1 & 0 & 1 & 0 & 0 & 1 & 0 \\ 1 & 1 & 1 & 0 & 0 & 0 & 0 & 1 \end{pmatrix}, \quad V_{[8,4,4]} = \begin{pmatrix} 1 & 0 & 0 & 0 \\ 0 & 1 & 0 & 0 \\ 0 & 0 & 1 & 0 \\ 0 & 0 & 0 & 1 \\ 0 & 1 & 1 & 1 \\ 1 & 0 & 1 & 1 \\ 1 & 1 & 0 & 1 \\ 1 & 1 & 1 & 0 \end{pmatrix}. \quad (4.10)$$

Other extended binary Hamming codes have a parity submatrix that may similarly be constructed by adding an overall parity bit to the corresponding binary Hamming code. Via Construction A, the $[8, 4, 4]$ extended binary Hamming code again generates the E_8 lattice.

4.1.6. Binary biorthogonal codes. The dual of the extended binary Hamming codes are the $[2^m, m + 1, 2^{m-1}]$ *binary biorthogonal codes* (a.k.a. *Hadamard codes*), and include $[4, 3, 2]$ (SED), $[8, 4, 4]$ (SECDED, self-dual), $[16, 5, 8]$ (TECQED), $[32, 6, 16]$, etc. The $[32, 6, 16]$ code was used on the Mariner 9 spacecraft. These codes are distinguished by the characteristic that their codewords are mutually orthogonal [that is, $\mathbf{w}^i \cdot \mathbf{w}^j = 0 \pmod{2}$ for $i \neq j$]. Note that the $[4, 3, 2]$ and $[8, 4, 4]$ codes have already been discussed above. The binary biorthogonal codes each have a parity submatrix that is simply the transpose of the parity submatrix of the corresponding extended binary Hamming code, the construction of which is described in §4.1.5. Via Construction B, the $[16, 5, 8]$ binary biorthogonal code generates the Λ_{16} lattice.

4.1.7. Binary quadratic residue codes. The $[n, (n + 1)/2, d]$ *binary quadratic residue codes* are defined for all prime n for which there exists an integer $1 < x < n$ such that $x^2 = 2 \pmod{n}$ [equivalently, for all prime n of the form $n = 8m \pm 1$ where m is an integer], and include $[7, 4, 3]$ (SEC, perfect, as introduced in §4.1.3), $[17, 9, 5]$ (DEC), $[23, 12, 7]$ (TEC, perfect, a.k.a. the *binary Golay code*), $[31, 16, 7]$ (TEC), $[41, 21, 9]$ (QEC), $[47, 24, 11]$, etc. Adding an overall parity bit to these codes, the $[n + 1, (n + 1)/2, d + 1]$ *extended binary quadratic residue codes* include $[8, 4, 4]$ (SECDED, quasi-perfect, self-dual, as introduced in §4.1.5), $[18, 9, 6]$ (DECTED), $[24, 12, 8]$ (TECQED, quasi-perfect, self-dual, a.k.a. the *extended binary Golay code*), $[32, 16, 8]$ (TECQED), $[42, 21, 10]$, $[48, 24, 12]$, etc. The venerable $[24, 12, 8]$ extended binary Golay code, which was used by the Voyager 1 & 2 spacecraft, is given by

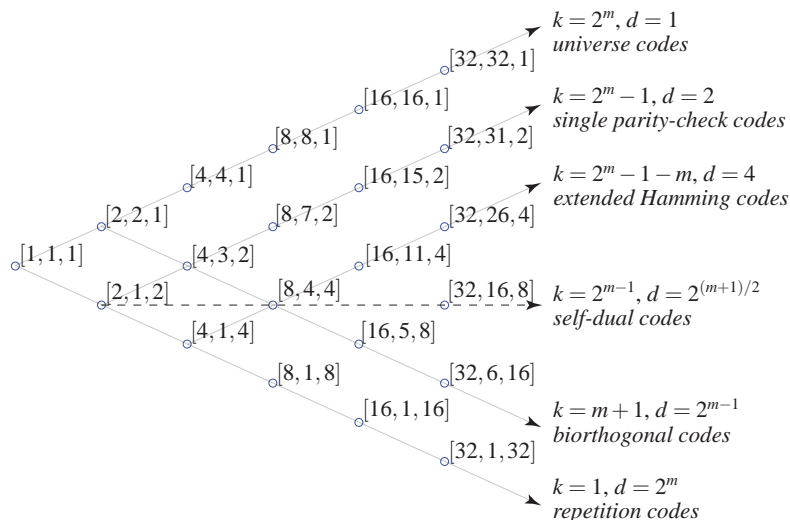
$$H_{[24,12,8]} = [P_{12 \times 12} \quad I_{12 \times 12}], \quad V_{[24,12,8]} = \begin{bmatrix} I_{12 \times 12} \\ P_{12 \times 12} \end{bmatrix},$$

$$P_{12 \times 12} = \begin{pmatrix} 0 & 1 & 1 & 1 & 1 & 1 & 1 & 1 & 1 & 1 & 1 & 1 \\ 1 & 1 & 1 & 0 & 1 & 1 & 1 & 0 & 0 & 0 & 1 & 0 \\ 1 & 1 & 0 & 1 & 1 & 1 & 0 & 0 & 0 & 1 & 0 & 1 \\ 1 & 0 & 1 & 1 & 1 & 0 & 0 & 0 & 1 & 0 & 1 & 1 \\ 1 & 1 & 1 & 1 & 0 & 0 & 0 & 1 & 0 & 1 & 1 & 0 \\ 1 & 1 & 1 & 0 & 0 & 0 & 1 & 0 & 1 & 1 & 0 & 1 \\ 1 & 1 & 0 & 0 & 0 & 1 & 0 & 1 & 1 & 0 & 1 & 1 \\ 1 & 0 & 0 & 0 & 1 & 0 & 1 & 1 & 0 & 1 & 1 & 1 \\ 1 & 0 & 0 & 1 & 0 & 1 & 1 & 0 & 1 & 1 & 1 & 0 \\ 1 & 0 & 1 & 0 & 1 & 1 & 0 & 1 & 1 & 1 & 0 & 0 \\ 1 & 1 & 0 & 1 & 1 & 0 & 1 & 1 & 1 & 0 & 0 & 0 \\ 1 & 0 & 1 & 1 & 0 & 1 & 1 & 1 & 0 & 0 & 0 & 1 \end{pmatrix}. \quad (4.11)$$

Note that P is symmetric. The $[23, 12, 7]$ binary Golay code may be obtained by *puncturing* the $[24, 12, 8]$ code listed above; that is, by eliminating any row of P (typically, the last).

Via Construction B, the $[24, 12, 8]$ extended binary Golay code generates the *Leech half-lattice* H_{24} , which may be joined with a translate of itself [that is, $H_{24} + \mathbf{a}$ where $a_1 = -3/2$ and $a_k = 1/2$ for $k = 2, \dots, 24$] to construct the Λ_{24} lattice.

Note that many of the binary codes introduced above fall within a larger family of codes collectively referred to as *Reed-Muller codes*, as illustrated in Figure 4.4.


 FIG. 4.4. The family of $[2^m, k, d]$ Reed-Muller binary codes for $m = 0$ to 5.

4.1.8. Extending, puncturing, and shortening. The (perfect) binary Hamming and binary Golay codes may be *extended* to quasi-perfect codes by adding an overall parity bit, thereby increasing n by 1 and, in the case of these specific codes, increasing d by 1. A code obtained by essentially the reverse of this process, removing a parity bit and thus reducing both n and d by 1, is sometimes said to be *punctured*. In contrast, a code obtained by removing $\ell \geq 1$ data bits, thus reducing both n and k by ℓ , is said to be *shortened*. A typical and common application is in error-correcting memory systems for computers, in which the data often comes naturally in blocks of 64 bits. Starting from the $[127, 120, 3]$ binary Hamming code, one may eliminate 56 data bits to create a shortened $[71, 64, 3]$ SEC code; alternatively, starting from the $[128, 120, 4]$ extended binary Hamming code, one may eliminate 56 data bits to create a shortened $[72, 64, 4]$ SECDED code. Many ECC Memory and RAID 6 storage systems are based on variants of such shortened binary Hamming codes, which are simple and fast to use. Note also that, via Construction B, the $[21, 9, 8]$ code obtained by shortening the $[24, 12, 8]$ extended binary Golay code by 3 data bits generates directly the Λ_{21} lattice.

4.2. Exemplary linear ternary codes (LTCs). We now summarize some of the families of LTCs available, presenting each in systematic form (4.1), noting that all have analogs in the binary setting.

4.2.1. Ternary single parity-check codes. The $[n, n-1, 2]_3$ ternary single parity-check codes are SED, and include $[2, 1, 2]_3$ (self-dual), $[3, 2, 2]_3$, $[4, 3, 2]_3$, etc. As illustrated for $n = 3$ in Figure 4.2a, the $[3, 2, 2]_3$ code is given by

$$H_{[3,2,2]_3} = \begin{pmatrix} 1 & 1 & 1 \end{pmatrix}, \quad V_{[3,2,2]_3} = \begin{pmatrix} 1 & 0 \\ 0 & 1 \\ 2 & 2 \end{pmatrix}, \quad W_{[3,2,2]_3} = \begin{pmatrix} 0 & 1 & 2 & 0 & 1 & 2 & 0 & 1 & 2 \\ 0 & 0 & 0 & 1 & 1 & 1 & 2 & 2 & 2 \\ 0 & 2 & 1 & 2 & 1 & 0 & 1 & 0 & 2 \end{pmatrix}. \quad (4.12)$$

Other ternary single parity-check codes have a parity submatrix P [see (4.3)] of similar form (a row of 2's). Via Construction $A_{\mathcal{G}}^{\theta}$, the $[3, 2, 2]_3$ ternary single parity-check code generates the E_6^* lattice.

4.2.2. Ternary repetition codes. The dual of the ternary single parity-check codes are the $[n, 1, n]_3$ ternary repetition codes, which include $[2, 1, 2]_3$ (SED, self-dual), $[3, 1, 3]_3$ (SEC), $[4, 1, 4]_3$ (SECDED), etc. As illustrated for $n = 3$ in Figure 4.2b, the $[3, 1, 3]_3$ code is given by

$$H_{[3,1,3]_3} = \begin{pmatrix} 2 & 1 & 0 \\ 2 & 0 & 1 \end{pmatrix}, \quad V_{[3,1,3]_3} = \begin{pmatrix} 1 \\ 1 \\ 1 \end{pmatrix}, \quad W_{[3,1,3]_3} = \begin{pmatrix} 0 & 1 & 2 \\ 0 & 1 & 2 \\ 0 & 1 & 2 \end{pmatrix}. \quad (4.13)$$

Other ternary repetition codes have a parity submatrix of similar form (a column of 1's). Via Construction $A_{\mathcal{E}}^\theta$, the $[3, 1, 3]_3$ ternary repetition code generates the E_6 lattice. Via Construction $B_{\mathcal{E}}^\theta$, on the other hand, the $[6, 1, 6]_3$ ternary repetition code generates the K_{12} lattice.

4.2.3. Ternary Hamming codes. The $[(3^m - 1)/2, (3^m - 1)/2 - m, 3]_3$ ternary Hamming codes are perfect and SEC, and include $[4, 2, 3]_3$ (self-dual, a.k.a. the *tetracode*), $[13, 10, 3]_3$, $[40, 36, 3]_3$, etc. To illustrate, the venerable $[4, 2, 3]_3$ tetracode is given by

$$H_{[4,2,3]_3} = \begin{pmatrix} 1 & 1 & 1 & 0 \\ 1 & 2 & 0 & 1 \end{pmatrix}, \quad V_{[4,2,3]_3} = \begin{pmatrix} 1 & 0 \\ 0 & 1 \\ 2 & 2 \\ 2 & 1 \end{pmatrix}. \quad (4.14)$$

The parity-check matrix H of the $[4, 2, 3]_3$ code has as columns those nonzero ternary vectors of length $(n - k) = 2$ whose first nonzero entry is 1; when expressed in systematic form, the $(n - k)$ columns of H corresponding to the identity matrix are shifted to the end, and the remaining k columns of H , in arbitrary order, make up the entries of $-P$. Other ternary Hamming codes may be built up similarly; for example, the $[13, 10, 3]_3$ code is given by

$$H_{[13,10,3]_3} = \begin{pmatrix} 0 & 0 & 1 & 1 & 1 & 1 & 1 & 1 & 1 & 1 & 1 & 0 & 0 \\ 1 & 1 & 0 & 0 & 1 & 1 & 1 & 2 & 2 & 2 & 0 & 1 & 0 \\ 1 & 2 & 1 & 2 & 0 & 1 & 2 & 0 & 1 & 2 & 0 & 0 & 1 \end{pmatrix}, \quad V_{[13,10,3]_3} = \begin{bmatrix} I_{10 \times 10} \\ P_{3 \times 10} \end{bmatrix}. \quad (4.15)$$

$\underbrace{\hspace{10em}}_{\triangleq -P_{3 \times 10}}$

Via Construction $A_{\mathcal{E}}^\theta$, the $[4, 2, 3]_3$ tetracode again generates the E_8 lattice.

4.2.4. Ternary simplex codes. The dual of the ternary Hamming codes are the $[(3^m - 1)/2, m, 3^{m-1}]_3$ ternary simplex codes, which include $[4, 2, 3]_3$ (SEC, perfect, self-dual), $[13, 3, 9]_3$ (QEC), $[40, 4, 27]_3$, etc. These codes are remarkable geometrically, as their codewords are all equidistant from one another. Ternary simplex codes have a parity submatrix given by the negative transpose of the corresponding ternary Hamming code.

4.2.5. Ternary quadratic residue codes. The $[n, (n+1)/2, d]_3$ ternary quadratic residue codes are defined for all prime n for which there exists an integer $1 < x < n$ such that $x^2 = 3 \pmod{n}$ [equivalently, for all prime n of the form $n = 12m \pm 1$ where m is an integer], and include $[11, 6, 5]_3$ (DEC, perfect, a.k.a. the *ternary Golay code*), $[13, 7, 5]_3$ (DEC), $[23, 12, 8]_3$ (TECQED), $[37, 19, 10]_3$, $[47, 24, 14]_3$, etc. Adding an overall parity bit to these codes, the $[n+1, (n+1)/2, d+1]_3$ extended ternary quadratic residue codes include $[12, 6, 6]_3$ (DECTED, quasi-perfect, self-dual, a.k.a. the *extended ternary Golay code*), $[14, 7, 6]_3$ (DECTED), $[24, 12, 9]_3$ (QEC), $[38, 19, 11]_3$, $[48, 24, 15]_3$, etc. The venerable $[12, 6, 6]_3$ extended ternary Golay code is given by

$$H_{[12,6,6]_3} = [-P_{6 \times 6} \quad I_{6 \times 6}], \quad V_{[12,6,6]_3} = \begin{bmatrix} I_{6 \times 6} \\ P_{6 \times 6} \end{bmatrix}, \quad P_{6 \times 6} = \begin{pmatrix} 0 & 1 & 1 & 1 & 1 & 1 \\ 1 & 0 & 1 & 2 & 2 & 1 \\ 1 & 1 & 0 & 1 & 2 & 2 \\ 1 & 2 & 1 & 0 & 1 & 2 \\ 1 & 2 & 2 & 1 & 0 & 1 \\ 1 & 1 & 2 & 2 & 1 & 0 \end{pmatrix}. \quad (4.16)$$

Note that P is symmetric. The $[11, 6, 5]_3$ ternary Golay code may be obtained by puncturing the $[12, 6, 6]_3$ code listed above.

Via Construction $B_{\mathcal{E}}^\theta$, the $[12, 6, 6]_3$ extended ternary Golay code generates an intermediate lattice which may be joined with two translates of itself to generate the Λ_{24} lattice.

4.3. Exemplary linear quaternary codes (LQCs). We now summarize some of the families of LQCs available, presenting each in systematic form (4.1).

4.3.1. Quaternary single parity-check codes. The $[n, n-1, 2]_4$ *quaternary single parity-check codes* are SED, and include $[2, 1, 2]_4$ (self-dual), $[3, 2, 2]_4$, $[4, 3, 2]_4$, etc. The $[3, 2, 2]_4$ code is given by

$$H_{[3,2,2]_4} = (1 \ 1 \ 1), \quad V_{[3,2,2]_4} = \begin{pmatrix} 1 & 0 \\ 0 & 1 \\ 1 & 1 \end{pmatrix}, \quad (4.17)$$

$$W_{[3,2,2]_4} = \begin{pmatrix} 0 & 1 & \omega & \bar{\omega} & 0 & 1 & \omega & \bar{\omega} & 0 & 1 & \omega & \bar{\omega} & 0 & 1 & \omega & \bar{\omega} \\ 0 & 0 & 0 & 0 & 1 & 1 & 1 & 1 & \omega & \omega & \omega & \omega & \bar{\omega} & \bar{\omega} & \bar{\omega} & \bar{\omega} \\ 0 & 1 & \omega & \bar{\omega} & 1 & 0 & \bar{\omega} & \omega & \omega & \bar{\omega} & 0 & 1 & \bar{\omega} & \omega & 1 & 0 \end{pmatrix}.$$

Other quaternary single parity-check codes have a parity submatrix P of similar form.

4.3.2. Quaternary repetition codes. The dual of the quaternary single parity-check codes are the $[n, 1, n]_4$ *quaternary repetition codes*, which include $[2, 1, 2]_4$ (SED, self-dual), $[3, 1, 3]_4$ (SEC), $[4, 1, 4]_4$ (SECEDED), etc. The $[3, 1, 3]_4$ code is given by

$$H_{[3,1,3]_4} = \begin{pmatrix} 1 & 1 & 0 \\ 1 & 0 & 1 \end{pmatrix}, \quad V_{[3,1,3]_4} = \begin{pmatrix} 1 \\ 1 \\ 1 \end{pmatrix}, \quad W_{[3,1,3]_4} = \begin{pmatrix} 0 & 1 & \omega & \bar{\omega} \\ 0 & 1 & \omega & \bar{\omega} \\ 0 & 1 & \omega & \bar{\omega} \end{pmatrix}. \quad (4.18)$$

Other quaternary repetition codes have a parity submatrix of similar form.

4.3.3. Quaternary Hamming codes. The $[(4^m - 1)/3, (4^m - 1)/3 - m, 3]_4$ *quaternary Hamming codes* are perfect and SEC, and include $[5, 3, 3]_4$, $[21, 18, 3]_4$, $[85, 81, 3]_4$, etc. To illustrate, the $[5, 3, 3]_4$ code is given by

$$H_{[5,3,3]_4} = \begin{pmatrix} 1 & 1 & 1 & 1 & 0 \\ 1 & \omega & \bar{\omega} & 0 & 1 \end{pmatrix}, \quad V_{[5,3,3]_4} = \begin{pmatrix} 1 & 0 & 0 \\ 0 & 1 & 0 \\ 0 & 0 & 1 \\ 1 & 1 & 1 \\ 1 & \omega & \bar{\omega} \end{pmatrix}. \quad (4.19)$$

The parity-check matrix H of the $[5, 3, 3]_4$ code has as columns those nonzero quaternary vectors of length $(n - k) = 2$ whose first nonzero entry is 1; when expressed in systematic form, the $(n - k)$ columns of H corresponding to the identity matrix are shifted to the end, and the remaining k columns of H , in arbitrary order, make up the entries of P . Other quaternary Hamming codes may be built up similarly.

4.3.4. Quaternary simplex codes. The dual of the quaternary Hamming codes are the $[(4^m - 1)/3, m, 4^{m-1}]_4$ *quaternary simplex codes*, which include $[5, 2, 4]_4$ (SECEDED), $[21, 3, 16]_4$, $[85, 4, 64]_4$, etc. These codes are remarkable geometrically, as their codewords are all equidistant from one another. Quaternary simplex codes have a parity submatrix given by the conjugate transpose of the corresponding quaternary Hamming code.

4.3.5. Quaternary quadratic residue codes. The $[n, (n+1)/2, d]_4$ *quaternary quadratic residue codes* are defined for all prime n of the form $n = 8m \pm 3$ where m is an integer, and include $[5, 3, 3]_4$ (SEC, perfect, see §4.3.3), $[11, 6, 5]_4$ (DEC), $[13, 7, 5]_4$ (DEC), $[19, 10, 7]_4$ (TEC), $[29, 15, 11]_4$, $[37, 19, 11]_4$, etc. The related $[n+1, (n+1)/2, d+1]_4$ *extended quaternary quadratic residue codes* include $[6, 3, 4]_4$ (SECEDED, quasi-perfect, self-dual, a.k.a. the *hexacode*), $[12, 6, 6]_4$ (DECTED), $[14, 7, 6]_4$ (DECTED, self-dual), $[20, 10, 8]_4$ (TECQED), $[30, 15, 12]_4$ (self-dual), $[38, 19, 12]_4$, etc. The venerable $[6, 3, 4]_4$ hexacode is given by

$$H_{[6,3,4]_4} = \begin{pmatrix} 1 & 1 & 1 & 1 & 0 & 0 \\ 1 & \omega & \bar{\omega} & 0 & 1 & 0 \\ 1 & \bar{\omega} & \omega & 0 & 0 & 1 \end{pmatrix}, \quad V_{[6,3,4]_4} = \begin{pmatrix} 1 & 0 & 0 \\ 0 & 1 & 0 \\ 0 & 0 & 1 \\ 1 & 1 & 1 \\ 1 & \omega & \bar{\omega} \\ 1 & \bar{\omega} & \omega \end{pmatrix}. \quad (4.20)$$

Note that P is symmetric. The $[5, 3, 3]_4$ quaternary quadratic residue code may be obtained by puncturing the $[6, 3, 4]_4$ code listed above.

Via Construction $A_{\mathcal{E}}^2$, the $[6, 3, 4]_4$ hexacode generates the K_{12} lattice.

$$\begin{array}{cccc}
& & & B_{110} \\
& & & A_{110} \quad A_{100} \\
& & B_{000} & B_{010} \quad B_{001} \\
A_{000} & A_{010} & A_{001} & A_{011} \\
& B_{100} & B_{111} & B_{101} \\
& & A_{111} & A_{101} \\
& & & B_{011}
\end{array}$$

FIG. 4.5. A labelling of 16 points of the D_2 lattice (due to Ungerboeck 1982). The A_{ijk} points have coordinates which are both even integers [e.g., $A_{000} = (0 \ 0)$], and the B_{ijk} points have coordinates which are both odd integers [e.g., $B_{000} = (1 \ 1)$]. The complete D_2 lattice is formed by repeating this 2D pattern as an infinite array with unit spacing, as in Figure 4.3; note that each of the subsets of D_2 corresponding to a particular label is itself an appropriate shift of a $4D_2$ lattice (that is, the D_2 lattice with the spacing quadrupled between the points).

The $[6, 3, 4]_4$ hexacode, with $4^3 = 64$ codewords, is of particular importance due to the structured role it plays in some convenient constructions of the $[24, 12, 8]$ extended binary Golay code (see §4.1.7), with $2^{12} = 4096$ codewords \mathbf{w} , and the corresponding Λ_{24} lattice. To construct the extended binary Golay code in this manner (see §11 of Conway & Sloane 1998), we may first arrange binary vectors of length 24 into 4×6 arrays with binary entries. The sum of the bits (mod 2) in any row or column of this array gives its *parity*, which is said to be *even* if the bits sum to 0 and *odd* if the bits sum to 1. We then define the *projection* of any binary vector $\mathbf{d} \in \mathbf{F}_2^4$ onto a symbol $x \in \mathbf{F}_4$ via the product $x = (0 \ 1 \ \omega \ \bar{\omega}) \mathbf{d}$ (on \mathbf{F}_4). The $[24, 12, 8]$ extended binary Golay code is then given by the set of all $\mathbf{w} \in \mathbf{F}_2^{24}$ such that, in the corresponding 4×6 array,

- the parity of all of the columns matches the parity of the top row, and
- the projection of the six columns of the array forms a codeword of the $[6, 3, 4]_4$ hexacode.

An alternative construction of the Λ_{24} lattice, due to Vardy & Be'ery (1993) and which also leverages cleverly the $[6, 3, 4]_4$ hexacode, is based on the Ungerboeck (1982) partitioning of the D_2 lattice (see §2.3) into A_{ijk} and B_{ijk} subsets, as depicted in Figure 4.5. Binary vectors of length 24 are now constructed as 2×6 arrays whose entries are points of D_2 , labelled as shown. When considering a pair of such points [say, $\mathbf{c} = (A_{i_1, j_1, k_1} \ A_{i_2, j_2, k_2})^T$],

- the pair is said to be *even* or *odd* based on the sum (mod 2) of the indices $\{i_1, j_1, i_2, j_2\}$,
- the index i_1 is known as the *h-parity* of the pair,
- the sum (mod 2) of k_1 and k_2 is known as the *k-parity* of the pair, and
- the *projection* of the pair is defined as above, based on the vector $\mathbf{d} = (i_1 \ j_1 \ i_2 \ j_2)^T$.

The Leech lattice Λ_{24} is then given by the set of all $\mathbf{u} \in \mathbb{Z}^{24}$ such that, in the corresponding 2×6 array,

- all array entries are either points in the A_{ijk} subsets of D_2 (referred to as a *type-A* array), or points in the B_{ijk} subsets of D_2 (referred to as a *type-B* array),
- the overall *k* parity of the array [that is, the sum (mod 2) of the *k*-parity of the 6 pairs of points] is even if the array is type *A* and odd if the array is type *B*,
- the pairs of points in the 6 columns of the array are either all even (referred to as an *even* array) or all odd (referred to as an *odd* array),
- the overall *h* parity of the array [that is, the sum (mod 2) of the *h*-parity of the 6 pairs of points] is even if the array even and odd if the array is odd, and
- the projection of the six columns of the array forms a codeword of the $[6, 3, 4]_4$ hexacode.

The union of all points corresponding to Type A arrays in this construction forms the *Leech half lattice* H_{24} mentioned in §4.1.7, whereas the union of all points corresponding to Type B arrays forms its translate, $H_{24} + \mathbf{a}$. The H_{24} lattice can be further decomposed into all points corresponding to even arrays, which forms the *Leech quarter lattice* Q_{24} , and all points corresponding to odd arrays, which forms its translate, $Q_{24} + \mathbf{b}$. The Λ_{24} lattice is then given by the union of Q_{24} , $Q_{24} + \mathbf{b}$, $Q_{24} + \mathbf{a}$, and $Q_{24} + \mathbf{a} + \mathbf{b}$; this construction is exploited in §5.5 when presenting a remarkably efficient algorithm for quantization from \mathbb{R}^{24} to Λ_{24} .

4.4. Decoding. The use of an $[n, k, d]_q$ linear code (a.k.a. *linear block code*) in practice to communicate data over a noisy channel is straightforward:

- arrange the original data into *blocks* of length k over an *alphabet* of q symbols;
- *code* each resulting data vector $\mathbf{d} \in \mathbf{F}_q^k$ into a longer codeword $\mathbf{w} \in \mathbf{F}_q^n$ via $\mathbf{w} = V_{[n,k,d]_q} \mathbf{d}$;
- transmit the corresponding codeword $\mathbf{w} \in \mathbf{F}_q^n$ over the noisy channel;
- receive the (possibly corrupted) message $\hat{\mathbf{w}} \in \mathbf{F}_q^n$ on the other end;
- *decode* the received message $\hat{\mathbf{w}}$ leveraging $H_{[n,k,d]_q}$; that is, find the most likely codeword \mathbf{w} corresponding to the received message $\hat{\mathbf{w}}$, and the data vector \mathbf{d} that generated it.

The decoding problem is quite rich; many creative schemes have been proposed over the years for decoding the various LCs that have been introduced thus far, as well as many others. This subject goes a bit beyond the scope of the present review, but we would be remiss if we didn't at least briefly introduce a few exemplary decoding strategies.

For the purpose of fast decoding of an LC, it is useful to consider convenient alternatives to the systematic form. If H and V are the parity-check and basis matrices of an $[n, k, d]_q$ LC in systematic form, with $HV = 0$ (on \mathbf{F}_q), then an *equivalent* LC, possibly not in systematic form, is given by taking

$$\tilde{H} = HQ \quad \text{and} \quad \tilde{V} = Q^{-1}V. \quad (4.21)$$

It follows immediately that, again, $\tilde{H}\tilde{V} = 0$ (on \mathbf{F}_q). In the simplest such transformation, Q is a permutation matrix, and thus $Q^{-1} = Q^T$; this transformation corresponds to reordering the rows of V and the corresponding columns of H (that is, reordering the data bits and parity bits in the corresponding LC). Other equivalent LCs may be constructed in this manner by relaxing the constraint that Q be a permutation matrix, effectively taking linear combinations (on \mathbf{F}_q) of the rows of V and the corresponding columns of H . Note further that reordering the columns of V and/or the rows of H leaves an LC unchanged.

4.4.1. Algebraic decoding. Certain LBCs may be decoded quickly by arranging the columns of the parity-check matrix in a convenient order and examining the binary number given by the product of the parity-check matrix and the (possibly, corrupted) received message. To illustrate, consider the $[7, 4, 3]$ binary Hamming code introduced in §4.1.3. Transforming as described above with

$$Q = \begin{pmatrix} 0 & 0 & 1 & 0 & 0 & 0 & 0 \\ 0 & 0 & 0 & 0 & 1 & 0 & 0 \\ 0 & 0 & 0 & 0 & 0 & 1 & 0 \\ 0 & 0 & 0 & 0 & 0 & 0 & 1 \\ 0 & 0 & 0 & 1 & 0 & 0 & 0 \\ 0 & 1 & 0 & 0 & 0 & 0 & 0 \\ 1 & 0 & 0 & 0 & 0 & 0 & 0 \end{pmatrix}$$

results in a modified basis matrix \tilde{V} , and a modified parity-check matrix \tilde{H} arranged such that the columns of \tilde{H} appear in binary order:

$$\tilde{H}_{[7,4,3]} = \begin{pmatrix} 0 & 0 & 0 & 1 & 1 & 1 & 1 \\ 0 & 1 & 1 & 0 & 0 & 1 & 1 \\ 1 & 0 & 1 & 0 & 1 & 0 & 1 \end{pmatrix}, \quad \tilde{V}_{[7,4,3]} = \begin{pmatrix} 1 & 1 & 0 & 1 \\ 1 & 0 & 1 & 1 \\ 1 & 0 & 0 & 0 \\ 0 & 1 & 1 & 1 \\ 0 & 1 & 0 & 0 \\ 0 & 0 & 1 & 0 \\ 0 & 0 & 0 & 1 \end{pmatrix}, \quad \tilde{\mathbf{w}} = \begin{pmatrix} b_3 \\ b_2 \\ d_1 \\ b_1 \\ d_2 \\ d_3 \\ d_4 \end{pmatrix}. \quad (4.22)$$

Taking the matrix $\tilde{H}_{[2^m-1, 2^m-1-m, 3]}$ of a binary Hamming code arranged in such a fashion (in the above example, $m = 3$) times (mod 2) any of the codewords $\tilde{\mathbf{w}}$ (generated via $\tilde{\mathbf{w}} = \tilde{V}_{[2^m-1, 2^m-1-m, 3]} \mathbf{d}$ where $\mathbf{d} \in \mathbf{F}_2^{2^m-1-m}$) gives the zero vector. On the other hand, taking the matrix $\tilde{H}_{[2^m-1, 2^m-1-m, 3]}$ times (mod 2) any invalid vector $\hat{\tilde{\mathbf{w}}}$ gives the nonzero *syndrome*

vector \mathbf{s} , of order $m = n - k$, which may be interpreted as a nonzero m -bit binary number called the *syndrome*, denoted s , of the received message. Conveniently, as a direct result of the structure of \tilde{H} used in this construction, the number s identifies precisely which bit of the received message vector $\hat{\mathbf{w}}$, arranged as shown above, must be flipped in order to determine the nearest codeword, thereby performing single error correction (SEC).

Consider now the class of $[2^m, 2^m - 1 - m, 4]$ extended binary Hamming codes introduced in §4.1.5. Define the syndrome s as in the corresponding binary Hamming code of length $(2^m - 1)$ as discussed above, neglecting the overall parity bit, and define p as the sum (mod 2) over all the bits, including the overall parity bit. There are zero bit errors if $s = p = 0$, there two bit errors (which may be detected but not uniquely corrected) if $s \neq 0$ and $p = 0$, and there is a single bit error if $p = 1$ (in which case, if $s = 0$, this error is in the overall parity bit, and, if $s \neq 0$, this error is in one of the other bits and may be corrected based on s just as in the corresponding binary Hamming code). This strategy thus performs single error correction and double error detection (SECDED).

The extended binary Golay code introduced in §4.1.7 may be decoded via syndrome computation in a similar fashion, though several more checks are involved, as the procedure performs triple error correction and quadruple error detection (TECQED) on the received message $\hat{\mathbf{w}}$. Recall the definitions of H , V , and $P = P^T$ for the $[24, 12, 8]$ extended binary Golay code in systematic form, as listed in (4.11). Note that $V^T V = 0$, and thus V^T serves as an alternative parity-check matrix for this code. Defining $w_H(\mathbf{s})$ as the Hamming weight (that is, the number of nonzero elements) of the vector \mathbf{s} , and defining \mathbf{p}^i as the i 'th column of P , \mathbf{e}^i as the i 'th Cartesian unit vector, and $\mathbf{0}$ as the zero vector, we may decode $\hat{\mathbf{w}}$ as follows:

```

set  $\mathbf{s} = V^T \hat{\mathbf{w}}$ , if  $w_H(\mathbf{s}) \leq 3$  then set  $\mathbf{c} = \begin{bmatrix} \mathbf{s}; & \mathbf{0} \end{bmatrix}$ , flag=0, return, end if (case A)
set  $\mathbf{r} = P\mathbf{s}$ , if  $w_H(\mathbf{r}) \leq 3$  then set  $\mathbf{c} = \begin{bmatrix} \mathbf{0}; & \mathbf{r} \end{bmatrix}$ , flag=0, return, end if (case B)
for  $i = 1 : 12$ 
  if  $w_H(\mathbf{s} + \mathbf{p}^i) \leq 2$  then set  $\mathbf{c} = \begin{bmatrix} \mathbf{s} + \mathbf{p}^i; & \mathbf{e}^i \end{bmatrix}$ , flag=0, return, end if (case C)
  if  $w_H(\mathbf{r} + \mathbf{p}^i) \leq 2$  then set  $\mathbf{c} = \begin{bmatrix} \mathbf{e}^i; & \mathbf{r} + \mathbf{p}^i \end{bmatrix}$ , flag=0, return, end if (case D)
end for
flag=1; return (4 total errors, can not be uniquely corrected)

```

Upon return, assuming the received vector $\hat{\mathbf{w}}$ has 4 or less bit errors, if flag = 0, then 3 or fewer errors are detected and the corrected vector is $\mathbf{w} = \hat{\mathbf{w}} + \mathbf{c}$, whereas if flag = 1, then 4 errors are detected and $\hat{\mathbf{w}}$ can not be uniquely corrected. To verify this algorithm, noting that $V^T \mathbf{w} = 0$ for any codeword \mathbf{w} , it is sufficient to analyze the algorithm for $\mathbf{w} = \mathbf{0}$ only. Block partitioning $\hat{\mathbf{w}} = \begin{bmatrix} \mathbf{x}; & \mathbf{y} \end{bmatrix}$, consider the following 4 correctable cases:

Case A (0 parity bit errors, up to 3 data bit errors): Due to the structure of P , parity bit errors (that is, $w_H(\mathbf{y}) \neq 0$) result in $w_H(\mathbf{s}) \geq 6$; if $w_H(\mathbf{s})$ is less than this, then $\mathbf{y} = \mathbf{0}$ and $\mathbf{s} = V^T \hat{\mathbf{w}} = I\mathbf{x} = \mathbf{x}$.

Case B (0 data bit errors, up to 3 parity bit errors): Note that $PV^T = H$, and thus $\mathbf{r} = H\hat{\mathbf{w}}$. By an analogous argument as that used in Case A, due to the structure of P , data bit errors (that is, $w_H(\mathbf{x}) \neq 0$) result in $w_H(\mathbf{r}) \geq 6$; if $w_H(\mathbf{s})$ is less than this, then $\mathbf{x} = \mathbf{0}$ and $\mathbf{r} = H\hat{\mathbf{w}} = I\mathbf{y} = \mathbf{y}$.

Case C (1 parity bit error, up to 2 data bit errors): In this case, we individually check each of the (12) possible cases corresponding to a single parity bit error, essentially repeating the analysis of Case A, mutatis mutandis. That is, for each i , we consider the possibility that $\mathbf{y} = \mathbf{e}^i$, and thus $\mathbf{s} = \mathbf{x} + \mathbf{p}^i$, and check to see if $w_H(\mathbf{x}) = w_H(\mathbf{s} + \mathbf{p}^i) \leq 2$.

Case D (1 data bit error, up to 2 parity bit errors): In this case, we individually check each of the (12) possible cases corresponding to a single data bit error, essentially repeating the analysis of Case B, mutatis mutandis (cf. Case C).

4.4.2. Cyclic form. A *cyclic code* is an LC that may be transformed [via (4.21)] into a form in which all cyclic shifts of codewords are themselves also codewords. The basis matrix $V = V_{n \times k}$ and parity-check matrix $H = H_{(n-k) \times n}$ of any $[n, k]_q$ cyclic code may be written in the standard form

$$H_{[n,k]_q} = \begin{pmatrix} h_k & h_{k-1} & \dots & h_0 & & & & 0 \\ & h_k & h_{k-1} & \dots & h_0 & & & \\ & & \ddots & \ddots & \ddots & \ddots & & \\ 0 & & & h_k & h_{k-1} & \dots & h_0 & \end{pmatrix}, \quad V_{[n,k]_q} = \begin{pmatrix} v_0 & & & & & & & 0 \\ v_1 & v_0 & & & & & & \\ \vdots & \vdots & \ddots & & & & & \\ v_{n-k} & \vdots & \ddots & \ddots & \ddots & \ddots & v_0 & \\ & v_{n-k} & & \ddots & \ddots & \ddots & v_1 & \\ & & & \ddots & \ddots & \ddots & \vdots & \\ 0 & & & & & & v_{n-k} & \end{pmatrix}. \quad (4.23)$$

A convenient construction which simplifies the analysis of an $[n, k]_q$ cyclic code, as defined above, is the *cyclic shift* operator z . The use of this operator as discussed here is akin to its use in the Z -transform analysis of discrete-time linear systems, with the major difference being that it is used here in a cyclic context on \mathbf{F}_q : that is, arithmetic with polynomials in z and coefficients in \mathbf{F}_q is performed as usual, except that the coefficients of each power of z are combined via the arithmetic rules on \mathbf{F}_q (see the second paragraph of §4), and higher powers of z^k are simplified via the cyclic condition

$$z^n = 1. \quad (4.24)$$

In the deployment of an $[n, k]_q$ cyclic code, the operator z appears in

$$\begin{aligned} \text{the data polynomial} & \quad d(z) = d_0 + d_1 z + \dots + d_{k-1} z^{k-1} \\ \text{the basis polynomial} & \quad v(z) = v_0 + v_1 z + \dots + v_{n-k} z^{n-k}, \\ \text{the codeword polynomial} & \quad w(z) = w_0 + w_1 z + \dots + w_{n-1} z^{n-1}, \\ \text{the received-message polynomial} & \quad \hat{w}(z) = \hat{w}_0 + \hat{w}_1 z + \dots + \hat{w}_{n-1} z^{n-1}, \text{ and} \\ \text{the parity-check polynomial} & \quad h(z) = h_0 + h_1 z + \dots + h_k z^k. \end{aligned}$$

The basis polynomial $v(z)$ and parity-check polynomial $h(z)$ are constructed in mutually-orthogonal manner that, taken together, enforces the cyclic condition (4.24):

$$v(z)h(z) = (z^n - 1), \quad (4.25a)$$

which may also be written

$$[v(z)h(z)] \bmod (z^n - 1) = 0; \quad (4.25b)$$

note that the mod command used in (4.25b) means that the polynomial $[v(z)h(z)]$ is divided by the polynomial $(z^n - 1)$ and the remainder is equal to 0. One such factorization of $(z^n - 1)$ on \mathbf{F}_q , which exists for any n and q , is

$$z^n - 1 = (z - 1)(z^{n-1} + z^{n-2} + \dots + z + 1); \quad (4.26)$$

this leads to the single parity check code $[n, n-1, 2]_q$ if one takes $v(z) = (z-1)$ and $h(z)$ equal to the rest, and to the repetition code $[n, 1, n]_q$ if one takes $h(z) = (z-1)$ and $v(z)$ equal to the rest. Other cyclic codes over \mathbf{F}_q for prime q may be built from the unique irreducible factors of the polynomial $(z^n - 1)$, grouping these factors appropriately to form $v(z)$ and $h(z)$; a few such factorizations for various values of n are listed in Table 4 for $q=2$ (in which $-1=1$) and Table 5 for $q=3$ (in which $-1=2$); others are easily found using Mathematica. Factoring

$$\begin{aligned}
z^5 - 1 &= (z+1)(z^4 + z^3 + z^2 + z + 1) \\
z^7 - 1 &= (z+1)(z^3 + z + 1)(z^3 + z^2 + 1) \\
z^{15} - 1 &= (z+1)(z^2 + z + 1)(z^4 + z + 1)(z^4 + z^3 + 1)(z^4 + z^3 + z^2 + z + 1) \\
z^{23} - 1 &= (z+1)(z^{11} + z^9 + z^7 + z^6 + z^5 + z + 1)(z^{11} + z^{10} + z^6 + z^5 + z^4 + z^2 + 1)
\end{aligned}$$

Table 4. Unique irreducible factors of $(z^n - 1)$ over \mathbf{F}_2 for various values of n .

$$\begin{aligned}
z^4 - 1 &= (z+2)(z+1)(z^2+1) \\
z^{11} - 1 &= (z+2)(z^5 + 2z^3 + z^2 + 2z + 2)(z^5 + z^4 + 2z^3 + z^2 + 2) \\
z^{13} - 1 &= (z+2)(z^3 + 2z + 2)(z^3 + z^2 + 2)(z^3 + z^2 + z + 2)(z^3 + 2z^2 + 2z + 2)
\end{aligned}$$

Table 5. Unique irreducible factors of $(z^n - 1)$ over \mathbf{F}_3 for various values of n .

$$z^5 - 1 = (z^2 + \omega z + 1)(z^3 + \omega z^2 + \omega z + 1)$$

Table 6. A useful (though nonunique) factorization of $(z^5 - 1)$ over \mathbf{F}_4 ; note that Table 4 provides an alternative factorization of $(z^5 - 1)$ over \mathbf{F}_2 which is also valid over \mathbf{F}_4 .

code	description	$v(z)$	$h(z)$
$[n, n-1, 2]_2$	§4.1.1	$z+1$	$z^{n-1} + z^{n-2} + \dots + z + 1$
$[n, 1, n]_2$	§4.1.2	$z^{n-1} + z^{n-2} + \dots + z + 1$	$z+1$
$[7, 4, 3]_2$	§4.1.3	$z^3 + z + 1$	$z^4 + z^2 + z + 1$
$[15, 11, 3]_2$	§4.1.3	$z^4 + z + 1$	$z^{11} + z^8 + z^7 + z^5 + z^3 + z^2 + z + 1$
$[31, 26, 3]_2$	§4.1.3	$z^5 + z^2 + 1$	$(z^{31} - 1)/(z^5 + z^2 + 1)$ over \mathbf{F}_2
$[63, 57, 3]_2$	§4.1.3	$z^6 + z + 1$	$(z^{63} - 1)/(z^6 + z + 1)$ over \mathbf{F}_2
$[127, 120, 3]_2$	§4.1.3	$z^7 + z^3 + 1$	$(z^{127} - 1)/(z^7 + z^3 + 1)$ over \mathbf{F}_2
$[23, 12, 7]_2$	§4.1.7	$z^{11} + z^9 + z^7 + z^6 + z^5 + z + 1$	$z^{12} + z^{10} + z^7 + z^4 + z^3 + z^2 + z + 1$
$[n, n-1, 2]_3$	§4.2.1	$z+2$	$z^{n-1} + z^{n-2} + \dots + z + 1$
$[n, 1, n]_3$	§4.2.2	$z^{n-1} + z^{n-2} + \dots + z + 1$	$z+2$
$[13, 10, 3]_3$	§4.2.3	$z^3 + z^2 + 2$	$z^{10} + 2z^9 + z^8 + 2z^6 + 2z^5 + z^4 + z^3 + z^2 + 1$
$[11, 6, 5]_3$	§4.2.5	$z^5 + 2z^3 + z^2 + 2z + 2$	$z^6 + z^4 + 2z^3 + 2z^2 + 2z + 1$
$[n, n-1, 2]_4$	§4.3.1	$z+1$	$z^{n-1} + z^{n-2} + \dots + z + 1$
$[n, 1, n]_4$	§4.3.2	$z^{n-1} + z^{n-2} + \dots + z + 1$	$z+1$
$[5, 3, 3]_4$	§4.3.3	$z^2 + \omega z + 1$	$z^3 + \omega z^2 + \omega z + 1$
$[85, 81, 3]_4$	§4.3.3	$z^4 + z^3 + \omega z + 1$	$(z^{85} - 1)/(z^4 + z^3 + \omega z + 1)$ over \mathbf{F}_4

Table 7. Some small cyclic codes. Note that a cyclic form of the $[4, 2, 3]_3$, $[40, 36, 3]_3$, and $[21, 18, 3]_4$ Hamming codes do not exist (that is, the best $[4, 2]_3$, $[40, 36]_3$, and $[21, 18]_4$ codes that may be cast in cyclic form have $d = 2$); in fact, a Hamming code of length $n = (q^m - 1)/(q - 1)$ over \mathbf{F}_q exists in cyclic form only if m and $(q - 1)$ are coprime (Blahut 2003).

$(z^n - 1)$ over \mathbf{F}_4 is more delicate, as the factorizations do not reduce to unique irreducible forms; one such factorization is listed in Table 6. Based on (4.25a) and such factorizations, a large number of cyclic codes may be constructed. However, only a few such codes have both favorable minimum distance d and an available simple error detection/correction scheme; some such codes are listed in Table 7.

Given a data vector $\mathbf{d} \in \mathbf{F}_q^k$, the use of an LC in cyclic form is again straightforward:

- form a data polynomial $d(z)$ with the k elements of \mathbf{d} as coefficients;
- code $d(z)$ into a codeword polynomial $w(z)$ leveraging the basis polynomial $v(z)$ [using nonsystematic coding, one simply takes $w(z) = d(z)v(z)$];
- transmit the corresponding codeword $\mathbf{w} \in \mathbf{F}_q^n$ over the noisy channel;
- receive the (possibly corrupted) message $\hat{\mathbf{w}} \in \mathbf{F}_q^n$ on the other end;
- decode the corresponding $\hat{w}(z)$ leveraging the parity-check polynomial $h(z)$.

Cyclic coding. For the purpose of fast decoding, we now present two methods with which the basis polynomial $v(z)$ may be leveraged to generate a codeword polynomial $w(z)$ in systematic form [that is, rather than taking $w(z) = d(z)v(z)$]. By convention, the systematic form in the cyclic case usually shifts the k data symbols in $d(z)$ to the end of the codeword, that is:

$$\begin{aligned} w(z) &= b(z) + z^{n-k}d(z) \\ &= b_0 + b_1z + \dots + b_{n-k-1}z^{n-k-1} + d_0z^{n-k} + d_1z^{n-k+1} + \dots + d_{k-1}z^{n-1}. \end{aligned} \quad (4.27)$$

If $k/n < 0.5$, a recursive approach may be used to determine the parity symbols in $b(z)$. By (4.25b) and the fact that each valid codeword polynomial $w(z)$ is itself a linear combination of the basis polynomials $v(z)$, it is seen that

$$u(z) \bmod (z^n - 1) = 0 \quad \text{where} \quad u(z) \triangleq h(z)w(z) = u_0 + u_1z + u_2z^2 + \dots$$

Initializing the last k symbols of $w(z)$ as shown in (4.27), the remaining symbols of $w(z)$ may thus be determined from the resulting convolution formulae for u_{n-1} through u_k as follows:

$$\begin{aligned} u_{n-1} &= h_0w_{n-1} + \dots + h_kw_{n-k-1} = 0 &\Rightarrow & w_{n-k-1} = -[h_0w_{n-1} + \dots + h_{k-1}w_{n-k-2}]/h_k, \\ u_{n-2} &= h_0w_{n-2} + \dots + h_kw_{n-k-2} = 0 &\Rightarrow & w_{n-k-2} = -[h_0w_{n-2} + \dots + h_{k-1}w_{n-k-3}]/h_k, \\ &\vdots && \\ u_k &= h_0w_k + \dots + h_kw_0 = 0 &\Rightarrow & w_0 = -[h_0w_k + \dots + h_{k-1}w_1]/h_k. \end{aligned}$$

If $k/n > 0.5$, a polynomial division approach to determine the parity symbols is more efficient. This is accomplished by writing the shift of the data symbols as some multiple of the basis polynomial $v(z)$ plus a remainder $r(z)$:

$$z^{n-k}d(z) = q(z)v(z) + r(z) \quad \Rightarrow \quad [z^{n-k}d(z)] \bmod v(z) = r(z),$$

where the mod command is interpreted as in (4.25b). Since the degree of $v(z)$ is $(n-k)$, the maximum degree of $r(z)$ is $(n-k-1)$. Calculating $r(z)$ as shown above, taking $b(z) = -r(z)$, and rearranging the above equations, it is seen that

$$w(z) = b(z) + z^{n-k}d(z) = q(z)v(z),$$

thus verifying that the polynomial $w(z)$ so generated is in fact a valid codeword polynomial, as it is a multiple of the basis polynomial $v(z)$.

Cyclic decoding. In single parity-check codes, single symbol errors are flagged if $h(z)\hat{w}(z) \neq 0$. In repetition codes, the symbols of $\hat{w}(z)$ may be corrected by simple majority vote.

Decoding of the binary Hamming and the extended binary Golay codes is introduced in §4.4.1. Such syndrome decoding methods extend easily to codes in cyclic form, in which the required syndrome computations are especially streamlined, as now shown. Note that any valid codeword polynomial $w(z)$ is a multiple of the basis polynomial $v(z)$; the *syndrome polynomial* $s(z)$ of the received-message polynomial $\hat{w}(z)$ is thus given by the remainder:

$$s(z) = \hat{w}(z) \bmod v(z).$$

Since the degree of $v(z)$ is $(n-k)$, the maximum degree of $s(z)$ is $(n-k-1)$, and thus the corresponding syndrome vector \mathbf{s} is of order $m = (n-k)$, as expected [see discussion after (4.22)].

The polynomial multiplications and divisions involved in the cyclic coding and decoding algorithms described above are easy to code and efficient to calculate in either an *application-specific integrated circuit (ASIC)* or a *field-programmable gate array (FPGA)*, in which repeated computations with shifted data may be performed quickly. The reduced storage associated with the vector representation of the basis matrix and the parity-check matrix in cyclic form help to facilitate such implementations.

4.4.3. Shannon's theorem and turbo codes. The low-dimensional LBC, LTC, and LQC constructions given above are now supplanted by the more complex *turbo* codes for high performance coding applications such as 10GBase-T ethernet and deep space communication. Though these codes are generally much longer than the simple codes discussed above, they are built on the same fundamental principles, and achieve a coding efficiency over a noisy channel that is very close to the celebrated Shannon limit (Shannon 1949). For more information on such codes, the reader is referred to Gallager (1963), Berrou *et al.* (1993), and Moon (2005). Note also that the study of ternary and quaternary codes is far more than a mathematical curiosity; new memory storage technology concepts leveraging, for example, DNA-based storage, with a four-character alphabet $\{A, T, G, C\}$, directly motivate the further development of non-binary error-correcting coding strategies.

4.4.4. Soft-decision decoding. The type of decoding discussed in §4.4.1-4.4.3, in which the received vector $\hat{\mathbf{w}}$ is assumed to be in \mathbf{F}_q^n , is known as *hard-decision decoding*.

Another formulation of the decoding problem assumes again that $\mathbf{w} \in \mathbf{F}_q^n$, but that $\hat{\mathbf{w}} \in \mathbb{R}^n$. The decoding problem in this case, called *soft-decision decoding*, is similar to that considered before (again, to find the most likely codeword \mathbf{w} corresponding to $\hat{\mathbf{w}}$, and the original data vector \mathbf{d} that generated it), but is now based on finding the codeword \mathbf{w} that minimizes the Euclidian distance to $\hat{\mathbf{w}}$ rather than that which minimizes the Hamming distance.

For example, consider the soft-decision decoding of a binary parity check code. Assume that the transmitted codeword $\mathbf{w} \in \mathbf{F}_2^n$ (that is, the symbols being transmitted are binary, and in this case rescaled to be ± 1) but that the received message $\hat{\mathbf{w}} \in \mathbb{R}^n$ (that is, the symbols received are real). In this case, we may decode the received message by initially taking $\mathbf{w} = \text{sign}(\hat{\mathbf{w}})$. If the resulting decoded vector fails the parity check, we simply take the decision that we were least certain about (that is, the element of $\hat{\mathbf{w}}$ that is closest to zero) and round it the other direction; this is known as *Wagner's decoding rule* (Silverman & Balser 1954).

Many soft-decision decoding algorithms are essentially generalizations of Wagner's decoding rule. Further, most soft-decision decoding algorithms may be framed as straightforward restrictions of a corresponding lattice quantization algorithm (see §5) to the appropriate subset of the lattice in question.

5. Quantization onto lattices. We now introduce some methods for quantization from an arbitrary point \mathbf{x} in \mathbb{R}^n onto a point $\tilde{\mathbf{x}}$ on a discrete lattice, which may be defined via integer linear combination of the columns of the corresponding basis matrix B . The solution to this problem is lattice specific, and is thus treated lattice by lattice in the subsections below. Note that §5.1 through §5.4 are adapted from Conway & Sloane (1998), and §5.5 is adapted from Vardy & Be'ery (1993). Note also that we neglect the problem of scaling of the lattices in this discussion, which is trivial to implement in code.

5.1. Quantization to \mathbb{Z}^n . Quantize to \mathbb{Z}^n simply by rounding each element of \mathbf{x} to the nearest integer.

5.2. Quantization to D_n . Quantize to D_n by rounding \mathbf{x} two different ways:

- Round each element of \mathbf{x} to the nearest integer, and call the result $\hat{\mathbf{x}}$.
- Round each element of \mathbf{x} to the nearest integer *except* that element of \mathbf{x} which is furthest from an integer, and round that element the wrong way (that is, round it down instead of up, or up instead of down); call the result $\hat{\hat{\mathbf{x}}}$.

Compute the sum s of the individual elements of $\hat{\mathbf{x}}$; the desired quantization is $\tilde{\mathbf{x}} = \hat{\mathbf{x}}$ if s is even, and $\tilde{\mathbf{x}} = \hat{\hat{\mathbf{x}}}$ if s is odd.

5.3. Quantization to A_n . The A_n lattice is defined in an n -dimensional subspace C of $Y = \mathbb{R}^{n+1}$. The subspace C is spanned by the n columns of the corresponding basis matrix B_{A_n} , and the orthogonal complement of C is spanned by the vector \mathbf{n}_{A_n} . Thus, the nearest

point in the subspace, $\mathbf{y}_C \in C$, to any given point $\mathbf{y} \in Y$ is given by

$$\mathbf{y}_C = \mathbf{y} - (\mathbf{y}, \mathbf{n}_{A_n}) \cdot \mathbf{n}_{A_n}.$$

An orthogonal basis \hat{B}_{A_n} of C may easily be determined from B_{A_n} via Gram Schmidt orthogonalization. With this orthogonal basis, the vectors $\mathbf{x} \in \mathbb{R}^n$ comprising the A_n lattice may be related to the corresponding vectors $\mathbf{y}_C \in C \subset Y$ (that is, on an n -dimensional subspace of \mathbb{R}^{n+1}) via the equation

$$\mathbf{y}_C = \hat{B}_{A_n} \mathbf{x}. \quad (5.1a)$$

Thus, starting from some point $\mathbf{x} \in \mathbb{R}^n$ but not yet quantized onto the lattice, we can easily determine the corresponding $(n+1)$ -dimensional vector \mathbf{y}_C which lies within the n -dimensional subspace C of \mathbb{R}^{n+1} via (5.1a). Given this value of $\mathbf{y}_C \in C$, we now need to quantize onto the lattice. We may accomplish this with the following simple steps:

- Round each component of \mathbf{y}_C to the nearest integer, and call the result $\hat{\mathbf{y}}$. Define the deficiency $\Delta = \sum_i \hat{y}_i$, which quantifies the orthogonal distance of the point $\hat{\mathbf{y}}$ from the subspace C .
- If $\Delta = 0$, then $\tilde{\mathbf{y}} = \hat{\mathbf{y}}$. If not, define $\mathbf{d} = \mathbf{y}_C - \hat{\mathbf{y}}$, and distribute the integers $0, \dots, n$ among the indices i_0, \dots, i_n such that

$$-1/2 \leq d(\hat{y}_{i_0}) \leq d(\hat{y}_{i_1}) \leq \dots \leq d(\hat{y}_{i_n}) \leq 1/2.$$

If $\Delta > 0$, then nudge $\hat{\mathbf{y}}$ back onto the C subspace by defining $\tilde{y}_{i_k} = \begin{cases} \hat{y}_{i_k} - 1 & k < \Delta, \\ \hat{y}_{i_k} & \text{otherwise.} \end{cases}$

If $\Delta < 0$, then nudge $\hat{\mathbf{y}}$ back onto the C subspace by defining $\tilde{y}_{i_k} = \begin{cases} \hat{y}_{i_k} + 1 & k > n + \Delta, \\ \hat{y}_{i_k} & \text{otherwise.} \end{cases}$

Back in n -dimensional parameter space, the quantized value $\tilde{\mathbf{y}} \in C$ corresponds to

$$\tilde{\mathbf{x}} = \hat{B}_{A_n}^T \tilde{\mathbf{y}}. \quad (5.1b)$$

5.4. Quantization to the union of cosets. The dual lattices D_n^* and A_n^* , the triangular lattice A_2 , and the packing D_n^+ (including the lattice $E_8 \cong E_8^* \cong D_8^+$) are described via the union of simple, real cosets in (2.4a), (2.7a), (2.6c), and (2.5), respectively. The lattices E_7 and E_7^* may be built via the union of simple, real cosets via Construction A [see (4.4a)], with coset representatives $\mathbf{w}_{[n,k,d]}^i$ defined in (4.8) and (4.9) respectively. To quantize a lattice described in such a manner (as a union of simple cosets), one may quantize to each coset independently, then select from these individual quantizations that lattice point which is nearest to the original point \mathbf{x} .

The lattices E_6 and E_6^* may be built via the union of complex cosets [which are scaled and shifted complex \mathcal{E} lattices $\mathbb{Z}[\omega]^3$] via Construction $A_{\mathcal{E}}^{\pi}$ [see (4.5a)], with coset representatives $\mathbf{w}_{[n,k,d]}^i$ given in (4.13) and (4.12) respectively. Following Conway & Sloane (1984), to discretize a point \mathbf{x} to coset i in these cases:

- Determine the complex vector $\mathbf{z} \in \mathbb{C}^3$ corresponding to $\mathbf{x} \in \mathbb{R}^6$. Shift and scale such that $\hat{\mathbf{z}} = (\mathbf{z} - \mathbf{a}_i)/\theta$.
- Determine the real vector $\hat{\mathbf{x}} \in \mathbb{R}^6$ corresponding to $\hat{\mathbf{z}} \in \mathbb{C}^3$. Quantize the first, second, and third pairs of elements of $\hat{\mathbf{x}}$ to the real triangular A_2 lattice to create the quantized vector $\hat{\hat{\mathbf{x}}}$.
- Determine the complex vector $\hat{\hat{\mathbf{z}}} \in \mathbb{C}^3$ corresponding to $\hat{\hat{\mathbf{x}}} \in \mathbb{R}^6$. Unscale and unshift such that $\tilde{\mathbf{z}} = \theta \hat{\hat{\mathbf{z}}} + \mathbf{a}_i$.
- Determine the real vector $\tilde{\mathbf{x}} \in \mathbb{R}^6$ corresponding to $\tilde{\mathbf{z}} \in \mathbb{C}^3$.

5.5. Quantization to Λ_{24} . We now jump to the Leech lattice in dimension $n = 24$. Recall from §2.6 that the best lattices in dimensions $n = 9$ to $n = 23$ may all be determined as lower-dimensional cross-sections of Λ_{24} ; once the (difficult) $n = 24$ case is mastered, quantization to these intermediate dimensions is relatively straightforward.

Efficient quantization to Λ_{24} is a problem that received intense scrutiny in the 1980s and early 1990s. The best algorithm described in the literature, due to Vardy & Be’ery (1993), is based on the construction of Λ_{24} described in the last paragraph of §4.3.5, and essentially represents a culmination of the previous efforts that led to it. This remarkable algorithm requires only about 3000 to 3600 floating-point operations and comparisons, and a comparable number of integer operations and comparisons, to compute the point of the Λ_{24} lattice that is closest to any given point $\mathbf{r} \in \mathbb{R}^{24}$. The algorithm leverages effectively many of the fundamental symmetries inherent in Λ_{24} , including its close relationships with both carefully-chosen subsets of the D_2 lattice (Figure 4.5) as well as the $[6, 3, 4]_4$ hexacode (§4.3.5).

Though it was proposed in 1993, the logic inherent to this algorithm is so intricate that, as of the writing of this review, an executable version of it did not appear to be readily available in the literature. We have thus written an efficient³⁰ Fortran90 implementation of this algorithm, which is available online at:

<http://renaissance.ucsd.edu/software/DecodeLeech.tgz>

This implementation is thoroughly commented, and is written in a notation consistent with that of Vardy & Be’ery (1993). Thus, in addition to being a useful code for new practical applications of the Leech lattice in science and engineering, it is hoped that this executable code can itself be a helpful guide in the understanding of this complex algorithm.

In short, using the notation introduced at the end of §4.3.5, this algorithm first splits the problem of quantizing a point $\mathbf{r} \in \mathbb{R}^{24}$ to the nearest Λ_{24} point into two subproblems:

- quantizing to H_{24} ; that is, when forming the original vector $\mathbf{r} \in \mathbb{R}^{24}$ into a 2×6 array of points $\mathbf{r}_{hn} \in \mathbb{R}^2$ for $h = 0, 1$ and $n = 0, \dots, 5$, quantizing each \mathbf{r}_{hn} to the best A_{ijk} points in the Ungerboeck partitioning of D_2 such that the overall k parity of the array is even, while the projection of the 2×6 array of points forms a codeword of the $[6, 3, 4]_4$ hexacode; and
- quantizing to $H_{24} + \mathbf{a}$; that is, quantizing to the best B_{ijk} points in the Ungerboeck partitioning of D_2 such that the overall k parity of the array is odd, while, again, the projection of the 2×6 array of points forms a codeword of the $[6, 3, 4]_4$ hexacode.

The best of the two lattice points selected by these subproblems is then returned.

During the execution of each of these two subproblems, the closest point to \mathbf{r}_{hn} in each A_{ijk} family (in the even overall k parity case) or in each B_{ijk} family (in the odd overall k parity case) is first identified, and the *squared Euclidian distance* (*SED*) to each of these points is calculated. For each i and j , the “preferred” value of k (that is, the one that leads to the least SED for that point) is determined, and the SED penalty δ for choosing the other value of k is computed. The algorithm then further splits the quantization to H_{24} (and, similarly to $H_{24} + \mathbf{a}$) into two smaller sub-subproblems:

- quantizing to Q_{24} ; that is, to arrays with the specified overall k parity such that, additionally, the overall h parity is even; and
- quantizing to $Q_{24} + \mathbf{b}$; that is, to arrays with the specified overall k parity such that, additionally, the overall h parity is odd.

The best of the two lattice points selected by these sub-subproblems is then returned.

³⁰Our implementation of this algorithm executes in about 0.3 milliseconds on a 2008 vintage laptop (2.53GHz Intel Core 2 Duo), which is sufficiently fast for many applications. It is also trivial to parallelize this code efficiently over four separate computational threads, as quantization to each Leech quarter lattice is handled independently.

The quantization to Q_{24} and its 3 translates is, in turn, decomposed into 5 distinct steps:

1. Only two sets of indices $\{i_0, j_0, i_1, j_1\}$ project to each symbol $p \in \mathbf{F}_4$; in this step, for each symbol p and for each column n of the 2×6 array, we identify the “preferred representation” as that set which, when taken together with their corresponding preferred values of k_0 and k_1 , minimize the SED of the column, and the other set, referred to as the “non-preferred representation”; we also calculate the SED penalty associated with choosing the non-preferred representation. Conveniently, it turns out that the preferred representation and the non-preferred representation necessarily have opposite h parity.
2. The three lists of penalties associated with changing the column-wise k parities (case 0), the column-wise h parities (case 1), or both (case 2) are then sorted (our implementation uses mergesorts, due to their cache efficiency; heapsorts or quicksorts are viable alternatives).
3. The SED for each preferred “block” (that is, each pair of columns) is then computed.
4. For each of the 64 codewords of the hexacode [see (4.20)], we then find the smallest possible correction(s) to the set of preferred representations such that the total k parity and the total h parity match the specified values required for the particular translate of Q_{24} being considered (of 4 possible cases). This step leverages the sorted lists computed in step 2.
5. For each of 16 sets of symbols [given by $w_0 \in \mathbf{F}_4$ and $w_1 \in \mathbf{F}_4$], calculate the total SED of corrected representations, determined in step 4, corresponding to the 4 valid codewords of the hexacode [given by $w_2 \in \mathbf{F}_4$ and $\{w_3, w_4, w_5\}$ selected according to $V_{[6,3,4]_4}$ defined in (4.20)]. We then find the minimum total SED amongst these 16 corrected representations, and return the corresponding lattice point.

6. Enumerating nearest-neighbor lattice points. In the practical use of lattices in engineering applications, in addition to effective quantization methods (§5), one occasionally needs to generate a list of all lattice points that are nearest neighbors to a given lattice point. It is sufficient to generate a list of all lattice points that are nearest neighbors of the origin, then to shift these points as necessary to the vicinity of any other lattice point. The present section describes two methods to generate such lists of nearest neighbors on a lattice.

6.1. Cases with $n \leq 8$. Noting first (see §2.1) that a basis matrix B of an n -dimensional lattice might itself have more than n rows, the following algorithm is found to be effective for all lattices up to about $n = 8$:

0. Initialize $p = 1$.
1. Define a distribution of points $\tilde{\mathbf{z}}^i$ such that each element of each of these vectors is selected from the set of integers $\{-p, \dots, 0, \dots, p\}$, and that *all possible vectors* that can be created in such a fashion, except the origin, are present (without duplication) in this distribution.
2. Compute the distance of each transformed point $\tilde{\mathbf{y}}^i = B\tilde{\mathbf{z}}^i$ in this distribution from the origin, and eliminate those points in the distribution that are farther from the origin than the minimum distance computed in the set.
3. Count the number of points remaining in the distribution. If this number equals the (known) kissing number of the lattice under consideration, as listed in Tables 2-3, then determine an orthogonal \hat{B} from B via Gram Schmidt orthogonalization, set $\tilde{\mathbf{x}}^i = \hat{B}^T \tilde{\mathbf{y}}^i$ for all i , and exit; otherwise, increment p and repeat from step 1.

Though this simple algorithm is not at all efficient, for $n \leq 8$ it really need not be, as the nearest neighbor distribution is identical around every lattice point, and thus this algorithm need only be run once for any given lattice.

6.2. Cases with $n > 8$. For $n > 8$, the algorithm described above is prohibitively expensive. We thus focus here on an efficient manner of obtaining the 196,560 nearest neighbors to the origin of the Leech lattice Λ_{24} , then on the restriction of this set of neighbors, one dimension at a time, down to $n = 9$.

To proceed, it is first necessary to enumerate the codewords of the binary Golay code following the approach described in §4.1.7. Recall that the basis matrix of the binary Golay

code has dimension 24×12 ; thus, the $2^{12} = 4096$ codewords of the binary Golay code follow immediately as a binary linear combination (that is, as a linear combination, mod 2, with binary coefficients) of the columns of this matrix.

Then, in order to identify all of the nearest neighbors of the Leech lattice, we may proceed (following Conway & Sloane 1998) by constructing three distinct sets of points:

- The first set, consisting of 98,304 points, is obtained using the binary Golay codewords discussed above. Construct first a 24×24 matrix A with -3 everywhere along the main diagonal and 1 everywhere else. Then, take each codeword of the binary Golay code, one at a time, replace each 0 with -1 , and perform elementwise multiplication of this modified codeword to each column of A , thereby generating 24 points for each of the 2^{12} binary Golay codewords, or $2^{12} \cdot 24 = 98,304$ points.
- The next set, consisting of 1,104 points, is composed of vectors with 22 zero elements and two elements that are either 4 or -4 . As there are 276 ways to select the locations of the nonzero elements, and $2^2 = 4$ valid ways to populate them, we obtain $2^2 \cdot 276 = 1,104$ points.
- The third set, consisting of 97,152 points, is obtained using the 759 vectors of the Witt design, which are just the 759 binary Golay codewords (discussed above) of weight 8. Note that each of these vectors has 8 ones and 16 zeros. Construct an 8×128 matrix C such that each element of each column is either a 2 or -2 , with an even number of minus signs in each column (note that there are $2^7 = 128$ such columns possible). We then distribute the elements in each of the 128 columns of C into each of 8 positions where the ones sit in each of the 759 vectors of the Witt design, thereby obtaining the remaining $128 \cdot 759 = 97,152$ points.

The $98,304 + 1,104 + 97,152 = 196,560$ points so generated are the nearest neighbors to the origin of Λ_{24} . Then, throwing out those points \mathbf{z} for which $\mathbf{z} \cdot \mathbf{n}_{\Lambda_{23}} \neq 0$ (see §2.6) leaves the 93,150 neighbors of Λ_{23} ; additionally throwing out those points \mathbf{z} for which $\mathbf{z} \cdot \mathbf{n}_{\Lambda_{22}} \neq 0$ leaves the 49,896 neighbors of Λ_{22} ; etc.

7. Conclusions. In short, §2 of this paper is about generalizing to higher dimensions the familiar triangular, BCC, and FCC lattices, which are dense alternatives to the Cartesian lattice with reduced nonuniformity, whereas §3 of this paper is about generalizing to higher dimensions a few (specifically, the most regular) of the many familiar nets arising in biology and crystallography, such as the honeycomb, diamond, and quartz graphs, which are rare alternatives to the Cartesian lattice with reduced coordination number. The primary successful application of n -dimensional sphere packing theory to date is in coding theory, as reviewed in §4. A working understanding of this material, including how to quantize to such lattices, as summarized in §5, and how to enumerate nearest neighbors on such lattices, as summarized in §6, is essential for new practical applications of sphere packing theory, such as those studied in Parts II and III of this work, both of which leverage heavily the foundational material discussed here.

Acknowledgements. The authors would like to thank Prof. Haoxiang Luo for helpful discussions related to this work.

REFERENCES

- [1] Anzin (2002) On the density of a lattice covering for $n = 11$ and $n = 14$ (in Russian), *Uspekhi Mat. Nauk* **57**, no. 2, 187188; English translation in *Math. Surveys* **57**, 407409.
- [2] Aste, T, & Weaire, D (2008) *The pursuit of the perfect packing*. Taylor & Francis.
- [3] Baranovskii, EP (1994) The perfect lattices $\Gamma(\mathcal{A}^n)$, and the covering density of $\Gamma(\mathcal{A}^n)$. *European Journal of Combinatorics* **15**, 317-323.
- [4] Belitz, P, & Bewley, T (2011) New Horizons in Sphere Packing Theory, Part II: Lattice Based Derivative Free Optimization via Global Surrogates. *SIAM Journal on Optimization*, submitted. http://fccr.ucsd.edu/pubs/BB_Part2.pdf
- [5] Berrou, C, Glavieux, A, & Thitimajshima, P (1993) Near Shannon limit error-correcting coding and decoding: Turbo-Codes. In *ICC'93*, Geneva, Switzerland. 1064-1070.

- [6] Beukemann, A, & Klee, WE (1992) Minimal nets. *Z. Krist.* **201**, 37-51.
- [7] Blahut, RE (2003) *Algebraic codes for data transmission*. Cambridge.
- [8] Blatov, VA (2006) Multipurpose crystallochemical analysis with the program package TOPOS. *IUCr CompComm Newsletter* **7**, 438.
- [9] Blatov, VA (2007) Topological relations between three-dimensional periodic nets. I. Uninodal nets. *Acta Cryst.* **A63**, 329-343.
- [10] Blatov, VA, Delgado-Friedrichs, O, O’Keeffe, M, & Proserpio, DM (2007) Three-periodic nets and tilings: natural tilings for nets. *Acta Cryst.* **A63**, 418-425.
- [11] Blatov, VA, O’Keeffe, M, & Proserpio, DM (2009) Vertex-, face-, point-, Schläfli-, and Delaney-symbols in nets, polyhedra and tilings: recommended terminology. *CrystEngComm.*, 2010, DOI: 10.1039/b910671e.
- [12] Blichfeldt, HF (1935) The minimum values of positive quadratic forms in six, seven and eight variables. *Math. Z.* **39**, 115.
- [13] Bonneau, C, Delgado-Friedrichs, O, O’Keeffe, M, & Yaghi, OM (2004) Three-periodic nets and tilings: minimal nets. *Acta Cryst.* **A60**, 517-520.
- [14] Brown, H, Bülow, R, Neubüser, J, Wondratschek, H, & Zassenhaus, H (1978) *Crystallographic groups of 4-dimensional space*. Wiley.
- [15] Cecil, T (2005) A numerical method for computing minimal surfaces in arbitrary dimension. *J. Comp. Phys.* **206**, 650-660.
- [16] Cessna, J, & Bewley, T (2011) New Horizons in Sphere Packing Theory, Part III: Structured Computational Interconnects. *SIAM Journal on Computing*, submitted. http://fccr.ucsd.edu/pubs/CB_Part3.pdf
- [17] Clark, WE (1930) *The Aryabhataiya of Aryabhata: An Ancient Indian Work on Mathematics and Astronomy*. University of Chicago Press.
- [18] Cohn, H, & Kumar, A (2009) Optimality and uniqueness of the Leech lattice among lattices, *Annals of Mathematics* **170**, 1003-1050.
- [19] Conway, JH, & Sloane, NJA (1984) On the Voronoï regions of certain lattices. *SIAM J. Alg. Disc. Meth.* **5**, 294-302.
- [20] Conway, JH, & Sloane, NJA (1997) Low-dimensional lattices. VII Coordination sequences. *Proc. R. Soc. Lond. A* **453**, 2369-2389.
- [21] Conway, JH, & Sloane, NJA (1998) *Sphere Packings, Lattices, and Groups*, Springer.
- [22] Coxeter, HSM (1951) Extreme forms. *Canadian Journal of Mathematics*, **3**, 391-441.
- [23] Coxeter, HSM (1970) *Twisted Honeycombs*. Regional Conference Series in Mathematics, No. 4, American Mathematical Society, Providence.
- [24] Coxeter, HSM (1973) *Regular Polytopes*. Dover.
- [25] Coxeter, HSM (1974) *Regular Complex Polytopes*. Cambridge.
- [26] Coxeter, HSM (1987) *Projective Geometry*. Springer.
- [27] Coxeter, HSM (1989) *Introduction to Geometry*. Wiley.
- [28] Croft, Falconer, & Guy (1991) *Unsolved Problems in Geometry*. Springer.
- [29] Curtis, RT (1976) A new combinatorial approach to M24. *Math. Proc. Camb. Phil. Soc.* **79**, 25-42.
- [30] Delgado-Friedrichs, O, Foster, MD, O’Keeffe, M, Proserpio, DM, Treacy, MMJ, & Yaghi, OM (2005) What do we know about three-periodic nets? *Journal of Solid State Chemistry* **178**, 2533-2554.
- [31] Delgado-Friedrichs, O, & Huson, DH (2000) 4-Regular Vertex-Transitive Tilings of E^3 . *Discrete & Computational Geometry* **24**, 279-292.
- [32] Delgado-Friedrichs, O, & O’Keeffe, M (2003) Identification of and symmetry computation for crystal nets. *Acta Cryst.* **A59**, 351-360.
- [33] Delgado-Friedrichs, O, & O’Keeffe, M (2007) Three-periodic nets and tilings: face-transitive tilings and edge-transitive nets revisited. *Acta Cryst.* **A63**, 344-347.
- [34] Delgado-Friedrichs, O, O’Keeffe, M, & Yaghi, OM (2003a) Three-periodic nets and tilings: regular and quasiregular nets. *Acta Cryst.* **A59**, 22-27.
- [35] Delgado-Friedrichs, O, O’Keeffe, M, & Yaghi, OM (2003b) Three-periodic nets and tilings: semiregular nets. *Acta Cryst.* **A59**, 515-525.
- [36] Delgado-Friedrichs, O, O’Keeffe, M, & Yaghi, OM (2003c) The $CdSO_4$, rutile, cooperite, and quartz dual nets: interpenetration and catenation. *Solid State Sciences.* **5**, 73-78.
- [37] Delgado-Friedrichs, O, O’Keeffe, M, & Yaghi, OM (2006) Three-periodic nets and tilings: edge-

- transitive binodal structures. *Acta Cryst.* **A62**, 350-355.
- [38] Dorozinski, TE, & Fischer, W (2006) A novel series of sphere packings with arbitrarily low density. *Z. Kristallogr.* **221**, 563-566.
- [39] Fejes Tóth, L (1959) Verdeckung einer Kugel durch Kugeln. *Publ. Math. Debrecen* **6**, 234-240.
- [40] Fejes Tóth, L (1972) *Lagerungen in der Ebene auf der Kugel und im Raum*. Springer.
- [41] Fejes Tóth, L (1975) Research problem 13. *Period. Math. Hungar.* **6**, 197-199.
- [42] Fischer, W (2005) On sphere packings of arbitrarily low density. *Z. Kristallogr.* **220**, 657662.
- [43] Friedman, E (2009) Erich's Packing Center: <http://www2.stetson.edu/~efriedma/packing.html>.
- [44] Gallager, RG (1963) *Low Density Parity Check Codes*. Monograph, M.I.T. Press.
- [45] Gandini, PM, & Willis, JM (1992) On finite sphere packings. *Math Pannon* **3**, 19-29.
- [46] Gandini, PM, & Zucco, A (1992) On the sausage catastrophe in 4-space. *Mathematica* **39**, 274-278.
- [47] Gauss, CF (1831) Untersuchungen über die Eigenschaften der positiven ternären quadratischen Formen von Ludwig August Seber, *Göttingische gelehrte Anzeigen*, 1831 Juli 9, also published in *J. Reine Angew. Math.* **20** (1840), 312320, and *Werke*, vol. 2, Königliche Gesellschaft der Wissenschaften, Göttingen, 1876, pp. 188196.
- [48] Gensane, T (2004) Dense packings of equal spheres in a cube. *Electronic J. Combinatorics* **11** (1), #R33, 1-17.
- [49] Grosse-Kunstleve, RW, Brunner, GO, & Sloane, NJA (1996) Algebraic description of coordination sequences and exact topological densities for zeolites. *Acta Cryst.* **A52**, 879-889.
- [50] Grover, P, Sahai, A, & Park, SY (2010) The finite-dimensional Witsenhausen counterexample. *IEEE Transactions on Automatic Control*, submitted. Draft available as: arXiv:1003.0514v1.
- [51] Hales, S (1727) *Vegetable Staticks*, London: Printed for W. and J. Innys; and T. Woodward.
- [52] Hales, TC (2005) A proof of the Kepler conjecture. *Annals of Mathematics*, **162**, 10651185.
- [53] Hales, TC (2006), Historical overview of the Kepler conjecture, *Discrete Comput Geom* **36**, 520.
- [54] Harriot, T (1614) *De Numeris Triangularibus Et inde De Progressionibus Arithmetis: Magisteria magna*, in Berry, J, and Stedall, J, editors (2009) *Thomas Harriot's Doctrine of Triangular Numbers: the 'Magisteria Magna'*, published by the European Mathematical Society.
- [55] Heath, TL (1931) *A Manual of Greek Mathematics*. Oxford University Press (republished in 2003 by Dover).
- [56] Heesch, H, & Laves, RT (1933) Über dünne Kugelpackungen, *Z. Krist.* **85**, 443-453.
- [57] Hyde, ST, Delgado-Friedrichs, O, Ramsden, SJ, Robins, V (2006) Towards enumeration of crystalline frameworks: The 2D hyperbolic approach. *Solid State Sci.* **8**, 740752.
- [58] Janssen, T (1986) Crystallography of quasi-crystals. *Acta Cryst.* **A42**, 261-271.
- [59] Kaku, M (1999) *Introduction to Superstring and M-Theory*. Springer-Verlag.
- [60] Kelvin, WT (1887) On the Division of Space with Minimum Partitional Area, *Philosophical Magazine* **24**, No. 151, p. 503.
- [61] Kepler, J (1611) *Strena seu de nive sexangula (The six-cornered snowflake)*.
- [62] Koch, E, & Fischer, W (1995) Sphere packings with three contacts per sphere and the problem of the least dense sphere packing. *Z. Krist.* **210**, 407414.
- [63] Koch, E, & Fischer, W (2006) Sphere packings and packings of ellipsoids. In *International Tables for Crystallography*, Vol C, Sec 9.1.1, pp 746-751.
- [64] Korkine, A, & Zolotareff, G (1873) Sur les formes quadratiques. *Math. Ann.* **6**, 366389.
- [65] Korkine, A, & Zolotareff, G (1875) Sur les formes quadratiques positives, *Math. Ann.* **11**, 242292.
- [66] Lagrange, JL (1773) Recherches darithmétique. *Nov. Mem. Acad. Roy. Sc. Bell Lettres Berlin* In *Œuvres*, **3**, Gauthier-Villars, Paris, 18671892, pp. 693758.
- [67] Leech, J (1956) The problem of the thirteen spheres. *Math. Gazette* **40**, 22-23.
- [68] MacWilliams, FJ, & Sloane, NJA (1977) *The Theory of Error Correcting Codes*. North Holland.
- [69] Meschkowski, H (1960) *Ungelöste und unlösbare Probleme der Geometrie*, Braunschweig.
- [70] Milnor, J (1976) Hilberts problem 18: on crystallographic groups, fundamental domains, and on sphere packings, in *Mathematical Developments Arising from Hilbert Problems*, Proceedings of Symposia in Pure Mathematics, vol. 28, AMS, Providence, RI, pp. 491506.
- [71] Moon, T (2005) *Error Correction Coding, Mathematical Methods and Algorithms*. Wiley.
- [72] Morelos-Zaragoza, RH (2006) *The Art of Error Correcting Coding*. Wiley.
- [73] Ockwig, NW, Delgado-Friedrichs, O, O'Keeffe, M, & Yaghi, OM (2005) Reticular Chemistry: Occurance and Taxonomy of Nets and Grammar for the Design of Frameworks. *Acc. Chem.*

- Res.* **38**, 176-182.
- [74] O’Keeffe, M (1991a) Dense and rare four-connected nets. *Z. Krist.* **196**, 21-37
- [75] O’Keeffe, M (1991b) N -dimensional diamond, sodalite, and rare sphere packings. *Acta Cryst.* **A47**, 748-753.
- [76] O’Keeffe, M (2008) Three-periodic nets and tilings: regular and related infinite polyhedra. *Acta Cryst.* **A64**, 425-429.
- [77] O’Keeffe, M, Eddaoudi, M, Li, H, Reineke, T, & Yaghi, OM (2000) Frameworks for Extended Solids: Geometrical Design Principles. *Journal of Solid State Chemistry* **152**, 3-20.
- [78] O’Keeffe, M, Peskov, MA, Ramsden, SJ, & Yaghi, OM (2008) The Reticular Chemistry Structure Resource (RCSR) Database of, and Symbols for, Crystal Nets. *Acc. Chem. Res.* **41**, 1782-1789.
- [79] Pless, V (1998) *Introduction to the Theory of Error-Correcting Codes*. Wiley.
- [80] Rukeyser, M (1972) *The Traces of Thomas Harriot*. Random House.
- [81] Sadoc, JF, & Rivier, N, editors (1999) *Foams and Emulsions*. Kluwer.
- [82] Schrijver, A (1986) *Theory of linear and integer programming*. Wiley.
- [83] Schürmann, A (2006) On packing spheres into containers; about Kepler’s finite sphere packing problem. *Documenta Mathematica* **11**, 393406.
- [84] Schürmann, A, & Vallentin, F (2006) Computational approaches to lattice packing and covering problems. *Discrete Comput. Geom.* **35**, 73-116.
- [85] Schütte, K, & van der Waerden, BL (1953) Das Problem der dreizehn Kugeln. *Math Annalen* **125**, 325-334.
- [86] Schwarzenberger, RLE (1980) *N -dimensional crystallography*. Pitman.
- [87] Shannon, CE (1949) Communication in the presence of noise. *Proc. Institute of Radio Engineers*, **37**, 1021.
- [88] Sikirić, MD, Schürmann, A, & Vallentin, F (2008) A generalization of Voronoi’s reduction theory and its application. *Duke Mathematical Journal* **142**, 127-164.
- [89] Silverman, RA, & Balser, M (1954) Coding for a constant data rate source. *IRE Trans. Inform. Theory* **IT-4**, 50-63.
- [90] Skelton, RE, & de Oliveira, MC (2009) *Tensegrity Systems*. Springer.
- [91] Sloan, IH, & Kachoyan PJ (1987) Lattice methods for multiple integration: theory, error analysis and examples. *SIAM J. Num. Anal.* **24**, 116-128.
- [92] Sloane, NJA (1987) Theta-Series and Magic Numbers for Diamond and Certain Ionic Crystal Structures, *J. Math. Phys.* **28**, 1653-1657.
- [93] Szpiro, G (2003) *Kepler’s conjecture: how some of the greatest minds in history helped solve one of the oldest math problems in the world*. Wiley.
- [94] Thompson, TM (1983) *From error-correcting codes through sphere packings to simple groups*. The Mathematical Association of America.
- [95] Thue, A (1892) Om nogle geometrisk talteoretiske Theoremer, *Forand. Skand. Natur.* **14**, 352353.
- [96] Tietäväinen, A (1973) On the nonexistence of perfect codes over finite fields, *SIAM J. Appl. Math.* **24**, 88-96.
- [97] Treacy, MMJ, Rivin, I, Balkovsky, E, Randall, KH, Foster, MD (2004) Enumeration of periodic tetrahedral frameworks. II. Polynodal graphs. *Microporous Mesoporous Mater.* **74**, 121132.
- [98] Ungerboeck, G (1982) Channel coding with multilevel/phase signals. *IEEE Trans. Inform. Theory*, **IT-28**, 55-67.
- [99] Vardy A & Be’ery Y (1993) Maximum likelihood decoding of the Leech lattice, *IEEE Trans. Inform. Theory* **39**, 1435-1444.
- [100] Weaire D & Phelan R (1994) A counterexample to Kelvin’s conjecture on minimal surfaces, *Phil. Mag. Lett.* **69**, 107110.
- [101] Wells, AF (1977) *Three-Dimensional Nets and Polyhedra*. Wiley.
- [102] Wells, AF (1979) *Further Studies of Three-dimensional Nets*. ACA Monograph No. 8.
- [103] Wells, AF (1983) Six New Three-Dimensional 3-Connected Nets $4.n^2$. *Acta Cryst.* **B39**, 652-654.
- [104] Wells, AF (1984) *Structural inorganic chemistry*. Oxford University Press.
- [105] Willis, JM (1983) Research problem 35. *Period. Math. Hungar.* **14**, 312-314.
- [106] Zong, C (1999) *Sphere Packings*. Springer.